9-27-2019 10:30 AM

Design of cell-instructive biomaterial scaffolds for intervertebral disc regeneration

Nadia Sharma
The University of Western Ontario

Supervisor
Flynn, Lauren E.
The University of Western Ontario Joint Supervisor
Séguin, Cheryle A.
The University of Western Ontario

Graduate Program in Biomedical Engineering
A thesis submitted in partial fulfillment of the requirements for the degree in Master of Engineering Science

Abstract

Biomaterials-based therapies targeting the nucleus pulposus (NP) have the potential to promote regeneration and restore mechanical function to the intervertebral disc. This study developed composite hydrogels incorporating decellularized NP (DNP) and assessed its effects on viability, retention and differentiation of U-CH1 cells, an NP progenitor-like cell line. A minimal protocol was developed to decellularize bovine NP that reduced nuclear content while preserving key extracellular matrix components predicted to be favourable for bioactivity. The resulting DNP demonstrated cell-instructive effects, supporting U-CH1 viability and retention within the hydrogels, and promoted the differentiation of the progenitor-like cells towards an NP-like phenotype. These studies established a 3-D platform that mimics the native NP microenvironment and holds promise for applications in cell culture and delivery. Further *in vitro* studies using this system will provide valuable insight into the effects of tissue-specific extracellular matrix on NP progenitor cell fate.

Keywords

Nucleus pulposus regeneration, cell-instructive biomaterials, naturally-derived materials, scaffolds, decellularization, extracellular matrix (ECM), decellularized nucleus pulposus, hydrogels, methacrylated chondroitin sulphate (MCS), U-CH1 cells

Summary for Lay Audience

Back pain is the most common cause of disability worldwide. While the cause of low back pain is complex, it is often linked to intervertebral disc (IVD) degeneration. Although IVD degeneration is multifactorial, it is believed to initiate in the central gel-like region of the disc, known as the nucleus pulposus (NP). Current treatments focus on pain management by medication, physiotherapy and/or exercise therapy; however, there are no disease-modifying treatments available for IVD degeneration. Surgical interventions can alter spine biomechanics, leading to further degeneration of adjacent discs. These limitations have inspired biomaterials-based therapies to regenerate the NP and restore mechanical function to the spine. This study developed injectable biomaterial scaffolds using extracellular matrix (ECM) from bovine NP tissues as a cell-instructive component. The ECM is a tissue-specific complex network of proteins and polysaccharides that provides structure and directs cell function. Existing techniques to isolate the NP ECM use harsh chemicals and strong detergents to remove donor cells, with the goal of creating off-the-shelf scaffolds that could be applied in humans without causing a negative immunological response. This thesis developed a new minimalistic protocol for isolating ECM from bovine NP tissues with the goal of better preserving the structure and composition of the native ECM to enhance bioactivity. Once the protocol was developed and validated, particles of the isolated NP ECM were incorporated into an injectable hydrogel, a gel material that can retain a large amount of water to support encapsulated cell populations and resembles the structure of the NP ECM. As a first step towards testing the regenerative potential of this material, the behaviour of human NP precursor-like cells within the hydrogels were assessed. The results indicated that the NP ECM enhanced the survival of the precursor cells within the gels and promoted a more mature NP-like cell phenotype. These studies represent a key first step in developing a new injectable biomaterial with potential clinical application for the repair or regeneration of the NP and to restore mechanical function to the IVD.

Acknowledgments

First and foremost, I would like to thank my supervisors Drs. Lauren Flynn and Cheryle Séguin for their continual guidance and support. Thank you for giving me the opportunity to work on this project and to grow both personally and as a scientist. It has been a privilege to work alongside and learn from such brilliant people as yourselves.

I would also like to thank my advisory committee members, Drs. Frank Beier and Aaron Price, for their thought-provoking and insightful feedback. It was a pleasure presenting and discussing my work with you during our committee meetings.

A big warm thank you to all of my dear Flynn and Séguin Lab members! You have made my time here unforgettable. Thank you for not only your excellent guidance in helping me learn concepts and techniques involved in the project, but also for all the laughs and fun times in and outside of the lab. A special thank you to Dr. Arthi Shridhar and Courtney Brooks for your patient technical guidance.

To Drs. Katherine Willmore and Keith Griffiths, thank you for believing in me and supporting me throughout my undergrad and till date. I am truly lucky to have mentors like you.

Last but not least, I would like to thank my family. Mama, Papa, Methely; thank you for your patience, guidance and endless love. You inspire me every day, and I am very blessed to have you in my life.

Table of Contents

List of Tables

List of Figures

List of Equations

Abbreviations

^{1}H NMR	Proton-nuclear magnetic resonance
3-D	Three-dimensional
ABAM	Antibiotic-antimycotic
ADAMTS	A disintegrin and metalloproteinase with thrombospondin
AF	Annulus fibrosus
ASCs	Adipose-derived stem/stromal cells
BMP	Bone morphogenetic protein
cDNA	Complimentary deoxyribonucleic acid
CEP	Cartilaginous endplates
COL	Bovine tendon collagen
CS	Chondroitin sulfate
CTGF	Connective tissue growth factor
DAPI	4',6-diamidino-2-phenylindole
DAT	Decellularized adipose tissue
dH_2O	Deionized water
DMMB	Dimethylmethylene blue
DNA	Deoxyribonucleic acid
DNP	Decellularized nucleus pulposus
dsDNA	Double stranded deoxyribonucleic acid
ECM	Extracellular matrix
EDTA	Ethylenediaminetetraacetic acid
ELISA	Enzyme-linked immunosorbent assay

EthD-1	Ethidium homodimer
F/T	Freeze-thaw cycles
FACIT	Fibril-associated collagens with interruptions in their triple helices
FBS	Fetal bovine serum
GAG	Glycosaminoglycan
H&E	Haematoxylin and Eosin
HIF	Hypoxia-inducible factor
Hyalectans	Hyaluronan- and lectin-binding proteoglycans
IHC	Immunohistochemistry
IKVAV	Isoleucine-lysine-valine-alanine-valine motif
IL	Interleukin
IVD	Intervertebral disc
KRT	Cytokeratin
MCS	Methacrylated chondroitin sulphate
MMP	Matrix metalloproteinase
NGF	Nerve growth factor
NP	Nucleus pulposus
PBS	Phosphate buffered saline
PCR	Polymerase chain reaction
PFA	Paraformaldehyde
PGE2	Prostaglandin E2
PMSF	Phenylmethane sulfonyl fluoride
RGD	Tri-peptide arginine-glycine-aspartic acid motif
RNA	Ribonucleic acid
RT-qPCR	Real-time quantitative polymerase chain reaction

SB	Sulfobetaine
SD	Standard deviation
SDS	Sodium dodecyl sulphate
SEM	Scanning electron microscopy
SEM	Standard error of the mean
sGAG	Sulphated glycosaminoglycan
Shh	Sonic hedgehog
SLRPs	Small leucine-rich proteoglycans
SPB	Sorensen's phosphate buffer
T	Brachyury
TBP	Tributyl phosphate
TGF-β	Transforming growth factor beta
TIMPs	Tissue inhibitors of metalloproteinases
TNF-α	Tumor necrosis factor α
Tris	Tris (hydroxymethyl)aminomethane
UV	Ultraviolet
VB	Vertebral body
VEGF	Vascular endothelium growth factor

Chapter 1

1 Introduction

1.1 Clinical significance of intervertebral disc degeneration

According to the most recent *Global Burden of Disease* study, low back pain is the leading cause of lifetime disability worldwide[1]. Between 1990 and 2015, years lived with disability from low back pain increased globally by 54%[2]. In Canada, the medical cost for low back pain-related cases is estimated to range from 6-12 billion dollars annually[3]. With an aging population, the incidence of low back pain is expected to rise further, imposing a substantial socioeconomic burden[4]. While back pain can originate from several anatomical structures of the spine, such as muscles, ligaments, nerve roots, vertebral bodies, facet joints and intervertebral discs (IVDs)[5], it is linked to IVD degeneration in ~40% of all cases[6,7]. Alarmingly, there are no disease-modifying therapies for IVD degeneration and the effect sizes of currently available treatments for back pain, such as physiotherapy, exercise therapy, acupuncture and pain management by medication, are low[8].

The IVD is a fibrocartilaginous joint situated between adjacent vertebrae in the spine, that facilitates multiaxial motion and dissipates high compressive loads (**Fig. 1.1A**)[9]. The IVD is composed of three distinct tissues: an inner nucleus pulposus (NP), an outer annulus fibrosus (AF), and the cartilaginous endplates (CEPs) that anchor the IVD to the superior and inferior vertebrae. The NP is enriched in proteoglycans relative to collagens, reflected in an estimated ratio of sulphated glycosaminoglycans (sGAGs) to hydroxyproline of ~27:1 in young adults (i.e. 15-25 years), resulting in a highly hydrated tissue (~80% H_2O by mass) that functions mechanically to resist compressive loads[10]. This tissue is populated by cartilage-like cells of notochordal origin referred to as NP cells that play an important role in tissue maintenance and mediate responses to changes in the IVD microenvironment (discussed in sections 1.3.2 and 1.4)[11]. The NP is enclosed by the AF, a flexible fibrocartilaginous tissue composed of concentric collagen-rich lamellae that function to resist tensile forces (**Fig. 1.1B**). The collagen bundles of the AF are oriented at an approximate 30° angle from the transverse plane, and alternate in direction with each subsequent lamella[12]. This arrangement of the fibers creates an angle-ply structure in the AF that supports radial forces exerted by the pressurized NP, as well as allows for bending

and twisting motions in the spine[13,14]. The cells in the AF typically extend parallel to the collagen fibers[15]. The CEP is a thin layer of hyaline cartilage rich in collagen type II and proteoglycans, populated by chondrocytes[16]. The CEPs function as an interface, connecting the IVD to adjacent vertebral bodies and allowing passive diffusion of nutrients to the largely avascular IVD[17].

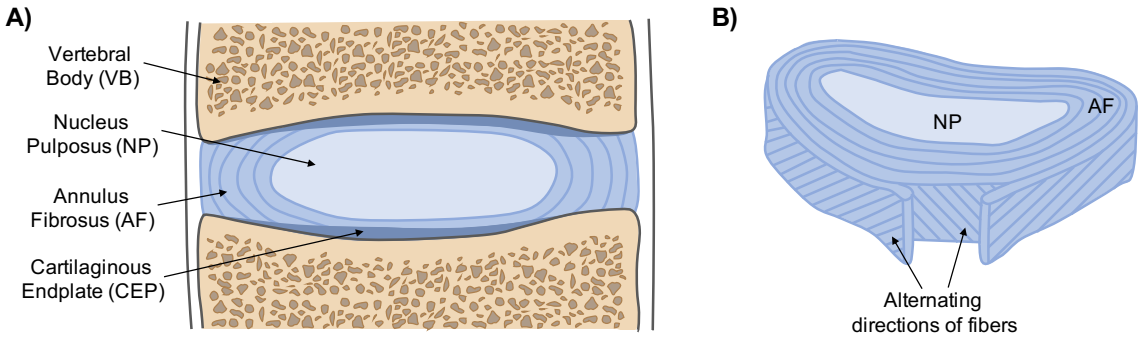

Figure 1.1: Schematic illustration of intervertebral disc (IVD) structure. A) The IVDs are situated between adjacent vertebral bodies (VB) in the spine, and are composed of three anatomically distinct, yet interdependent tissues: an inner gel-like nucleus pulposus (NP), an outer fibrous annulus fibrosus (AF), and the cartilaginous end plates (CEP) that line the superior and inferior vertebral bodies. **B)** The gelatinous NP is enclosed by the highly organized, lamellar AF with collagen fibers arranged in alternating directions. Figure adapted from Pattappa, *et al*[16].

Degeneration of the IVD is associated with increased fibrotic matrix synthesis, inflammation, innervation and vascularization to the largely aneural and avascular tissue[9,18]. Although the etiology of disc degeneration is unknown, it is believed to initiate with changes in the cellular microenvironment of the NP. The NP plays a critical role in maintaining IVD function by absorbing and dissipating axial compressive loads to the surrounding AF[16]. Degenerative changes lead to the loss of hydration in the NP, which reduces the overall disc height and the ability of the NP to resist axial compression[11]. As a result, the load is redistributed to the AF, creating an altered mechanical environment that can cause structural changes leading to disc herniation or rupture, resulting in severe pain[9,11,19].

The disc has a limited capacity for repair, and there are currently no disease-modifying treatments for disc degeneration. Surgical intervention, such as spinal fusion or artificial disc replacement surgery, is required in ~10% of patients with disc degeneration due to severe and persistent pain[20]. While the surgical treatments can alleviate pain, they are associated with numerous neurological complications, and can alter spine mechanics, leading to further degeneration of adjacent discs[21]. These limitations have motivated research in biomaterials-based therapies to deliver pro-regenerative cell populations to the NP to restore function[22].

1.2 The extracellular matrix

The extracellular matrix (ECM) is a complex three-dimensional meshwork of proteins, glycoproteins and proteoglycans assembled in a unique tissue-specific microarchitecture[23]. The ECM is an integral component of all tissues, providing structural support, mechanical strength, cell-adhesion sites, and serving as a chemical reservoir for signaling molecules that influence cell phenotype and function[23,24]. Cells interact with the ECM through complex mechanisms that can modulate functions such as attachment, migration, proliferation, differentiation, and apoptosis[25–27]. Direct binding of cells to structural ECM components can initiate a cascade of intracellular signaling and transmit mechanical forces via cytoskeleton organization[25–27]. Cells can directly bind to various ECM components via cell-surface receptors such as integrins[28]. Integrins are heterodimeric transmembrane receptors that have α and β subunits with large modular extracellular domains, single transmembrane helices and short cytoplasmic regions that can couple to the cytoskeleton and transduce intracellular signaling[28,29]. In vertebrates, there are 18 α and 8 β subunits that can form 24 different integrins with varying affinities to ECM proteins[28]. The integrins function as a link between the cytoskeleton and the ECM, providing bidirectional signals. The extracellular domains can recognize various specific sequences in the ECM, and the cytoplasmic region can initiate cytoskeleton coupling and transduce intracellular signaling that can influence cell behaviour[30]. The ECM is in 'dynamic equilibrium', constantly remodeled by cell-secreted proteases (e.g. matrix metalloproteinases (MMPs) and a disintegrin and metalloproteinase with thrombospondin (ADAMTS) family members) to accommodate tissue growth or to repair damage[25–27]. The cell-secreted proteases can liberate sequestered growth factors and cytokines in the ECM that can interact with cell-

surface receptors to elicit signal transduction and regulate gene transcription[31]. While the amino acid sequence and quaternary structure of many components of the ECM are conserved across species, each tissue-specific ECM is unique in protein composition depending on factors including tissue type, location and age of host[32]. Broadly, the ECM is composed of 1) fibrous proteins (e.g. collagen, elastin), 2) glycosaminoglycans (GAGs) (e.g. chondroitin sulphate, keratin sulphate), 3) proteoglycans (e.g. aggrecan, biglycan, decorin, fibromodulin), and 4) cell-adhesive glycoproteins (e.g. fibronectin, matricellular proteins, laminin)[28,33]. The proportion and organization of these components, as well as the presence of specialized macromolecules varies between tissue type[31].

1.2.1 Collagens

Collagens are proteins that form a right-handed triple helix of polypeptide chains, and play an important role by providing structural integrity and tensile strength to the ECM, while also interacting with cell-surface receptors to modulate processes including cell adhesion, migration, proliferation and differentiation[34,35]. At least 28 different types of collagens have been identified and classified into fibrillar (e.g. type I, II, III, V, XI), network forming (type IV, VIII, X), fibril-associated collagens with interruptions in their triple helices (FACIT) (e.g. type IX, XII, XIV, XVI), short chain collagens (e.g. type VIII, X), anchoring fibrils (e.g. type VII) and other membrane-type collagens (e.g. type VI)[34–36]. While the collagen types vary in size, function and distribution, they are all comprised of three α-chains that can be either identical to form homodimers (e.g. collagen type II, III, VII, VIII, X) or different to form heterotrimers (e.g. collagen type I, V, VI, IX, XI)[34,37]. The triple helix sequences of each α-chain contain glycine-X-Y amino acid repeats, with the X and Y positions often occupied by proline and 4-hydroxyproline, respectively[35].

The structure of each collagen type provides a specific function in the ECM. Fibrillar collagens, such as collagen types I and II, are arranged in highly organized aggregates known as fibrils, crosslinked at the telopeptide regions by the enzyme lysyl oxidase, providing tensile strength and resistance to compressive loads in tissues[38,39]. FACIT collagens do not form fibrils, but are associated with the surface of collagen fibrils[34]. The structure consists of short triple helical domains inter-dispersed with other non-triple helical and non-collagenous domains[40]. FACIT collagens, such as type IX, can contribute to the stabilization of the fibrillar collagen network and anchorage of other ECM

components, such as proteoglycans[41]. Collagens that do not fall in any category, can bind to different components of the ECM, aiding in cell-ECM interactions, and have important roles in cell signaling. For example, collagen type VI has been shown to regulate autophagy, cell differentiation and have cytoprotective effects, including counteracting apoptosis and oxidative damage in connective tissues[42].

1.2.2 Elastin

Elastin is a hydrophobic protein that can stretch and recoil, providing long-range elasticity to various connective tissues including cartilage, ligaments, blood vessels, and skin[28]. The monomeric soluble precursor tropoelastin, the main component of the elastin, is synthesized intracellularly and transported into the extracellular space via exocytosis, where it is crosslinked through the enzyme lysyl oxidase[43,44]. Members of the fibulin protein family integrate the newly-forming elastin to existing microfibrils in the ECM[45]. In addition to the structural support, elastin also plays a role in cell adhesion, migration and signaling[45].

1.2.3 Glycosaminoglycans

GAGs are highly anionic linear unbranched polysaccharides with disaccharide repeating units composed of uronic acid (D-glucoronic acid or L-iduronic acid) joined by a glycosidic bond to an amino sugar (D-galactosamine or D-glucosamine)[46]. The sugars typically contain carboxylic acid or sulphate groups, which are deprotonated at physiological pH, giving the GAGs a high negative charge density[46,47]. This results in the attraction and retention of water through osmosis, which provides the tissue with low compressibility and shock absorbing properties[46]. Further, the GAGs can bind and sequester soluble growth factors and cytokines that can be liberated through selective degradation of the matrix, regulating their spatial and temporal availability and activity[48]. In addition to these contributions, the GAGs can be bound to cell surface receptors (e.g. hyaluronan binding CD44 receptor) and matrix components (e.g. laminin, fibronectin, collagen type I) aiding in cell-ECM interactions that modulate a range of cell functions including adhesion, growth, differentiation[46,49].

There are two main types of GAGs: sulphated GAGs (chondroitin suphate, keratin sulphate, heparan sulphate) and non-sulphated GAGs (hyaluronan). The geometry of the

glycosidic linkage between the two units of the disaccharides, as well as the type of hexosamine or hexuronic acid unit provides further distinction between the various types of GAGs[46,47]. The GAGs play a major role in cell signaling and development, and deficient GAG synthesis is associated with numerous defects in embryogenesis and postnatal diseases[50,51].

1.2.4 Proteoglycans

Proteoglycans are a class of glycosylated proteins with one or more sulphated GAG chain covalently linked to a specific protein core[31]. ECM proteoglycans can be divided into two main groups: 1) hyaluronan- and lectin-binding proteoglycans (hyalectans) and 2) small leucine-rich proteoglycans (SLRPs)[52]. The hyalectans are a family of proteoglycans (e.g. aggrecan, versican, neurocan, brevican) that contain a large protein core and have a hyaluronan-binding N-terminal domain, a central domain harboring the GAG side chains, and a lectin-binding C-terminal region[52,53]. Aggrecan is the most commonly studied hyalectan, as it is the principal load-bearing proteoglycan in cartilaginous and NP tissues[52]. As the name indicates, aggrecan can aggregate into large supramolecular complexes (> 200 MDa) with hyaluronan and link protein to generate a densely packed hydrated gel that can be supported by a network of reinforcing collagen fibrils, glycoproteins, and other proteoglycans[52,54]. In aggrecan, following the N-terminal hyaluronan-binding domain, the central GAG-binding domain contains numerous keratin sulphate chains, followed by >100 chondroitin sulphate chains that generate electrostatic repulsion forces that contribute towards the compressive moduli of tissues[52]. The C-terminal region can bind to collagen type II, other ECM proteins or cell surface constituents, and can provide mechanosensitive feedback to cells[52]. The SLRPs are a class of proteoglycans (e.g. fibromodulin, biglycan, decorin) containing a relatively small protein core (~36–42 kDa) as compared to aggregating proteoglycans, and encompass a central region constituted by leucine-rich repeats. SLRPs have many biological functions varying from regulating collagen fibrillogenesis to binding to growth factors and cytokines such as transforming growth factor beta (TGF-β) and bone morphogenetic protein (BMP), influencing cell proliferation, differentiation, apoptosis and other cellular functions[31,52].

1.2.5 Glycoproteins

Glycoproteins are proteins with covalently bound carbohydrates that can function as adhesive intermediates that link components of the ECM and can promote cell attachment to the matrix[31,55]. Integrins can recognize and bind to specific sequences on glycoproteins to enable cell adhesion and regulate downstream processes such as transcription factor activity and protein expression[56]. Two examples of commonly studied glycoproteins are fibronectin and laminin, which have commonly been used in cell culture and biomaterial synthesis to enhance cell attachment and survival[57,58]. Fibronectin exists in a dimer conformation with multiple binding sites (heparin, fibrin, collagen, and cell surface binding domains) along each of the two polypeptide chains, connected at the C-terminus domain with two disulphide bonds[59]. The cell attachment domain contains a tri-peptide arginine-glycine-aspartic acid motif (RGD), that binds to αvβ3 and α5β1 integrins on cells[60]. The multiple binding sites along fibronectin allow for different cells types, cytokines and ECM components to interact simultaneously[59]. Laminin is comprised of three polypeptide chains (i.e. α-chain, β-chain, and γ-chain) that form a cross-like structural network, interwoven with collagen type IV[28]. Similar to the RGD sequence on fibronectin, the laminin α1 chain contains an isoleucine-lysine-valine-alanine-valine motif (IKVAV) that can bind to integrins (e.g. α1β1, α2β1, α3β1) and modulate cell attachment, proliferation and maintenance of cells in the differentiated state[61,62].

1.3 The nucleus pulposus

1.3.1 The extracellular matrix in the nucleus pulposus

The ECM of the NP is composed primarily of large aggregating proteoglycans held together by a loose, irregular meshwork of collagen type II and elastin fibers (**Fig. 1.2**). Proteoglycans are the largest component of the NP, with aggrecan as the major proteoglycan[63,64]. The negatively charged GAGs within the proteoglycans attract water, exerting a high osmotic swelling pressure that, in combination with the collagen network, provides stiffness in the NP, enabling it to resist compressive loads[65]. Additionally, the GAGs sequester growth factors in the IVD (e.g. IGF-1, TGF-β, BMP 2/4/6) that can regulate matrix production and direct cell proliferation, differentiation, migration, and apoptosis[66]. The NP ECM also contains low amounts of other ECM macromolecules

including: fibronectin, collagens (fibrillar type I, III, V, XI; FACIT type VI; and category-less collagen type IX), and SLRPs (biglycan, decorin and fibromodulin)[67,68]. The specific combination, concentrations and organization of the various macromolecules gives the tissue its unique biochemical and biomechanical properties that allows the tissue to function as a viscoelastic material capable of absorbing compressive loads by variations of osmotic pressures[69].

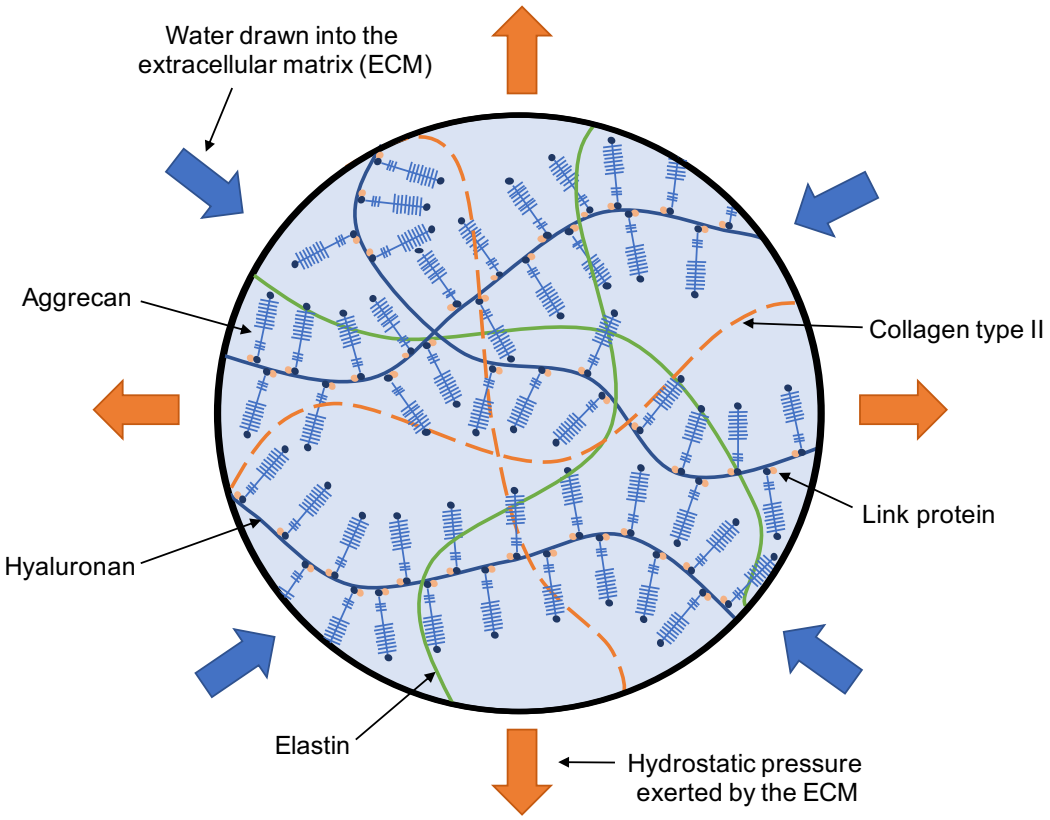

Figure 1.2: Schematic illustration of the extracellular matrix (ECM) structure and function within the nucleus pulposus (NP). The unique load-bearing properties of the NP are provided by a high osmotic swelling pressure created by aggrecan, the major proteoglycan of the NP, which draws water into the ECM. Aggrecan is immobilized in the NP by forming biocomplexes with hyaluronan and link protein. The irregular meshwork of collagen type II and elastin fibers reinforce tensile strength within the ECM, exerting a high hydrostatic pressure that allows the NP to absorb compressive loads in the spine. Figure adapted from Hardingham[70].

1.3.2 Cell populations in the nucleus pulposus

The NP is composed of a heterogeneous population of cells that change drastically by the first decade of human life[9]. At birth, the NP is composed primarily of large (~25–85 μm) physaliphorous notochord cells, derived from the embryonic notochord[9,71]. In most vertebrates, the population of notochord cells within the NP begins to decline shortly after birth and are undetectable by early adolescence, replaced by small (~10 μm) spherical cartilage-like cells, termed NP cells[71–73].

Lineage-tracing experiments in mice by our group[74] and others[75] have shown that notochord cells give rise to the terminally differentiated NP cells. In the developing embryo, the notochord is a transient rod-like structure that forms the primitive anterior/posterior axis. It plays an important role as a signaling center, secreting growth factors and morphogens that pattern the surrounding tissues[9]. Postnatally, the notochord cells within the IVD maintain their role in cell signalling by secreting factors that inhibit NP cell death and apoptosis[76], and protect NP cells from degenerative changes by upregulating anabolic gene expression while downregulating catabolic gene expression[9,76,77]. The co-localization of notochord and NP cells appears to be fundamental in maintaining disc homeostasis[72,78].

In healthy tissue, notochord cell-secreted factors such as connective tissue growth factor (CTGF), transforming growth factor beta (TGF-β) and sonic hedgehog (Shh), can limit enzymatic degradation of the ECM by inhibition of MMP production and stimulation of tissue inhibitors of metalloproteinases (TIMPs) production[69]. MMPs are a family of nine or more highly homologous endopeptidases that can collectively cleave most of the ECM constituents[79]. An imbalance in their production and activation, relative to their inhibition by TIMPS can cause degenerative changes in the NP[79]. Apoptosis and tissue neovascularization is prevented through inhibition of the expression of vascular endothelium growth factor (VEGF), interleukins 6 and 8 (IL-6 and IL-8) in the NP cells by notochord-secreted factors[69]. The stimulation of NP ECM synthesis by notochord-derived CTGF and Shh also results in the secretion of TGF-β1 from NP cells that in turn stimulate CTGF synthesis by notochord cells[76,80,81]. This molecular exchange between notochord and NP cells promotes the expression of anti-catabolic and pro-anabolic factors that contribute to NP tissue homeostasis[69].

The loss of notochord cells is associated with the onset of disc degenerative changes to the IVD[9]. The differentiation of notochord cells towards mature NP cells is not well understood, and further work is required to identify the temporal and spatial regulation of gene expression during differentiation. Many genes (e.g. Brachyury (T), cytokeratins-8/-18 (KRT-8, KRT-18), CD24) expressed in the notochord are also expressed in mature NP cells, in keeping with the finding that all cells of the NP have a shared ontogeny[82,83]. Some work has focused on identifying genes differentially expressed in notochord and NP cells. For example, a recent study showed that notochordal cells abundantly express the transcription factor T, and the cell-surface antigen CD24, which show decreased expression in mature NP cells[84]

While the phenotypic profile of NP cells during development, growth, maturation, and degeneration has yet to be defined, recent attempts have been made to identify the phenotype of the "healthy" NP cell by detailing a panel of potential gene, protein and metabolic markers. Based on the criteria of 1) expression specific to healthy NP cells, 2) requirement for healthy NP function and physiological relevance, and 3) mRNA and protein expression validated across species, the ORS Spine Research Interest Group proposed a list of the following primary markers: stabilized expression of stabilized hypoxia-inducible factor-1α and -2α (HIF-1α and HIF-2α), the glucose transporter GLUT1, the signaling factor sonic hedgehog (Shh), T, the carbonic anhydrases CA3 and CA12, the CD24 antigen, and the keratins KRT-8, KRT-18, and KRT-19[83,85].

1.4 Changes in the nucleus pulposus associated with intervertebral disc degeneration

Degenerative changes in the NP are thought to be induced by multiple factors including aging, genetics, biomechanics, and environmental factors (e.g. nutrient supply, pH)[9,69]. The healthy NP is a gel-like, highly hydrated tissue rich in proteoglycans that allow it to generate an intradiscal pressure that separates the two vertebrae and evenly distributes the pressure to the AF and over the two adjacent CEPs[86]. A degenerated NP contains an ECM that is disorganized and fibrous, unable to bind water under compression and appropriately distribute loads in the spine[86]. Overall, degenerative changes in the NP are marked by a decrease in the number of NP cells, increased catabolic and deceased anabolic factors that lead to an altered ECM environment and change the NP tissue biomechanics. With changes

in mechanical and/or biochemical cues from the microenvironment, the cells of the NP decrease proteoglycans and collagen type II production[87,88], and increase the production of collagen type I, which results in an increasingly fibrotic NP matrix[87,89,90]. The decrease in healthy ECM production (i.e. rich in proteoglycans) will lead to reduced hydrostatic pressure that alters biomechanics in the NP. The shift in tissue biomechanics can further impact cellular physiology, resulting in increased NP cell senescence and altered gene expression that further decreases anabolic and increases catabolic activity in the NP[89,91]. These interactions serve as a positive feedback loop that leads to progressive degeneration of the tissue[89,91].

The phenotypic change in NP cells associated with degeneration includes increased production of matrix degrading enzymes and pro-inflammatory cytokines, and decreased production of anabolic factors and synthesis of healthy ECM[69]. While the molecular mechanisms regulating disc degeneration is currently under investigation, a common finding is that NP cells increase synthesis of ADAMTS-1, -4, -5, -9 and -15, as well as MMP-1 and -3, which degrade aggrecan and type II collagen[69]. The aggrecan biocomplex can be cleaved from the hyaluronan backbone at the N-terminal binding domain and several locations along the GAG-binding domain[92,93]. The cleaved aggrecan fragments cannot aggregate, reducing their efficacy in binding to water[94]. Fragments of collagen type II have been shown to inhibit collagen synthesis, cell attachment to collagen, as well as induce matrix degradation in cartilage, and it may play a similar role in promoting degenerative changes in the NP[79]. An increase in pro-inflammatory cytokines including IL-6, IL-8, and prostaglandin E2 (PGE2) stimulates nerve growth factor (NGF) production, combined with an upregulation of VEGF can promote abnormal nerve ingrowth and vascularization into the previously avascular and anural tissue[95]. Further, with the induction of vascularization and increased synthesis of cytokines that stimulate the recruitment of immune cells (e.g. IL-8, CCL2, 3, 4, 5, 7), there is an increase of IL-1β and tumor necrosis factor α (TNFα) production[95]. These two major pro-inflammatory cytokines further promote the production of matrix degrading MMPs and ADAMTS, while suppressing the expression of TIMPs, dysregulating the balance between catabolism and anabolism in the NP[95].

Local differences in tissue tension and pressure can produce mechanical stimuli that directly influence cell phenotype and matrix production by influencing catabolic, anabolic

and inflammatory cell responses in the IVD[86]. For example, a hydrostatic pressure of 0.3 MPa was found to have ~20% higher proteoglycan production, lower MMP-3 production and higher TIMP production as compared to 0.1 MPa in human and IVD explants[96,97]. Similar to other load-bearing tissues including cartilage and bone, an increase in shear stress can upregulate the production of collagen type I[86]. Further, increased shear stress can also increase production of nitric oxide, a reactive oxygen metabolite that can reduces proteoglycan production, and increases apoptosis in cells of the IVD[86]. As such, reduction in intradiscal pressure, which translates to a shift of hydrostatic pressure to shear stress, can result in further degeneration of the NP[86]. This complex disease involves multiple factors that may initiate at any stage and accelerate due to the interdependency of altered cellular physiology, the ECM and NP tissue biomechanics.

1.5 Regenerative therapies targeting the nucleus pulposus

Regenerative approaches aim to restore IVD tissue biochemical composition and biomechanical function. A scaffold that mimics the native NP ECM is an attractive approach to deliver and support the survival of pro-regenerative cells for IVD regeneration. In theory, while the delivered cells regenerate the NP ECM, a mechanically robust scaffold could restore IVD tissue biomechanical function.

Naturally-derived and synthetic materials that have non-toxic and sterile components, match the structural and mechanical properties of the native NP, and biodegrade are the target objectives when designing potential scaffolds for IVD regeneration. Naturally-derived materials, such as collagen, hyaluronan, alginate, chitosan, and decellularized matrices, can mimic the native ECM biochemistry and structural properties, providing inherent cell-instructive cues to promote regeneration[98]. Since collagen type II and hyaluronan are major components of the NP ECM[67], they have been commonly studied as scaffolds for NP regeneration[98]. For example, composite collagen type II-hyaluronan hydrogels have been shown to support the survival and proliferation of rat MSCs[99] or bovine NP cells[100] cultured within the scaffold, and promote GAG production[99,100]. Other natural materials, such as alginate and chitosan have also shown potential as cell-supportive scaffolds. For example, alginate and chitosan-gelatin hydrogels promoted the survival and proliferation of human NP cells cultured *in vitro* for up to 21 days, with alginate gels better supporting viability as compared to chitosan-gelatin hydrogels at later timepoints[101]. While

inherently cell-supportive, many natural materials are mechanically weak and show low stability unless chemically crosslinked, raising concerns that they will be unable to withstand loads in the spine[102]. Further, with some naturally-derived materials there can be considerable batch-to-bath variability in bioactivity, which may result in inconsistent outcomes when applied *in vivo*[103]. Synthetic materials, such as poly(ethylene glycol) and poly(lactic-co-glycolic acid), can address some of these limitations, as they can be designed to be more mechanically robust and have more tunable mechanical properties[104]. Further, their composition and material properties can be more precisely and reproducibly controlled[105]. However, these materials lack the innate biological cues to support long-term survival and direct cell function[104]. The incorporation of bioactive ligands or growth factors within synthetic scaffolds may help to circumvent these issues[98]. For example, conjugating laminin to poly(ethylene glycol) noticeably increased cell attachment *in vitro*, and promoted the *in vivo* survival and retention of porcine NP cells[58]. While modifications may improve cell-attachment and retention, many traditional synthetic materials may still degrade very slowly *in vivo* through non-enzymatic hydrolysis[105,106]. This can lead to fibrous capsule formation and other foreign-body immune responses upon implantation[105,107]. When designing biomaterials, it is important to consider that their degradation products must also be non-cytotoxic and be readily metabolized or eliminated from the body[106]. Combining naturally-derived, synthetic and/or semi-synthetic materials to develop new scaffold platforms that better mimic the native NP environment and have tunable properties could aid in the development of new biomaterials-based therapeutic approaches for NP regeneration. Further, these systems could have utility as tissue-specific 3-D culture models for studying NP cell function.

1.6 Decellularized tissue bioscaffolds

Decellularized tissue bioscaffolds are one of the most promising scaffolds for regenerative medicine applications as they most closely mimic the native tissue environment. The decellularization process aims to remove cellular and nuclear content while preserving the ECM composition and ultrastructure. The matricellular proteins, growth factors, cytokines, and other secreted signals embedded in the ECM are known to play an important role in directing cell phenotype[28,108]. The ECM composition, ultrastructure and mechanical properties of decellularized scaffolds vary greatly depending on the processing and

preparation methods employed[24]. Commercially available allogenic and xenogeneic decellularized tissue bioscaffolds developed from skin, pericardium, and small intestinal submucosa have shown variable efficacy in the clinic, which can be attributed in part to processing methods[109]. This variability emphasizes the need for detailed evaluation of decellularized tissue bioscaffolds to quantify nuclear content and levels of key structural and bioactive ECM components.

Since decellularization techniques are unable to remove 100% of DNA content, it is important to identify the level of residual double stranded DNA (dsDNA) in the processed tissues[110]. While there are no established criteria, the minimal guidelines for decellularized tissues were suggested by the Badylak group to be: 1) <50 ng dsDNA/mg of tissue dry weight, and 2) lack of visible nuclei in tissues stained with 4',6-diamidino-2-phenylindole (DAPI)[111,112]. While these suggestions were shown to reduce a proinflammatory host response to decellularized porcine small intestinal submucosal[112], the level of residual cell and nuclear content that may elicit a negative immunogenic response in other tissue types remains unknown[113]. Protocols must be optimized for each specific tissue-type since they have unique cellularity, composition and structure. There is a general need to develop more rigorous standards and release criteria for the acceptable amount of residual cellular material in the scaffolds to ensure safe use in clinic[32,114].

Previously reported strategies to decellularize tissues include a combination of physical, chemical, and/or biological treatments. The specific decellularization reagents, processing times, and processing sequence can vary depending on the tissue-specific cellularity, porosity and ECM composition. In general, decellularization treatments typically lyse cell membranes, and the cellular and nuclear components must be separated from the ECM, solubilized or digested, and removed from the tissue[115]. Physical decellularization strategies include freeze/thaw cycles, incubation or agitation in hypotonic or hypertonic solutions, mechanical abrasion, tissue compression, and exposure to supercritical fluids[113]. These methods seek to disrupt the cell membrane, thereby making the cellular and nuclear content more accessible for extraction[113]. Chemical treatments including detergents, acids, bases, organic solvents, and alcohols, aid in solubilizing the cellular and nuclear components in order to separate them from the ECM[113]. Biological treatments are included to selectively cleave cell adhesion proteins to dissociate cells from tissues (i.e. protease;

trypsin, dispase), hydrolyze cell phospholipids (i.e. esterases; phospholipase A2), and digest the nuclear remnants (i.e. nucleases; DNase/RNase)[113]. Wash steps between, and following treatments aim to clear the processed tissues of treatment solutions and solubilized components.

All NP decellularization protocols to date use a combination of detergents to aid in the removal of cells by destabilizing the cell membrane and enabling cell lysis[116–121]. Based on their hydrophilic head groups, detergents are separated into nonionic, zwitterionic, and ionic. Non-ionic detergents, such as Triton X-100, may better preserve tissue structure and composition as compared to zwitterionic and ionic detergents, which can interact more strongly with charged components in the ECM[113]. However, these detergents may be less effective in extracting cells as compared to zwitterionic and ionic detergents[113]. Zwitterionic detergents, such as sulfobetaine-10 and -16 (SB-10 and SB-16), have a hydrophilic head group with a net zero electric charge, and are thought to protect the native state of proteins[113]. While ionic detergents, such as sodium dodecyl sulphate (SDS), sodium deoxycholate and Triton X-200, have been shown to effectively extract cells from a number of different tissues, they are also known to denature proteins, remove growth factors from the ECM, and remain in the ECM even after many washes[113]. The detergent residues from these strong ionic detergents can have cytotoxic effects, posing a barrier to the goal of eventual clinical translation[113].

The first effort to decellularize the NP by Mercuri *et al* explored the use of Triton X-100 and deoxycholic acid at varying concentrations for 72 h (room temperature; 150 rpm), followed by nucleic acid digestion using 720 mU/mL DNase and 720 mU/mL RNase for 48 h (37°C; 150 rpm) on porcine NP sectioned into halves[116]. While an increase in concentrations of detergents resulted in a decrease of visible nuclei within the processed tissues, incubation alone in these solutions were found be insufficient in effectively reducing nuclear content (~50% reduction)[116]. The addition of ultrasonication, which is thought to disrupt cell membranes by the formation and subsequent collapse of microscopic cavitation, resulted in processed tissues devoid of visible nuclei and DNA fragments as assessed by histology and agarose gel electrophoresis, respectively[116]. While the final protocol by Mercuri *et al* effectively reduced cell nuclei, it resulted in noticeable disruptions in the ECM structure, with a significant loss in sGAG content (~50% reduction)

and a qualitative decrease in aggrecan, collagen types II, IX and XI within the decellularized NP (DNP)[116].

Subsequent efforts by other groups have explored the effects of varying the concentration and incubation times of other detergent-based treatments to decellularize the NP. Consistently, it has been shown that the NP ECM structure is further disrupted with increased processing time[118,119,122]. For example, Lin *et al* explored the effects of freeze-thaw cycles as a method to lyse cell membrane, followed by detergent extraction and enzymatic digestion of DNA content on whole rabbit IVDs[118]. The protocol, which consisted of an incubation in 2% Triton X-100 for 24 h (4°C; 100 rpm), followed by extraction in 1% SDS for 24 h (4°C; 100 rpm), and finally enzymatic digestion with 200 U/mL DNase for 12 h (37°C; 100 rpm), resulted in no detectable nuclei and >97% reduction of DNA content in the processed tissues[118]. Additionally, there was a qualitative preservation of aggrecan, collagen types I and II based on immunohistochemical analyses[118]. However, these proteins were not quantified in the processed tissues. In establishing this protocol, Lin *et al* found that DNase was important in reducing nuclear content, as higher concentrations of Triton X-100 and SDS (3% and 2%, respectively) without the use of DNase were not as effective in reducing DNA within the processed tissues[118]. Performing the incubations at 4°C was postulated to reduce ECM degradation caused by proteases released from lysed cells, which can also be addressed with the supplementation of phenylmethylsulfonyl fluoride (PMSF), a serine protease inhibitor[113].

In an attempt to reduce the processing time for decellularizing the NP, Illien-Jünger *et al* increased the surface area of the processed NP by grinding the tissue prior to treatment with detergents[120]. The protocol involved 5 freeze-thaw cycles, lyophilization and tissue grinding of the bovine NP prior to processing with 2% sodium deoxycholate for 1 h (37°C, with agitation), and subsequently DNase for 1 h (37°C, with agitation)[120]. While this protocol involving relatively short durations of detergent/DNase incubations was effective in significantly reducing DNA content within the processed tissues, it also significantly decreased sGAG content (~83% reduction)[120]. The findings from this work indicate that the surface area of NP could be adjusted prior to processing in order to find a suitable surface area that minimizes decellularization treatments required while improving GAG retention. All decellularization methods will alter the ECM to some degree. Further work

is required to develop a minimal procedure that effectively removes cellular/nuclear content while preserving as much of the microarchitecture and complex tissue-specific composition of the ECM as possible.

1.7 Hydrogels

Hydrogels are three-dimensional hydrophilic networks of synthetic or natural polymers that are able to absorb and retain large amounts of water[123]. Hydrogels maintain their structure by chemical bonds (covalent bonds), physical interactions (chain entanglement, ionic and hydrophobic interactions, hydrogen bonding) or by a combination of both[124]. Hydrated hydrogels can be promising cell delivery platforms as they closely resemble soft tissues, and facilitate nutrient, oxygen and waste transfer by diffusion[125]. Furthermore, their physicochemical properties (pore size and electric charge), mechanical properties (stiffness and tensile strength), and bioactivity (cell adhesion, migration and scaffold biodegradation) can be tailored by chemical modifications[126].

Hydrogels can undergo *in situ* gelation (i.e. crosslinking following delivery to the desired site) via photo-initiated, thermal-initiated or physical-initiated crosslinking. Chemical crosslinking (i.e. photo- and thermal-initiated) typically results in polymer networks that have superior mechanical strength as compared to physical-initiated crosslinking[127]. However, commonly used crosslinkers (e.g. glutaraldehyde, ethylene glycol diglycidyl ether) and/or residual unreacted radicals can have cytotoxic effects on encapsulated cells[127,128]. Physical crosslinking overcomes these limitations; however, the resulting polymer network possesses limited mechanical properties and is not as stable as those formed by chemical crosslinking[127].

Cell-seeded hydrogels have been investigated for NP regeneration and have shown promise as a potential therapy. For example, human MSCs cultured at 5% O_2 within a thermoresponsive Laponite® crosslinked pNIPAM-co-DMAc (L-pNIPAM-co-DMAc) polymer, had an increased expression of NP-associated markers (HIF1α, FOXF1, PAX1) following 6 weeks of culture as compared to cells grown in monolayer culture[129]. When injected into bovine IVD tissue explants, the MSCs within the L-pNIPAM-co-DMAc hydrogels were found to secrete NP ECM components (collagen type II, aggrecan and chondroitin sulphate) following 6 weeks of *in vitro* culture at 5% O_2, mimicking the oxygen

level in the native NP environment[130]. The hydrogel system was reported to restore disc height and stiffness in an *ex vivo* collagenase digested bovine disc explant model by filling micro and macro fissures[130]. As another example of hydrogels for NP regeneration, studies using methacrylated gellan gum hydrogels have shown that MSCs[131] or human IVD cells[132] survive within the gels for up to 21 days, secrete NP ECM components (collagen type II and aggrecan), display low cytotoxicity[131] and an acute inflammatory response[132] when implanted subcutaneously in mouse[131] or rat[132] models. While further detailed *in vivo* investigation is required to radiographically assess restoration of disc height, as well as detailed gene and protein expression analyses to evaluate differentiation towards an NP-like phenotype, studies may suggest that hydrogel systems hold promise as a potential therapy for IVD degeneration.

1.7.1 Chondroitin sulphate-based hydrogels

Chondroitin sulphate (CS) is the most abundant GAG in the NP ECM[133]. CS consists of repeating 4- or 5- sulphated D-glucuronic acid and N-acetyl galatosamine disaccharide units[134]. Interestingly, CS exhibits anti-inflammatory properties in animals and osteo-arthritic patients[135], and has water and nutrient absorption capabilities[136]. By conjugating polymerizable moieties, such as methacrylate groups, onto the pendant hydroxyl groups, this compound has previously been used to derive biocompatible hydrogels for tissue-engineering applications[137]. The polymerizable moieties can be crosslinked to form a gel using ultraviolet (UV) light, changes in temperature, or pH with an appropriate initiator[137]. Previously, groups have functionalized CS with polymerizable methacrylate groups to obtain methacrylated CS (MCS), and have successfully encapsulated chondrocytes within UV-crosslinked MCS[138]. They have shown in a large animal (goat) model that MCS hydrogels photopolymerized into critical-size chondral defects enhanced cartilage tissue repair over 6 months, as compared to untreated defects[137].

1.7.2 Hydrogel composites

Although natural and synthetic scaffolds have their merits in tissue engineering applications, composite hydrogel scaffolds incorporating both natural and synthetic/semi-synthetic components can overcome limitations associated with each individual class. Functionalizing or incorporating natural materials into synthetic polymers can combine the

cell-supportive and cell-instructive properties of naturally-derived materials with the enhanced mechanical tunability offered by synthetic or semi-synthetic platforms. In particular, incorporating ECM particles as a cell-instructive component within hydrogels has shown promising results. Our group has previously develop functional platforms that support cell viability and differentiation by incorporating porcine cartilage ECM and human adipose ECM particles into UV- and thermally-crosslinked MCS at a degree of methacrylation of 17-20%, which enabled crosslinking while maintaining high cell viability[139]. Further, we have explored MCS as a tunable platform by varying parameters such as ECM particle size and concentration and exploring the effects on proliferation and differentiation of adipose-derived stem/stromal cells (ASCs)[140]. In comparing the effects of varying particle concentrations (3 w/v% vs 5 w/v%), incorporating a higher density of the adipose ECM within the MCS hydrogels resulted in higher ASC viability over 14 days of culture[141]. When comparing the effects of varying particle sizes (278 ± 3 μm vs 38 ± 6 μm), we found that adipogenic differentiation was significantly enhanced in scaffolds with small ECM particles and a higher density of ASCs, postulated to be due to enhanced cell-cell interactions[142]. *In vivo* investigation complimented these findings with mature adipocytes visualized within ASC-seeded and unseeded composite MCS+ECM scaffolds at 12 weeks, indicating that the constructs promoted adipogenesis in a subcutaneous Wistar rat model[141].

1.8 Project rationale, hypothesis and aims

1.8.1 Rationale

Currently, there are no disease-modifying treatments for IVD degeneration. Biomaterials-based therapies targeting the NP have the potential to improve mechanical function, and may establish a pro-regenerative microenvironment to support delivered or endogenous cell populations. Once thought to simply provide structural support, the ECM is now recognized as a bioactive microenvironment that directs and influences cell function[28,108]. This study aimed to develop biomaterials that harness the regenerative potential of tissue-specific ECM for NP regeneration and assesses their ability to direct the function of NP cells. Since primary notochord cells are difficult to obtain and current protocols for NP cell monolayer culture do not effectively maintain cell phenotype *in vitro*, the current study used the human chordoma-derived U-CH1 cell line[143]. These cells demonstrate a stable

notochord-like phenotype *in vitro*, marked by the expression of the embryonic notochord markers brachyury, CD24, KRT19, epithelial marker antigen, vimentin, and cytokeratin[144–146], making them an attractive model to investigate human NP progenitor cell response within our constructs.

1.8.2 Hypothesis

Given the important role the ECM plays in directing cell phenotype, I hypothesize that ECM derived from DNP will have cell-instructive effects and will promote the lineage-specific differentiation of human notochord-like cells.

1.8.3 Specific aims

Aim 1: To develop a decellularization protocol for bovine NP, and characterize the retention of key ECM components including GAG and collagen in the processed tissues.

Aim 2: To fabricate and characterize the physical properties of composite scaffolds incorporating decellularized nucleus pulposus (DNP) or non-tissue-specific bovine tendon collagen (COL) within *in situ* crosslinking methacrylated chondroitin sulphate (MCS) hydrogel carriers.

Aim 3: To assess the viability, retention, and differentiation of human notochord-like cells cultured within MCS ± DNP/COL constructs.

Chapter 2

2 Methods

2.1 Materials

All chemical reagents were purchased from Sigma-Aldrich Canada Ltd. (Oakville, Ontario) unless otherwise indicated.

2.2 Development of a protocol for nucleus pulposus decellularization

Bovine tails (from animals 9-30 months of age) were obtained 2 hours post-mortem from the Mount Brydges Abattoir (Mount Brydges, Ontario). The muscle, soft tissues and ligaments surrounding the caudal spinal column were removed aseptically and the nucleus pulposus (NP) was removed by dissection from 8 IVDs. The pooled NP was then sectioned into quarters using a scalpel (Protocol 1) or biopsy punched (2 mm, Protocols 2 and 3) before being processed for decellularization with ~15 g of NP/100 mL solution in a 500 mL tub. For all protocols, the incubation steps were performed at 37°C under agitation (125 rpm). All solutions, with the exception of the enzymatic digestion steps, were supplemented with 1 v/v% antibiotic-antimycotic (ABAM) (Gibco®, Invitrogen, Burlington, Ontario) and 0.27 mM phenylmethylsulfonyl fluoride (PMSF); the enzymatic digestions were supplemented with only 1 v/v% ABAM.

Protocol 1: The original protocol investigated was based on established protocols in the Flynn lab for the decellularization of porcine auricular cartilage, which were adapted from published methods for the decellularization of human nasoseptal cartilage[147]. Minced NP was subjected to 3 freeze-thaw cycles (-80°C overnight / 37°C for 3 h) in Solution A [10 mM tris (hydroxymethyl)aminomethane (Tris), 5 mM ethylenediaminetetraacetic acid (EDTA), (pH 8.0)], with buffer replaced following each thaw. Tissues were then incubated for 24 h in Solution A followed by 48 h incubation in Solution B [1.5 M KCl with 2 v/v% Triton X-100 and 50 mM Tris buffer, (pH 8.0)]. Tissues were rinsed 3 x 30 min in phosphate buffered saline (PBS) prior to 5 h incubation in Sorensen's phosphate buffer digest solution [SPB digest; 0.55 M sodium phosphate dibasic heptahydrate ($Na_2HPO_4 \cdot 7H_2O$), 0.17 M potassium phosphate (KH_2PO_4), 0.049 M magnesium sulphate

heptahydrate ($MgSO_4 \cdot 7H_2O$), (pH 7.3)] supplemented with 15,000 U DNase Type II (from bovine pancreas) and 12.5 mg RNase Type III (from bovine pancreas). Tissues were then incubated for 3 days in Solution C [50 mM Tris buffer with 1 v/v% tributyl phosphate (TBP), (pH 8.0)]. Following 3 x 30 min rinses in deionized water (dH_2O) and 3 x 30 min rinses in PBS, tissues were incubated for 48 h in Tris buffer [50 mM tris buffer, (pH 9.0)] with solutions replaced ~ every 12 h. Tissues were rinsed 3 x 30 min in dH_2O and 3 x 30 min in PBS prior to collection.

Protocol 2: Biopsy-punched NP (2 mm x 2 mm) was subjected to 3 freeze-thaw cycles in either dH_2O (**2A**) or Solution A (**2B**), with buffer replaced following each thaw cycle. Next, tissues were rinsed 3 x 30 min in dH_2O and 3 x 30 min in PBS prior to 5 h incubation in SPB digest supplemented 15,000 U DNase Type II and 12.5 mg RNase Type III. Tissues were then incubated in 1 v/v% Triton X-100 in 50 mM tris buffer for 2 h. Tissues were rinsed 3 x 30 min in dH_2O and 3 x 30 min in PBS prior to collection.

Protocol 3: Biopsy punched NP (2 mm x 2 mm) was subjected to 1 freeze-thaw cycle in dH_2O. Tissues were then split equally into three treatment groups: 5 h incubation in SPB digest supplemented with 15,000 U DNase Type II and 12.5 mg RNase Type III (**3A**), 2 h incubation in SPB digest supplemented with 15,000 U DNase Type II and 12.5 mg RNase Type III (**3B**), and 2 h incubation in PBS supplemented with 15,000 U DNase Type II and 12.5 mg RNase Type III (**3C**). Tissues were rinsed 3 x 30 min in PBS prior to collection.

2.3 Characterization of decellularized tissues

2.3.1 Histological analyses

Native NP and decellularized nucleus pulposus (DNP) sampled at specified stages of decellularization were fixed overnight in 4% paraformaldehyde (PFA). Following standard histological processing (Robarts Molecular Pathology Laboratory, London ON), samples were embedded in paraffin and sectioned (7 μm sections) using a Leica RM2235 microtome (Leica Biosystems, Concord, ON, Canada). Serial sections were deparaffinized and stained used standard methods for safranin-O/fast green or toluidine blue to visualize glycosaminoglycan (GAG), Masson's trichrome or picrosirius red to visualize collagen, and DAPI using fluoroshield mounting medium (ab104139, Abcam) to visualize cell nuclei within the tissues. Stained tissue sections were imaged using a Leica DM1000 microscope

with Leica Application Suite software. Fluorescent images were acquired using a Zeiss Imager M2 microscope (Zeiss Canada, Toronto, ON, Canada).

2.3.2 Scanning electron microscopy

Native NP and DNP samples were frozen at -80°C overnight and lyophilized using a Labconco Freezone 4.5 lyophilizer (Labconco, Kansas City, MO, United States) for 72 h. Lyophilized samples of native NP and DNP (2 mm x 2 mm biopsy punch samples) were submerged in liquid nitrogen and cryofractured. Samples were then collected in glass vials and stored for future use under a desiccator. Prior to imaging, samples were coated with osmium and visualized using a LEO1530 scanning electron microscope (Nanofabrication facility, Western University).

2.3.3 Preparation of cryomilled ECM particles

Native NP and DNP samples were lyophilized as described above. The lyophilized tissues were transferred into Retsch 25 mL cryo-milling grinding jars with two 10 mm stainless steel milling balls. The sealed chambers were immersed in liquid nitrogen for 3 min, and then milled for 3 min at 30 Hz (Retsch Mixer Mill MM 400 milling system). This cycle was repeated three times and the resulting particles were stored within a desiccator for future use, as previously reported[148].

2.3.4 Biochemical analyses

Ten mg of each lyophilized cryomilled sample was digested in 1 mL of proteinase K digestion buffer (0.2 mg/mL in Tris-EDTA (TE) buffer) overnight at 56°C under agitation (1200 rpm) and sonicated (3 x 1 sec) using the Sonic Dismembrator model 100 (Fisher Scientific) 1 h prior to thermal enzyme deactivation (92°C for 5 min under agitation).

Dimethylmethylene blue assay: Proteinase K-digested samples were diluted (1:30) in 1% bovine serum albumin (BSA) in PBS and assayed for sulphated glycosaminoglycan (sGAG) content using the dimethylmethylene blue (DMMB) dye binding assay, as previously reported[149]. Briefly, sGAG standards were prepared from chondroitin sulfate sodium salt (Sigma C-6737, 4°C) (10 mg/mL of 1% BSA), and an 8-point standard curve was prepared by serial dilution, with a starting concentration of 250 µg/mL in 1% BSA. Ten µL of each sample and standard were combined with 200 µL of DMMB reagent

(0.016 mg/mL in 0.2% formic acid (pH 5.3)) in technical triplicates, and the absorbance was read at 525 nm using the BMG LABTECH CLARIOstar® microplate reader. GAG concentrations of samples were determined based on the standard curve, and reported as µg of sGAG/mg of tissue dry weight.

Hydroxyproline assay: Proteinase K-digested samples were hydrolyzed in 12 M hydrochloric acid for 24 h at 110°C, neutralized by the addition of 5.7 M sodium hydroxide, and centrifuged (400 x *g*, 1 min). Activated charcoal was added (25 mg/mL), samples were vortexed, centrifuged (10,000 x *g*, 5 min) and the supernatant was collected to assess collagen content using the hydroxyproline assay, as previously described[149]. Briefly, samples were diluted (1:80) in deionized water and standards were prepared from a stock solution of hydroxyproline (100 µg/mL in deionized water). An 8-point standard curve was prepared by serial dilution, with a starting concentration of 16 µg/mL in deionized water. Fifty µL of each standard and sample were pipetted into a 96-well plate in triplicates and 50 µL of chloramine-T (0.05 M) was added. Samples were mixed and allowed to incubate at room temperature for 20 min. Fifty µL of perchloric acid (3.15 M) was then added to each well, and the samples were mixed and incubated at room temperature for 5 min. Finally, 50 µL of Ehrlich's reagent (200 mg/mL of 4-dimethylaminobenzaldehyde in 2-methoxyethanol) was added, mixed and incubated at 60°C for 20 min. The plate was cooled at 4°C for 5 min, then read at an absorbance of 560 nm using the CLARIOstar® microplate reader. Hydroxyproline concentrations of samples were determined based on the standard curve, and reported as µg of hydroxyproline/mg of tissue dry weight.

PicoGreen assay: Samples used for the Quant-iT™ PicoGreen® double stranded DNA (dsDNA) assay were prepared according to the manufacturer's instructions for the DNeasy Blood & Tissue Kit (Qiagen, Hilden, Germany). The PicoGreen assay was performed according to manufacturer's instructions. Briefly, standards were prepared from λ-DNA (100 µg/mL of TE buffer) provided in the Quant-iT™ kit, and an 8-point standard curve was prepared by serial dilution with a starting concentration of 250 ng/mL in TE buffer. Fifty µL of each sample and standard were combined with 150 µL of Quant-iT™ reagent (1:200 dilution) in technical triplicates, and absorbance was read at 520 nm using the CLARIOstar® microplate reader. DNA concentrations of samples were determined based on the standard curve, and reported as ng of dsDNA/mg of tissue dry weight.

2.3.5 Particle size distribution

Cryomilled DNP and bovine tendon collagen (COL) (Sigma-Aldrich) particles were independently sieved through a 125 µm stainless steel mesh and collected on a 45 µm mesh to remove larger particles and aggregates. This size range was selected based on previous work showing that it was favourable for promoting adipogenesis in adipose-derived stem/stromal cells encapsulated within MCS + decellularized adipose tissue (DAT) hydrogel constructs[140]. The particle size distributions were analyzed using a Malvern Mastersizer 2000 (Malvern Instruments Ltd., Worcestershire, United Kingdom). For each sample, ~100 mg of lyophilized ECM particles were hydrated in PBS and analyzed according to the manufacturer's instructions.

2.4 Composite hydrogel fabrication and characterization

2.4.1 Methacrylation of chondroitin sulfate

Chondroitin sulfate (CS) was methacrylated to enable hydrogel formation, as previously described[139]. Briefly, CS was reacted with methacrylic anhydride to form O-methacrylate chondroitin sulphate (**Fig. 2.1**).

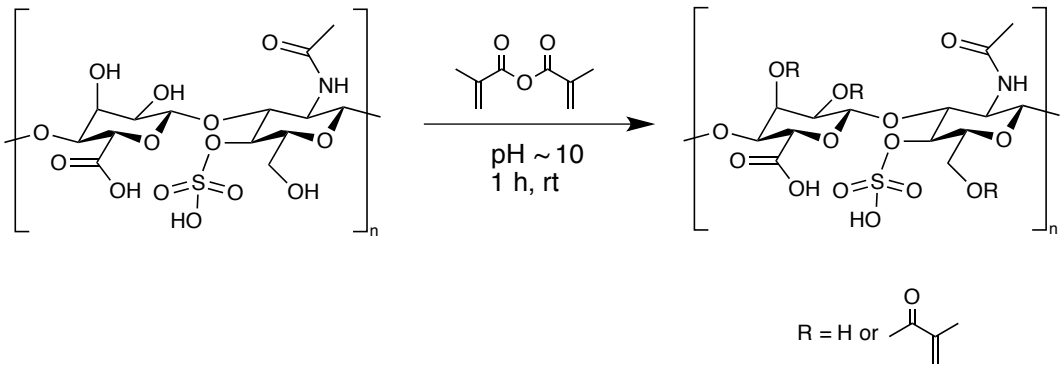

Figure 2.1: Chemical structure of chondroitin sulphate before and after methacrylation using methacrylic anhydride at pH ~ 10 for 1 hour at room temperature.

In brief, 200 mg of CS salt (LKT Laboratories Inc., MN, United States) was dissolved in 1 mL of 0.2 M sodium phosphate monobasic buffer (NaH_2PO_4), the pH was adjusted to ~10, and 60 µL of methacrylic anhydride (Sigma-Aldrich) was added dropwise with

continuous stirring (700 rpm). The reaction was allowed to proceed for 1 h at room temperature with the pH maintained at 10, using 3 M sodium hydroxide. The product was precipitated by the addition of 10 mL of absolute ethanol. Excess solvent was decanted, and the precipitate was dissolved in 10 mL of deionized water. The solution was then transferred to a 3.5 kDa MWCO dialysis membrane (Spectra/Por) and dialyzed against 4 L of deionized water for 72 h, with solvent changes every 8 h. Throughout, the sample was protected from light to avoid crosslinking. Following dialysis, the methacrylated chondroitin sulphate (MCS) was neutralized using 3 M sodium hydroxide, and snap frozen in liquid nitrogen. The samples were lyophilized for 72 h and proton-nuclear magnetic resonance (^{1}H NMR) was performed on the Inova 600 NMR spectrometer to confirm the targeted degree of methacrylation (17-20%[141]) was achieved. The samples were stored under nitrogen gas, protected from light and moisture at -20°C until future use.

2.4.2 Fabrication of composite MCS ± DNP/COL scaffolds

The composite scaffolds were fabricated based on previously-established methods[139]. Briefly, MCS was disinfected by UV exposure for 30 min in a biological safety cabinet. Cryomilled DNP and COL particles were decontaminated with an overnight incubation in 70% ethanol, and hydrated with 3 x 30 min washes in PBS. The pre-polymer solutions were then made by dissolving the MCS in PBS (20 w/v%), with the addition of Irgacure 2959 (10 w/v%), with or without cryomilled DNP or COL particles (5 w/v%). U-CH1 cells (passage 2-3 post thaw) were resuspended in chordoma media (IMDM/RPMI 4:1 with 10% FBS (Invitrogen, Life Technologies)) to obtain 10 x 10^6 cells/mL of final gel volume. The final gel volume consisted of 80% pre-polymer solution and 20% cell suspension. The solution was stirred with an 18G needle for 45 sec and immediately transferred to a 1 mL sterile syringe mold and photo-crosslinked by UV exposure (365 nm at an intensity of 12 mW/cm^2) for 2 min on each side of the syringe. The molds used to generate scaffolds were fabricated from 1 mL slip-tip syringes, cut cross-sectionally to remove the bore of the syringe, with a second plunger added to the cut end. Following crosslinking, the gel was extruded from the syringe and cut into individual 20 µL hydrogel scaffolds. The scaffolds were then transferred to cell culture inserts (Greiner Bio-one, Germany) within 12-well tissue culture plates. The gels were rinsed (2 x 15 min) with chordoma media, and the scaffolds were cultured in chordoma media for *in vitro* studies at 37°C with 5% CO_2.

2.4.3 Gel content analysis

Single-phase (i.e. no ECM) and composite MCS hydrogel scaffolds were synthesized as described above (section 2.4.2) without U-CH1 cells, and with dH_2O in place of PBS. Immediately following crosslinking, gels were snap-frozen in liquid nitrogen and lyophilized for 24 h. The initial dry mass (m_1) was recorded and the samples were rinsed in 10 mL of dH_2O for 3 x 3 h. The samples were then snap-frozen and lyophilized again for 24 h, and the final dry mass (m_2) was recorded. The following equation was used to calculate gel content:

$$\text{Gel content (\%)} = \left(\frac{m_2}{m_1}\right) \times 100 \quad (1)$$

2.4.4 Bulk compression testing

The single-phase and composite MCS hydrogel scaffolds were incubated in PBS at 37°C overnight prior to mechanical testing. The height and diameter of each scaffold was measured using calipers immediately before testing. Unconfined bulk compression testing was perform using the UniVert system (CellScale Biomaterials Testing, Waterloo, ON) with a 0.5 N load cell in an immersion bath containing PBS maintained at 37 °C. Sandpaper sheets were affixed to the UniVert platens by double-sided tape, and the samples were placed between the sheets to prevent the gel from slipping. Samples were pre-conditioned for 2 cycles of 10% strain at a rate of 0.05%/s. Cyclic compression testing was then performed for 4 cycles, at the same strain and rate parameters[150]. Nominal stress was calculated from the applied force divided by the initial cross-sectional area of each sample. Strain values of 4% and 10% were used as boundary conditions from the linear region of the nominal stress-strain curve to estimate the Young's modulus.

2.5 Cell characterization

2.5.1 Cell culture

U-CH1 cells[143] originally obtained from Dr. Michael Kelley (Duke University, North Carolina, United States) were maintained in monolayer on 0.1% gelatin-coated tissue culture plastic plates in chordoma media at 37°C with 5% CO_2. Cells were enzymatically dissociated with 0.25% trypsin (Gibco, Life Technologies) when then reached 80-90%

confluency, and plated at a ratio of 1:2-1:3 for cell expansion. For all cell-encapsulated hydrogel studies, cells were maintained for 2-3 passages prior to encapsulation. All cell studies were performed with four biological replicates (N=4).

2.5.2 Cell viability in hydrogel scaffolds

The LIVE/DEAD® Viability/Cytotoxicity Assay (Invitrogen) enables the simultaneous visualization of live and dead cells through the use of calcein AM (494 nm/517 nm) and ethidium homodimer (EthD-1) dyes (528 nm/617 nm), respectively. This assay was used to qualitatively evaluate viability and retention of U-CH1 cells within MCS±DNP/COL scaffolds following 24 h, 3 days and 7 days of *in vitro* culture. For each timepoint, the cell-seeded scaffolds were rinsed in sterile 5% FBS in PBS solution, then incubated in dye solution (4 µM EthD-1 and 2 µM Calcein AM in 5% FBS in PBS) for 30 min at 37°C[151]. Scaffolds were then washed in sterile 5% FBS in PBS solution and imaged using a Zeiss LSM800 Confocal Microscope with Airyscan. The tiling feature was used to capture and stitch together images to visualize the entire cross-sectional area of the scaffolds. For each scaffold, 4 depths were imaged starting at the surface of the gels, separated by 50 µm.

2.5.3 Gene expression analyses

For each group (MCS±DNP/COL) following 24 h or 3 days in culture, three 20 µL cell-seeded hydrogel scaffolds were pooled together in 1 mL of PureZOL. Samples were mechanically dissociated using a microtube pestle and sonicated 10 x 1 sec for three cycles. Total RNA was extracted using the Aurum Total RNA Fatty and Fibrous Tissue kit (Bio-Rad), according to manufacturer's instructions. RNA concentrations were determined using a Nanodrop 1000 spectrophotometer (Thermo Scientific), and 275 ng of RNA/sample was used for cDNA synthesis using the iScript™ cDNA Synthesis Kit (Bio-Rad). Controls with no reverse transcriptase were also prepared for each sample. Gene expression was assessed by real-time qPCR using the BioRad CFX-384 system. All reactions were run in triplicates, with each reaction containing 312.5 nM of forward and reverse primers, and 2x SsoFast Evagreen Supermix (Bio-Rad). PCR primers were previously validated for efficiency and specificity (primer sequences provided in **Table 2.1**). The following 2-step RT-PCR protocol was used: initial denaturing at 95°C for 2 min, denaturing at 95°C for 10 sec and annealing/elongation at 60ºC for 30 sec, repeated for 45

cycles, followed by a melt curve. Transcript levels were analyzed using the ΔΔCT method, normalized to the geometric mean of the housekeeping genes GUSB and GAPDH. No-reverse transcriptase controls were run for all primer pairs to detect genomic contamination.

Table 2.1: RT-qPCR Primer Sequences.

Gene	Primer Sequence (5' to 3')
Brachyury (T)	FWD – TGAGACCCAGTTCATAGCGG REV – TGCTGGTTCCAGGAAGAAGC
CD24	FWD – CTCCTACCCACGCAGATTTATTC REV – AGAGTGAGACCACGAAGAGAC
FOXA1	FWD – GGTGGCTCCAGGATGTTAGG REV – TGTTCCAGTCGCTGGTTTCA
Aggrecan (ACAN)	FWD – TGAGGAGGGCTGGAACAAGTACC REV – GGAGGTGCTAATTGCAGGGAACA
SOX9	FWD – AGCGAACGCACATCAAGAC REV – CTGTAGGCGATCTGTTGGGG
Collagen type I (COL1A1)	FWD – AAGAGGAAGGCCAAGTCGAG REV – CACACGTCTCGGTCATGGTA
Collagen type II (COL2A1)	FWD – CCAGATGACCTTCCTACGCC REV – TTCAGGGCAGTGTACGTGAAC
GUSB	FWD – ACGCAGAAAATATGTGGTTGGA REV – GCACTCTCGTCGGTGACTGTT
GAPDH	FWD – GAGTCAACGGATTTGGTCGT REV – GACAAGCTTCCCGTTCTCAG

2.6 Statistical analyses

All numerical data are presented as mean ± standard deviation (SD), unless noted otherwise. All statistical analyses were performed using GraphPad Prism 7 Software (GraphPad Software, San Diego, CA). A Kolmogorov–Smirnov test was performed to compare the size distributions of the DNP and COL particles. Data from the biochemical analyses was analyzed by one-way ANOVA with a Tukey's post-hoc comparison of the means. The gene expression data was analyzed by two-way ANOVA with a Tukey's post-hoc comparison of the means. Differences of $p < 0.05$ were considered statistically significant unless noted otherwise.

Chapter 3

3 Results

3.1 Development of a protocol to decellularize bovine nucleus pulposus

The first phase of the project focused on the systematic development of a decellularization protocol for bovine nucleus pulposus (NP), with the goal of enhancing cell extraction while preserving glycosaminoglycan (GAG) and collagen content. While many iterations of treatment testing were performed (**Appendix; Supplemental Table 1**), the following body of work details three protocols that were key in informing the development of a reliable and reproducible bovine NP decellularization protocol.

The initial decellularization protocol was based on an established 10-day method in the Flynn Lab for porcine auricular cartilage decellularization (**Fig. 3.1**), which was adapted from published methods for the decellularization of human nasoseptal cartilage[147]. Whole NP samples were cut into quarters and treated with the 10-day decellularization protocol, summarized in **Fig. 3.1A**. Tissue samples were collected for qualitative assessment by histology immediately following dissection and after rinsing following the final decellularization treatment step (3 x 30 min in deionized water (dH_2O) and 3 x 30 min in phosphate buffered saline (PBS)). Safranin-O/fast green staining for GAG revealed a notable loss of GAG in the DNP as compared to the native NP samples (**Fig. 3.1B**). Masson's trichrome staining revealed more intense collagen staining in the DNP, potentially due to collagen fibers being more accessible as a result of substantial GAG loss. DAPI staining confirmed successful removal of nuclei in the processed tissues.

In an attempt to preserve more GAG, the subsequent protocol was reduced to three main steps: mechanical disruption by freeze-thaw (F/T) cycles in hypotonic solutions to lyse cell membranes, enzymatic digestion of nuclear content, and detergent washes to solubilize and remove cellular and nuclear debris.

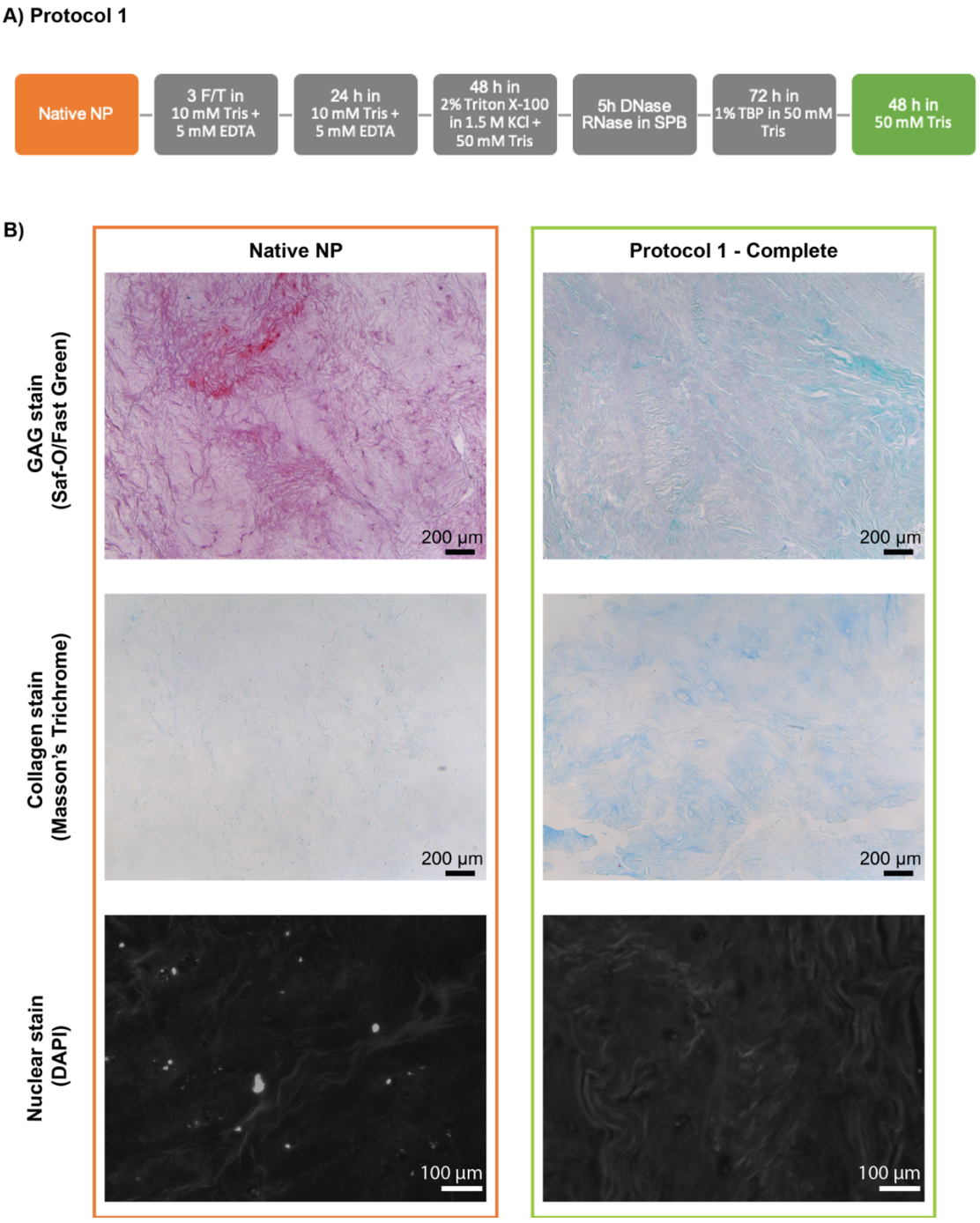

Figure 3.1: Histological analyses of bovine NP tissue processed with decellularization Protocol 1. A) Protocol overview, with sampling points shown in colour. Acronyms: F/T = freeze-thaw cycles, Tris = tris (hydroxymethyl)aminomethane, EDTA = ethylenediaminetetraacetic acid, SPB = Sorensen's phosphate buffer, TBP = tributyl phosphate. **B)** Representative safranin-O/fast green staining of GAG (red) and collagen (blue-green), Masson's trichrome staining of collagen (blue), and DAPI nuclear staining (white), (n=3, serial sections throughout the tissue sample). Scale bars for safranin-O/fast green and Masson's trichrome = 200 µm. Scale bars for DAPI stain = 100 µm.

The importance of mechanical disruption by F/T cycles was established in a supplemental protocol (**Appendix; Supplemental Fig. 1**), where incubation in hypotonic 10 mM tris (hydroxymethyl)aminomethane (Tris) + 5 mM ethylenediaminetetraacetic acid (EDTA) buffer alone did not effectively disrupt the cells, resulting in the presence of abundant nuclei throughout the processed tissues following the final treatment step.

Decellularization protocol 2, summarized in **Fig. 3.2A**, was designed to compare the effects of F/T cycles in two hypotonic solutions: dH_2O and 10 mM Tris + 5 mM EDTA buffer. The NP was cut into 2 mm x 2 mm pieces to increase the surface area treated and improve uniformity in decellularization. Tissue samples were collected for assessment by histology and biochemical assays immediately following dissection and after rinsing (3 x 30 min in dH_2O and 3 x 30 min in PBS) following the final decellularization treatment steps. Toluidine blue staining was performed in place of safranin-O/fast green staining as it was found to better visualize GAG content within the processed tissues and showed a better correlation with the quantitative results of sulphated GAG (sGAG) content measured using the DMMB assay. Toluidine blue staining in **Fig. 3.2B** revealed more intense staining in the decellularized nucleus pulposus (DNP) generated with Protocol 2A as compared to Protocol 2B, suggesting that F/T cycles in dH_2O better preserved GAG. Quantification of sGAG content by the DMMB assay (**Fig. 3.2C**) corroborated these qualitative findings, showing slightly enhanced sGAG retention in Protocol 2A as compared to Protocol 2B (~17% versus ~14% retention). Collagen distribution visualized by Masson's Trichrome staining revealed similar patterns in the native NP and DNP samples from both treatment groups (**Fig. 3.2B**). Quantitative analysis of collagen content through the hydroxyproline assay suggested an enrichment in collagen content relative to tissue dry weight in the processed tissues, consistent with the loss of GAG (**Fig. 3.2C**). Although nuclei visualized by DAPI staining appeared qualitatively reduced in both treatment groups (**Fig. 3.2B**), quantification of dsDNA revealed that F/T cycles in dH_2O more effectively reduced nuclear content as compared to F/T cycles in the 10 mM Tris + 5 mM EDTA buffer (~77% versus ~61% reduction). Interestingly, the DNA content was similar in Protocol 2A following both the DNase/RNase and Triton X-100 detergent extraction treatment steps (**Fig. 3.2C**) (~79% versus ~77% reduction).

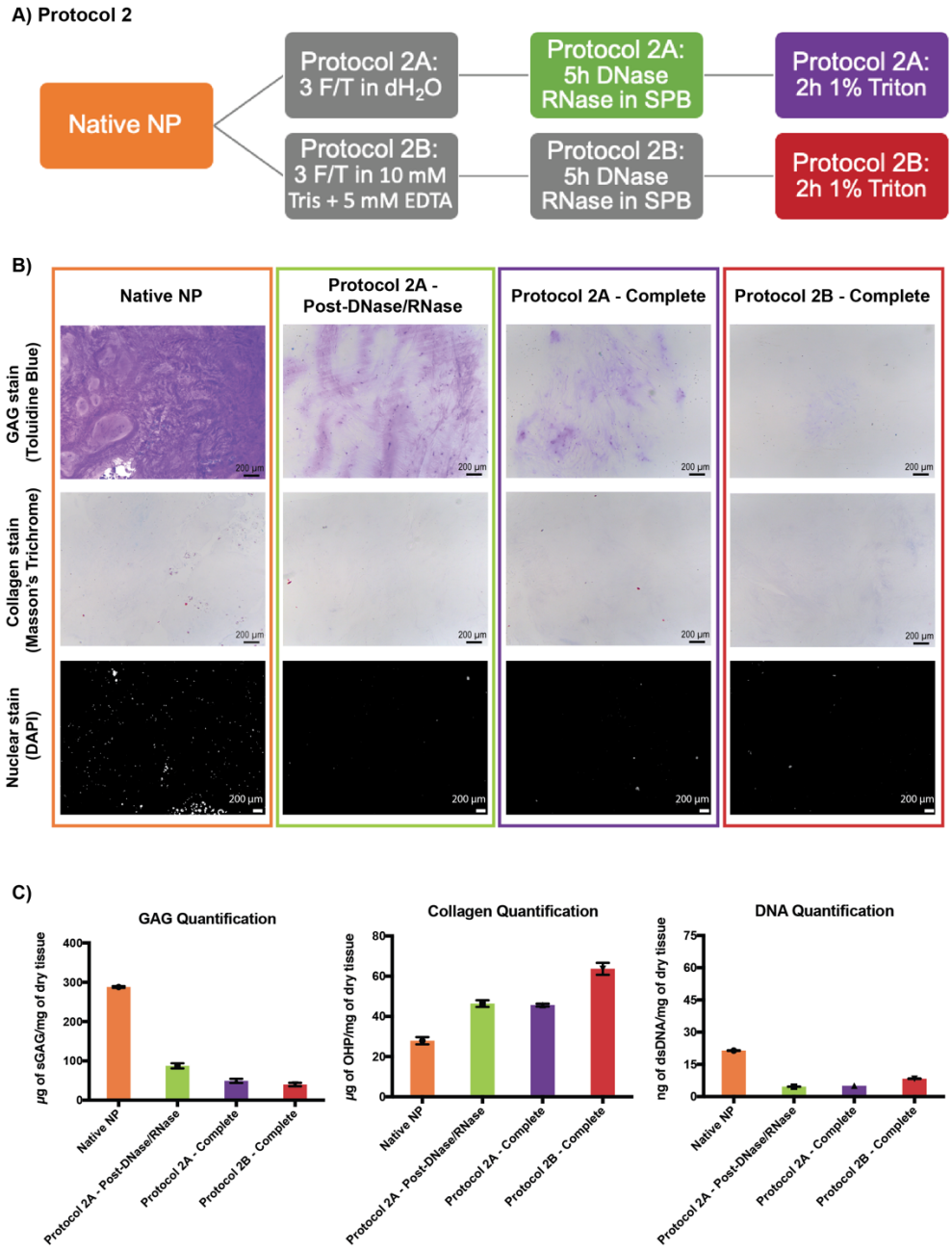

Figure 3.2: Histological and quantitative analyses of bovine NP tissue processed with decellularization Protocol 2. A) Protocol overview, with sampling points shown in colour. Acronyms: F/T = freeze-thaw cycles, Tris = tris (hydroxymethyl)aminomethane, EDTA = ethylenediaminetetraacetic acid, SPB = Sorensen's phosphate buffer. **B)** Representative Toluidine blue staining of GAG (purple), Masson's trichrome staining of collagen (blue), and DAPI nuclear staining (white) (n=3, serial sections halfway through the tissue). Scale bars = 200 µm. **C)** Quantitative biochemical analysis of the processed DNP and native tissues including sGAG content as determined by the DMMB assay, hydroxyproline content as a measure of total collagen content by the hydroxyproline assay, and dsDNA content as determined by the PicoGreen assay (n=3, N=1 for all assays). Data are presented as mean ± SD.

Given that the detergent treatment reduced the GAG content without enhancing DNA extraction, the subsequent decellularization protocol excluded the Triton X-100 detergent extraction (**Fig. 3.3**). Since follow up testing revealed that GAG was lost with each F/T cycle (**Appendix; Supplemental Fig. 2**), the testing in Protocol 3 included only one F/T cycle. Additionally, in a final effort to preserve GAG, the effects of reducing the duration of the enzymatic digestion from 5 h (Protocol 3A) to 2 h (Protocol 3B) and changing the incubation solution to PBS (Protocol 3C) were explored (**Fig. 3.3A**).

Toluidine blue staining (**Fig. 3.3B**) and sGAG quantification (**Fig. 3.3C**) both indicated that Protocol 3B and 3C were more effective in preserving GAG as compared to Protocol 3A. Collagen distribution was evaluated with Picrosirius red staining, as it was found to better visualize the collagen fibers within the processed tissues as compared to the faint staining observed with Masson's trichrome. The Picrosirius red staining suggested that the collagen structure was qualitatively similar between all treatment steps evaluated and the quantitative results showed an increasing trend in relative collagen content following treatment, as seen in our previous protocols (**Fig. 3.2C**). Although DAPI staining revealed a qualitatively greater number of residual nuclei within tissues processed with Protocols 3B and 3C as compared to Protocol 3A, the quantitative analysis showed a marked reduction in dsDNA content of Protocols 3A and 3B, as compared to native NP.

Since Protocols 3A and 3B appeared most promising, the treatments were repeated for a minimum of three biological replicates each (N=3) to validate the efficacy of both protocols. Statistical analyses were performed on the biological replicates to compare Protocols 3A and 3B. Although there was a significant reduction in sGAG content from native NP in both treatment groups, Protocol 3B was shown to retain ~36% sGAG as compared to ~28% in Protocol 3A. Collagen quantification results were similar between Protocols 3A and 3B, however there was greater variability in Protocol 3A, which may be attributed in part to the native tissue source. In particular, the data points at the high range in terms of collagen content for Protocol 3A correlated to the samples that had higher sGAG content in the native tissues and consequently showed greater relative loss of sGAG during processing. Both Protocols 3A and 3B had a notable reduction in dsDNA content, with ~88% and ~89% loss of dsDNA, respectively.

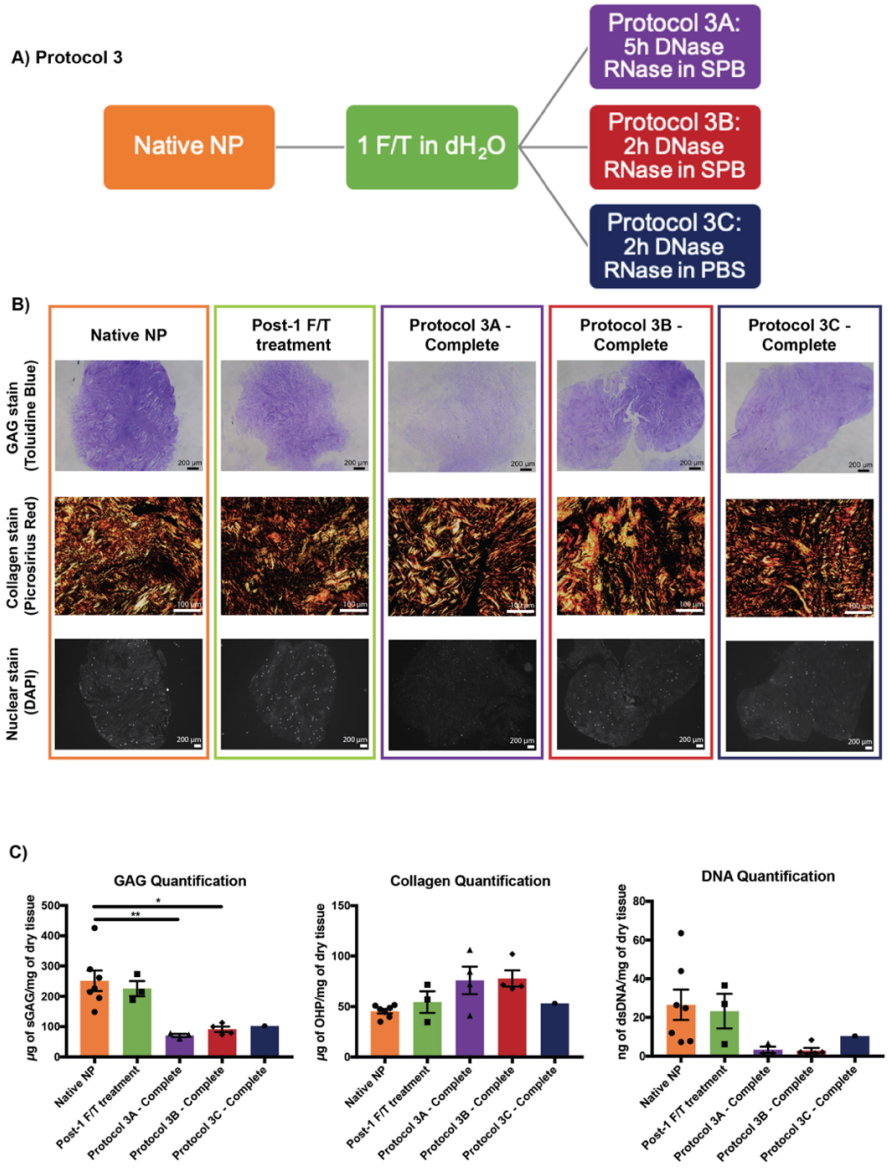

Figure 3.3: Histological and quantitative analyses of bovine NP tissue processed with decellularization Protocol 3. A) Protocol overview, with sampling points shown in colour. Acronyms: F/T = freeze-thaw cycle, SPB = Sorensen's phosphate buffer, PBS = phosphate buffered saline. **B)** Representative Toluidine blue staining of GAG (purple), Picrosirius red staining of collagen (red/orange), and DAPI nuclear staining (white) (n=3, serial sections halfway through the tissue; *Native NP*: N=7, *Post-1 F/T treatment*: N=3, *Protocol 3A - Complete*: N=3-4, *Protocol 3B - Complete*: N=5, *Protocol 3C - Complete*: N=1). Scale bars = 200 μm. **C)** Quantitative biochemical analysis of the processed DNP and native tissues including sGAG content as determined by the DMMB assay, hydroxyproline content as a measure of total collagen content by the hydroxyproline assay, and dsDNA content as determined by the PicoGreen assay (n=3 for all assays; *Native NP*: N=7, *Post-1 F/T treatment*: N=3, *Protocol 3A - Complete*: N=3-4, *Protocol 3B - Complete*: N=5, *Protocol 3C - Complete*: N=1). Data are presented as mean ± SEM. * = $p<0.05$, ** = $p<0.005$. One-way ANOVA with Tukey's post-hoc correction was performed to compare all groups, excluding *Protocol 3C - Complete* (N=1).

Based on enhanced GAG retention with similar efficacy in terms of cell extraction, Protocol 3B was selected as the 'final' decellularization protocol and was used for all future studies.

The scanning electron microscopy (SEM) images (**Fig. 3.4**) revealed an intricate mesh-like ECM ultrastructure in the native bovine NP that was qualitatively preserved in the DNP generated with Protocol 3B.

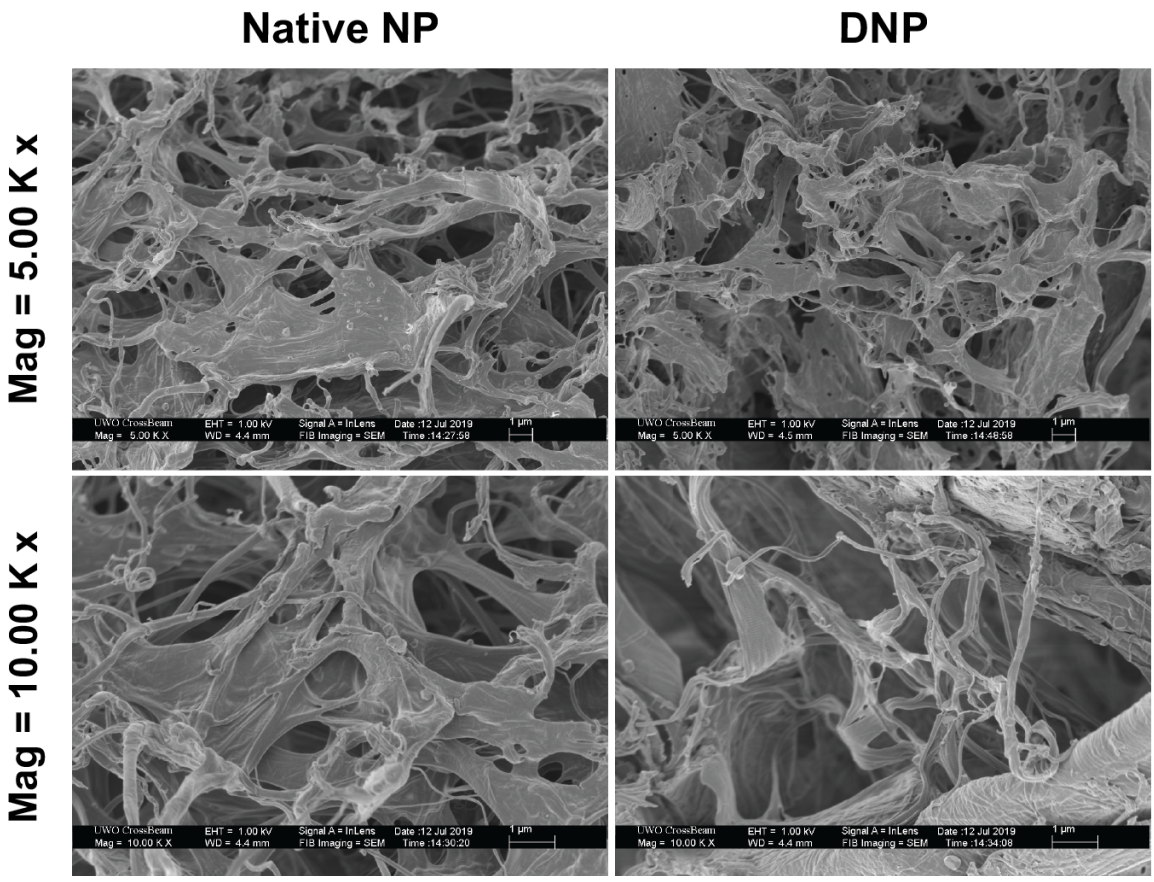

Figure 3.4: Scanning electron microscopy (SEM) images visualizing the ECM ultrastructure of the native bovine NP and DNP generated with Protocol 3B. Scale bars = 1 µm.

3.2 Characterization of cryomilled decellularized nucleus pulposus and bovine tendon collagen particles

The DNP generated with Protocol 3B (pooled from N=4) and commercially-sourced bovine tendon collagen (COL) controls were lyophilized and cryomilled to obtain ECM particles for use in the fabrication of the methacrylated chondroitin sulphate (MCS) ± DNP/COL constructs. The volume fraction (**Fig. 3.5A**) and size distribution (**Fig. 3.5B**) of the DNP and COL particles were assessed using a Malvern Mastersizer 2000. While a range of particle sizes was observed, the majority of particles were in the expected size range of 45 µm to 125 µm. The Kolmogorov–Smirnov test with $p<0.05$ revealed that the size distributions of DNP and COL particles were not significantly different, eliminating differences in particle size as a potential confounding variable.

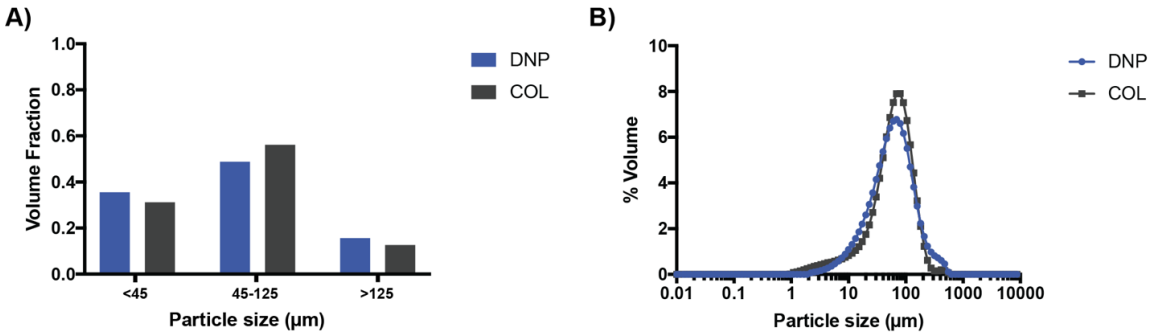

Figure 3.5: Characterization of the size distribution of the DNP and COL cryomilled particles. A) Volume fraction and **B)** particle size distribution of the cryomilled DNP and COL particles sieved between 45 µm and 125 µm stainless steel meshes. There was no significant difference in the particle size distributions between the two ECM sources as determined by Kolmogorov–Smirnov test with $p<0.05$.

3.3 Characterization of methacrylated chondroitin sulphate

Following MCS synthesis, dialysis and lyophilization, successful methacrylation of chondroitin sulphate was confirmed by ^{1}H NMR spectroscopy (**Fig. 3.6**). Peaks at 6.03 ppm (i.) and 5.59 ppm (ii.) on the ^{1}H NMR correspond to protons on the vinyl group, while the peak at 1.79 ppm (iii.) corresponds to the protons on the methyl group of the

methacrylate. The peak at 1.89 ppm (iv.) corresponds to the N-acetyl residues from the starting CS material. Integration of protons revealed that the targeted degree of methacrylation (17-20%) was achieved, with 18% in this specific batch of polymer. Additionally, the absence of extra unidentified peaks indicates that the polymer is free of contaminants.

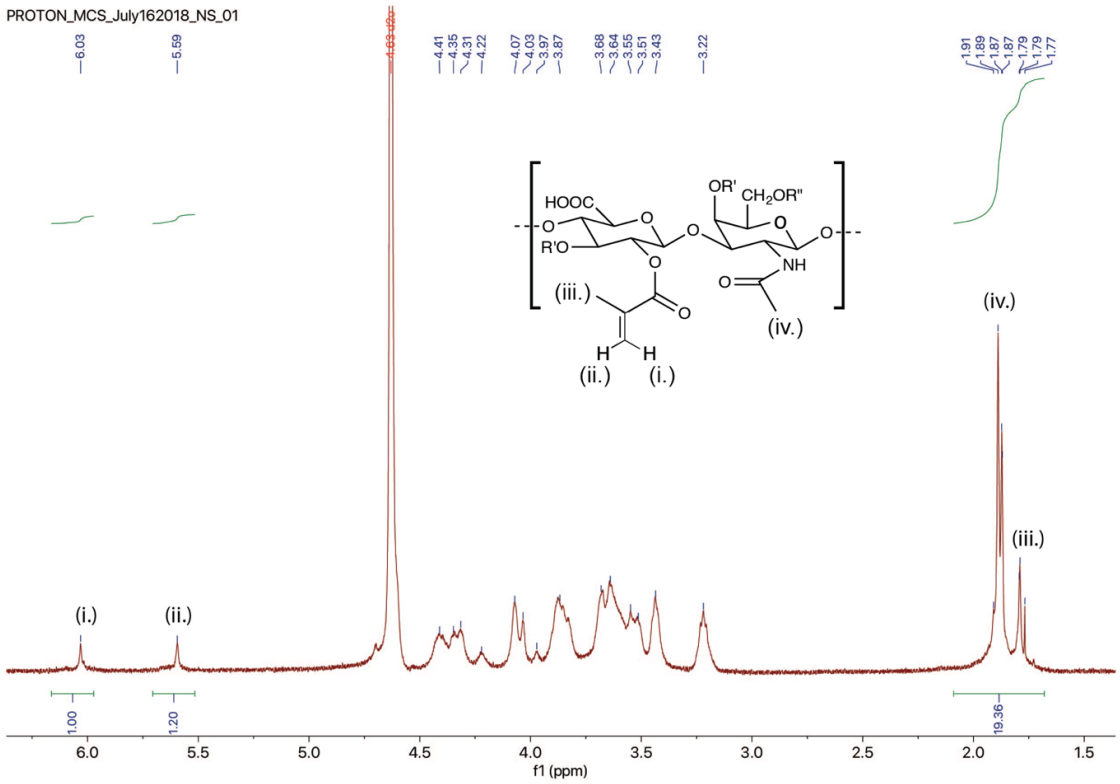

Figure 3.6: ^{1}H NMR of MCS with key peaks on the spectrum labelled and correlated to the chemical structure.

3.4 Hydrogel physical characterization

Following the fabrication of the MCS ± DNP/COL hydrogel constructs via UV crosslinking, the gels were macroscopically similar in appearance, but varied somewhat in colour (**Fig. 3.7A**). Single-phase MCS hydrogels were colourless, whereas MCS+DNP and MCS+COL constructs were off-white and white in colour, respectively. While handling

the gels, single-phase MCS constructs were qualitatively more brittle than the MCS + DNP/COL constructs. No differences were noted in the dimensions of the hydrogels between the three groups following swelling for samples that were prepared for bulk compression testing.

Gel content analysis was performed as a measure of the crosslinking efficacy of the hydrogels. In comparing the three hydrogel groups, there was no significant difference in gel content (**Fig. 3.7B**), with values of 82.2 ± 5.1%, 80.0 ± 5.8%, and 79.9 ± 5.4% for the MCS+DNP, MCS+COL, and single-phase MCS constructs, respectively. These findings indicate that integration of the DNP and COL at 5 w/v% did not compromise the overall formation of the hydrogel network. Unconfined bulk compression testing was performed to compare the Young's moduli of the three hydrogel groups (**Fig. 3.7C**). The MCS+DNP, MCS+COL, and single-phase MCS constructs showed moduli of 42.1 ± 8.6 kPa, 35.5 ± 7.9 kPa, and 53.7 ± 9.7 kPa, respectively. The results showed a significant difference between the MCS+COL and single-phase MCS constructs, suggesting that the incorporation of the COL may have introduced defects or inhomogeneities into the polymer network. No significant differences were found between other groups.

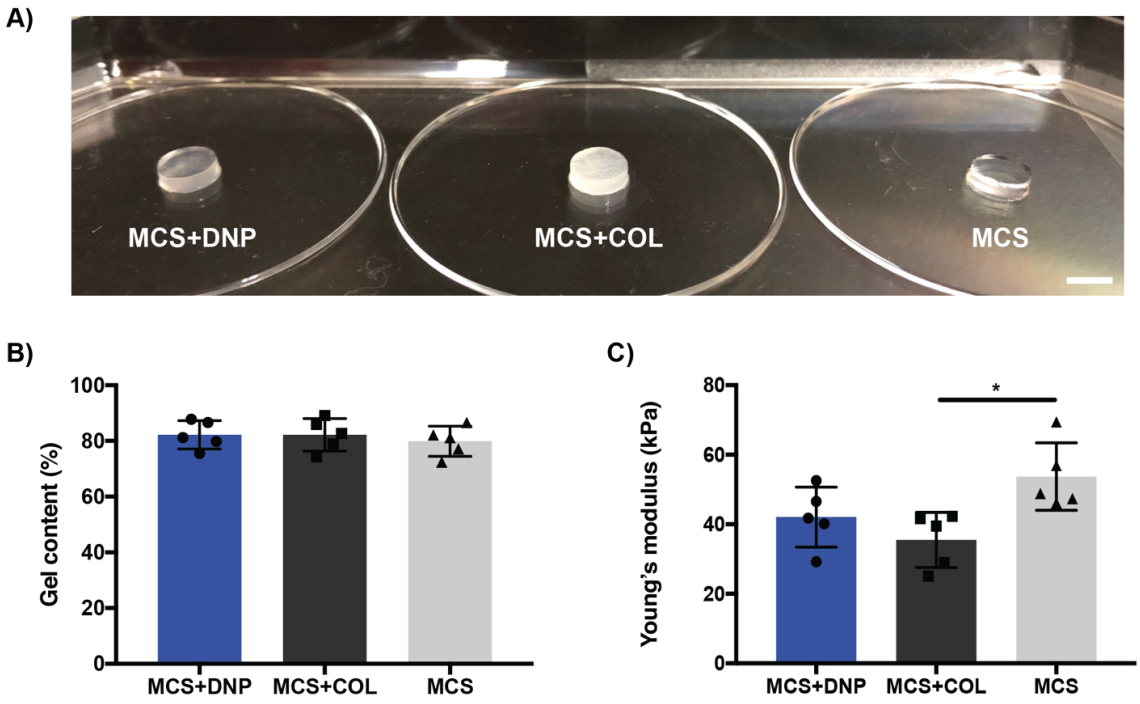

Figure 3.7: Physical characterization of MCS ± DNP/COL hydrogel constructs. A) Macroscopic images of MCS+DNP, MCS+COL and single-phase MCS gels. Scale bar = 1 cm. **B)** Gel content analysis, showing no significant differences between the groups (n=5). **C)** Unconfined bulk compression testing showing that the MCS+COL composites had a significantly lower Young's modulus than the single-phase MCS hydrogels, with no significant differences between the other groups as determined by a one-way ANOVA with a Tukey's post-hoc comparison of means (n=5). * = $p<0.05$.

3.5 Viability and retention of U-CH1 cells encapsulated within MCS ± DNP/COL constructs

The LIVE/DEAD® assay with confocal imaging was used to qualitatively assess the viability and retention of U-CH1 cells within MCS ± DNP/COL constructs following 24 h, 3 days and 7 days of *in vitro* culture (**Fig. 3.8**). Images were acquired at a maximum depth of ~200 µm, limited by the focal length capability of the microscope. Initially, at the 24 h timepoint, the viability and retention of U-CH1 cells within all of the constructs appeared similar. At the 3 and 7 day timepoints, the MCS+DNP and MCS+COL groups showed qualitatively enhanced cell viability and retention as compared to the single-phase MCS. At both 3 and 7 days, there was noticeable cell death and a marked decrease in the cell density in the U-CH1 cells encapsulated within single-phase MCS. Interestingly,

preliminary studies investigating the viability of U-CH1 cell cultured within thermally-crosslinked MCS ± DNP/COL constructs (**Appendix; Supplemental Fig. 3**) showed similar trends, with a qualitatively higher cell density observed in the MCS+DNP constructs at 7 and 14 days, and a dramatic reduction in the presence of viable cells in the single-phase MCS hydrogels over time.

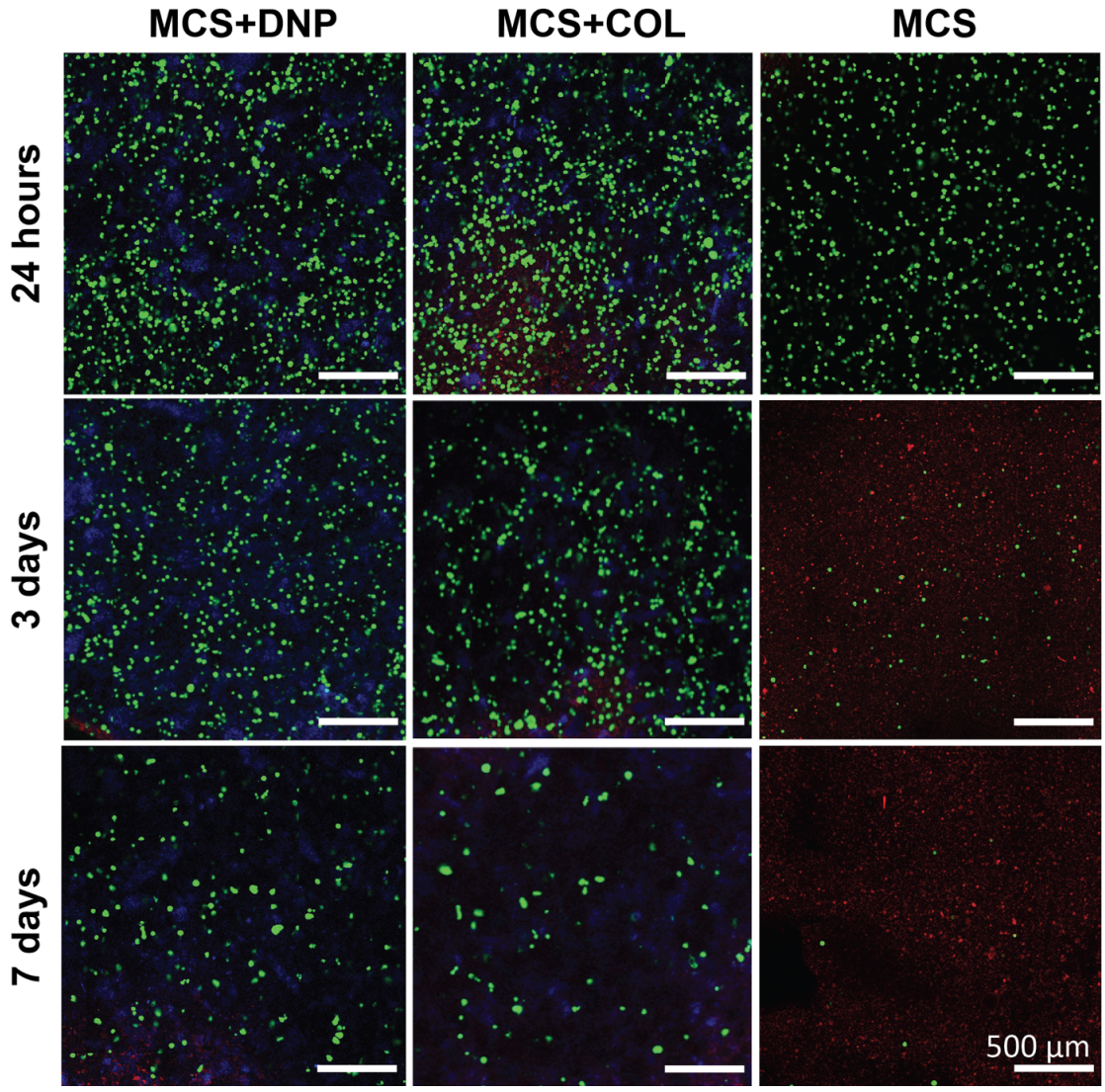

Figure 3.8: Representative confocal microscopy images showing LIVE/DEAD® staining of U-CH1 cells encapsulated within the MCS ± DNP/COL hydrogel constructs through UV crosslinking and cultured *in vitro* over 7 days. Live cells were stained with calcein-AM (green) and dead cells were stained with ethidium homodimer-1 (red). The DNP and COL particles appear blue due to ECM autofluorescence. Images were captured at a depth of ~100 µm. Scale bars = 500 µm.

3.6 Gene expression of U-CH1 cells encapsulated within MCS+DNP/COL constructs

A panel of notochord-associated (*T* and *CD24*), NP-associated (*FOXA1* and *SOX9*), and ECM (*ACAN, COL2A1* and *COL1A1*) genes was quantified in U-CH1 cells encapsulated in the MCS+DNP and MCS+COL constructs, as well as U-CH1 cells maintained on standard tissue culture plastic (TCP) as control following 24 h and 3-days in culture using RT-qPCR (**Fig. 3.9**). The 7-day timepoint and single-phase MCS groups were not assessed due to low RNA yields.

U-CH1 cells encapsulated within the MCS+DNP hydrogels showed a significant decrease in *T* (3d) and *CD24* (24 h and 3d) expression as compared to the TCP controls, associated with a significant increase in *SOX9* (3d) expression compared to the TCP controls. Following 3 days in culture, cells within the MCS+DNP group showed a significant decrease in expression of the ECM gene *COL2A1* (3d) compared to the TCP controls, accompanied by decreased expression of *ACAN*, (mRNA levels falling below detection in two of the three biological replicates). There were no significant differences in *FOXA1* or *COL1A1* expression in U-CH1 cells cultured in MCS+DNP hydrogels, as compared to the TCP controls.

Although the U-CH1 cells within the MCS+COL hydrogels showed no significant differences in *T*, *SOX9*, or *COL1A1* expression compared to the TCP controls, there was a significant decrease in *ACAN* (3 d; and from 24 h to 3 d) and *CD24* (24 h and 3d; with a significant increase from 24 h to 3 d) expression, a significant increase in *FOXA1* expression (3 d, and from 24 h to 3 d), and a significant decrease in *COL21* expression (24 h and 3 d), compared to the TCP controls.

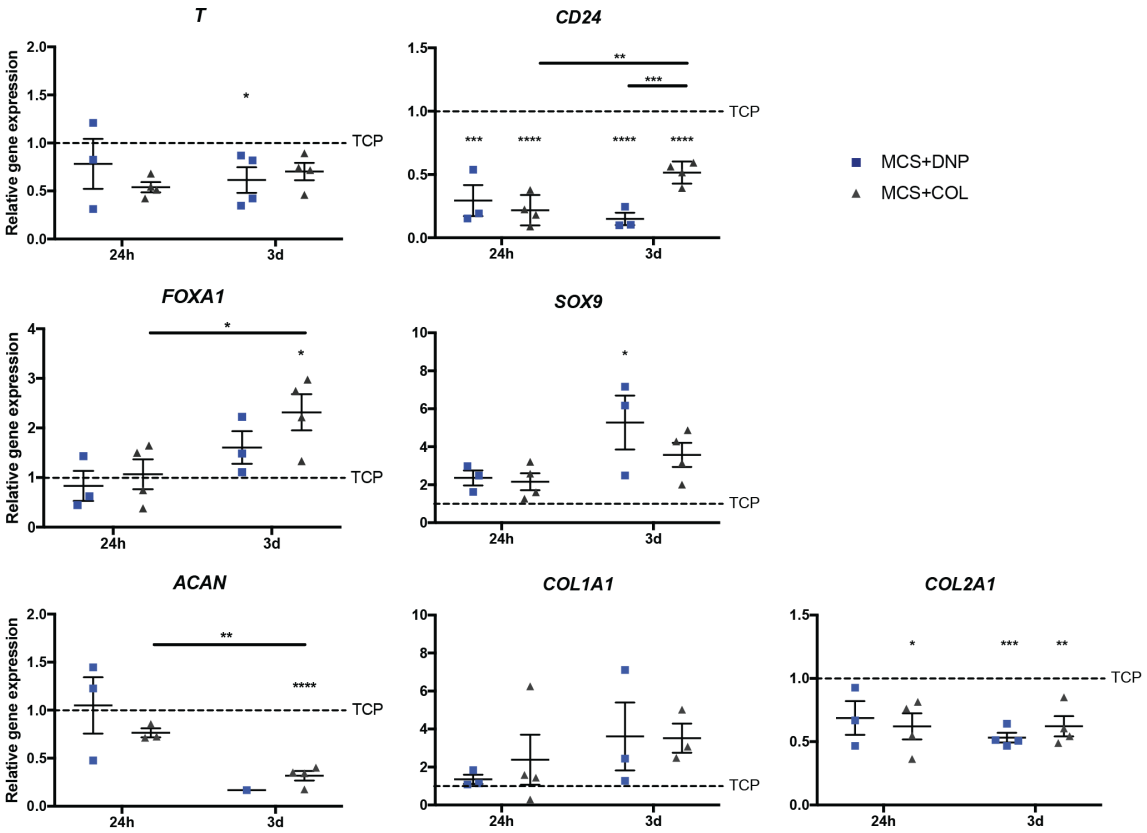

Figure 3.9: RT-qPCR analysis of gene expression of U-CH1 cells encapsulated within MCS+DNP/COL hydrogels and cultured *in vitro* for 24 h or 3 days. Analysis was performed on *T* and *CD24* as markers of a notochord-like phenotype, *FOXA1* and *SOX9* as markers of an NP-like phenotype, and *ACAN, COL2A1* and *COL1A1* as markers of NP ECM production. Dashed lines indicate levels in control cells cultured using standard protocols on tissue culture plastic (TCP). Relative gene expression was calculated using the $\Delta\Delta C_t$ method normalized to the geometric mean of the housekeeping genes GUSB and GAPDH, with U-CH1 cells cultured on TCP as control. Data are presented as mean ± SEM, N=3-4 (n=3-6 technical replicates averaged per biological replicate). * = $p<0.05$, ** = $p<0.005$, *** = $p<0.0005$, **** = $p<0.0001$. The ROUT method (Q=1%) was used to identify outliers prior to statistical analyses. One-way ANOVA with Tukey's post-hoc correction was performed for groups within each timepoint. Welch's t-test was performed to evaluate changes in gene expression within a group over time. *ACAN* expression for MCS+DNP at 3d was excluded from statistical analyses as two of the three biological replicates had no amplification.

Chapter 4

4 Discussion

Back pain is the most common cause of disability worldwide, with intervertebral disc (IVD) degeneration as the primary contributor in ~40% of cases[1]. Although the etiology of disc degeneration is not understood, it is believed to initiate in the central gel-like structure of the IVD, known as the nucleus pulposus (NP)[9]. Changes in the NP, such as decreased production of proteoglycans[87,88] and other extracellular matrix (ECM) components[87], lead to a loss of hydration[11], disc height, and overall impaired mechanical function[91]. The IVD has a limited capacity for repair and there are currently no disease-modifying treatments for disc degeneration. As such, there is a growing interest in the design and application of biomaterials-based therapies targeting the NP to improve mechanical function by restoring disc height, and to establish a pro-regenerative microenvironment that supports delivered or endogenous cell populations for the regeneration of this tissue. Recognizing the role of the ECM in influencing cell function[28,108], natural and synthetic scaffolds have been designed to mimic biochemical composition and/or biomechanical function of the native NP ECM. One especially promising approach to mimic the native tissue is to decellularize the NP tissue to obtain the NP ECM for use as a cell-instructive scaffold.

Decellularization methods aim to remove cellular and nuclear content while preserving the ECM composition and ultrastructure. Since there are currently no standardized criteria to develop and characterize these materials, the bioactivity of the resulting scaffolds may vary greatly[24]. For each tissue type, decellularization protocols must be developed and refined based on the tissue-specific composition, structure and cellularity[113]. In general, decellularization treatments typically lyse cell membranes, and the cellular and nuclear components must be separated from the ECM, solubilized or digested, and removed from the tissue[115]. To date, efforts made to decellularize the NP have employed multiple detergents and harsh chemicals such as sodium dodecyl sulphate and deoxycholic acid[119–122,152–154]. Although effective in reducing cell content, these treatments can alter the ECM structure, strip the tissues of cell-instructive soluble factors, and leave residues that can lead to cytotoxicity[155]. All treatments that decellularize tissues will also alter the ECM to some degree, impacting the innate bioactivity. With this in mind, the focus of this project was on the development of a reproduceable method with minimal processing that

effectively reduced cellular/nuclear content in the bovine NP, while preserving glycosaminoglycan (GAG) and collagen content, which are key ECM components within the native tissues. Following protocol establishment, the effects of the resulting decellularized NP (DNP) on cell viability, retention and differentiation were explored using NP progenitor-like cells encapsulated within a tunable 3-D hydrogel platform comprised of methacrylated chondroitin sulphate (MCS) that mimics the GAG-rich composition of the native NP[64].

The initial protocols tested employed the use of Triton X-100 and tributyl phosphate (TBP) detergents to aid in solubilizing fragmented cellular and nuclear content. Detergents have a hydrophilic head group and a hydrophobic tail that can solubilize amphiphilic cell membranes. Based on their hydrophilic head groups, detergents are separated into nonionic, zwitterionic, and ionic. Non-ionic detergents, such as Triton X-100, are gentler and may better preserve tissue structure and composition than zwitterionic and ionic detergents[113]. Zwitterionic detergents, such as TBP, are harsher than non-ionic detergents, but gentler than ionic detergents that are known to denature proteins and remove growth factors from the ECM[113]. The NP decellularization protocols in the literature to date[117–121,154,156] frequently use zwitterionic and ionic detergents to decellularize the tissues. While the efficacy of cell extraction using Triton X-100 has been variable with some tissue types, it is thought to maintain protein–protein interactions that are disrupted with the use of TBP[113]. As noted by the EDTA incubation, these interactions may be important in preserving GAG and the ECM structure in general. Since the NP ECM is not as dense as other tissues tested using Triton X-100, we selected this non-ionic detergent over TBP in our initial refinements of the protocols. Interestingly, in the decellularization treatments investigated in the current study, treatment with Triton X-100 detergent was found to strip the tissues of GAG without having a noticeable effect on DNA content. We postulate that at the enzymatic digestion step, the nuclei were fragmented and solubilized enough to extract these components from the ECM without the need of added detergents. Thus, the detergent wash step was omitted from the finalized decellularization protocol.

The finalized 1-day detergent-free method involved one freeze-thaw cycle in hypotonic deionized water (dH_2O), followed by a 2 h enzymatic digestion with DNase and RNase in Sorensen's phosphate buffer (SPB). After validation with four independent biological

replicates, this protocol was found to consistently extract ~89% of double stranded DNA (dsDNA) while preserving ~36% sulphated GAG (sGAG), as compared to <14% sGAG in initial protocols tested. The collagen distribution was qualitatively preserved in the DNP, with a quantitative enrichment in collagen content relative to tissue weight in the processed tissues, consistent with the loss of GAG. This increase in relative collagen content has been previously noted in the quantification results of other groups decellularizing the NP[118–121,154].

Although there was a substantial quantitative reduction in dsDNA content, the qualitative histological analysis revealed residual nuclei in the DNP tissues. The discrepancy in these results may be attributed in part to variability within NP samples from the different levels of IVDs, and between tissue donors. While the specific cellularity and ECM composition at various levels of IVDs in the spine have yet to be characterized, many groups recognize these parameters may vary depending on the specific tissue source. For example, in studies aiming to understand aging[157,158], matrix homeostasis[159] and degeneration of the discs[160], the level of IVDs were stratified during analyses to account for potential source variations. Donor variability in the age and breed of the cattle are also recognized as possible contributing factors in the current study. The quantification of DNA and sGAG content in the native NP samples during protocol validation demonstrates this variability, with dsDNA content ranging from ~7-64 ng/mg dry tissue and sGAG content ranging from ~128-425 µg/mg dry tissue in biological replicates. The sample pooling and tissue processing (i.e. lyophilization and cryomilling) in the biochemical analyses may have reduced sample variability as compared to the histological analyses, which looked at individual 2 mm x 2 mm NP samples. Nonetheless, our decellularization protocol consistently resulted in a reduction of DNA, while qualitatively preserving the intricate mesh-like ECM ultrastructure of the native bovine NP in the DNP.

The first treatment step in the protocol involved mechanical disruption by a freeze-thaw cycle in a hypotonic solution to lyse cell membranes. Hypotonic solutions cause an influx of water into cells, exerting an osmotic stress that results in cell lysis[113]. In earlier protocols tested, incubation with agitation alone in a hypotonic solution (50 mM tris (hydroxymethyl)aminomethane (Tris) + 10 mM ethylenediaminetetraacetic acid (EDTA)) was found to be insufficient in lysing cell membranes in the NP tissues. Mechanical

disruption by freeze-thaw cycles in the same solution aided in cell lysis, likely making the nuclear content more accessible for enzymatic digestion in future steps. The 50 mM Tris + 10 mM EDTA solution was also found to solubilize a substantial amount of GAG. EDTA is a divalent metal cation chelator that dissociates cells from the ECM by sequestering calcium. Although effective in dissociating cells from the matrix, EDTA can also destabilize protein-protein interactions dependent on calcium binding. This effect was postulated to result in the increased solubilization of GAG. In an effort to better preserve this important ECM component, dH_2O was compared to 50 mM Tris + 10 mM EDTA as the hypotonic solution used for the freeze-thaw cycles. The quantification results revealed that dH_2O was more effective in reducing dsDNA content (~77% versus ~61% reduction post-freeze-thaws), while better preserving GAG (~17% versus ~14% retention post-decellularization). No noticeable differences in collagen distribution were visualized by histology, however there was a greater enrichment in collagen content in tissues processed with 50 mM Tris + 10 mM EDTA, as expected with the increased loss of GAG. Thus, dH_2O was selected as the hypotonic solution in our decellularization protocol. In a final attempt to preserve more GAG at this step in the decellularization, the number of freeze-thaw cycles were reduced from 3 to 1. Freeze-thaw cycles are thought to increase tissue porosity and induce cell lysis by ice crystal formation[161]. A decrease in the number of freeze-thaw cycles was found to better preserve GAG in the NP, while maintaining its efficacy in reducing cellular/nuclear content.

The second treatment step in our protocol involved a 2 h enzymatic digestion with DNase and RNase in SPB, to fragment the cellular and nuclear content and remove these components from the NP ECM. DNase and RNase are endonucleases that hydrolyze deoxyribonucleotides and ribonucleotides, respectively. The activity of these enzymes can be reduced over time as lysed cells release natural protease inhibitors[113]. With this in mind, enzymatic digestion incubation times of 5 h and 2 h were compared. A qualitatively greater number of nuclei were visible by histology at 2 h as compared to 5 h; however, quantification revealed similar levels of dsDNA between both treatments. As mentioned earlier, the discrepancies between the histological and biochemical analyses may be in part due to donor and sample variability. The 2 h incubation also revealed a greater qualitative and quantitative preservation of GAG as compared to the 5 h incubation. There were no noticeable differences in collagen distribution, and quantification between the two

incubation times tested. Based on the quantitative data, the enzymatic digestion step was set at 2 h in the finalized decellularization protocol. In a final effort to reduce loss of GAG, SPB and phosphate buffered saline (PBS) were compared as the digestion incubation solutions. PBS is a commonly used buffer that has a pH, ion concentration and osmolarity that simulate physiological conditions and is thought to maintain tissues. The quantitative results revealed that enzymatic digestion performed in SPB had a greater reduction in dsDNA content as compared to those carried out in PBS. There were no noticeable differences in the quantitative retention of sGAG between the two treatment groups. Similarly, the collagen distribution and the enrichment in collagen content were similar between the two groups. The additional ions and their specific concentrations in the SPB (0.55 M sodium phosphate dibasic heptahydrate, 0.17 M potassium phosphate, 0.049 M magnesium sulphate heptahydrate) are postulated to increase enzyme activity as compared to the PBS. Thus, the enzymatic digestion step with DNase and RNase was performed in SPB for 2 h.

In addition to the treatments discussed above, balancing the NP surface area exposed during incubations, standardizing the tissue-to-solution volume ratio and speed of agitation during incubation are important factors in the decellularization of the NP. A possible reason as to why previous methods required harsher treatments to effectively decellularize the tissues may be related to the surface area of the NP samples used prior to processing. Published protocols have maintained the original size of the native NP tissues[117,118,121,154], used halved[116] or 8 mm NP biopsied segments[119], or milled the NP tissues[120] prior to processing. Our finalized protocol sectioned the native NP into 2 mm x 2 mm pieces prior to treatment in order to improve the efficacy of the decellularization while maintaining a surface area that minimized GAG solubilization. Selecting a tissue-to-solution volume ratio of ~15 g of NP tissues/100 mL of solution in a 500 mL tub standardized the process and created a balance that reduced tissue aggregation. An incubation speed of 125 rpm was selected as higher speeds tested resulted in undesired aggregation of the NP tissue pieces, while lower speeds have been reported in the literature to be less effective in removing nuclei[113]. It is postulated that a combination of these factors contributed towards the successful decellularization with minimal treatments.

Since our protocol requires noticeably less tissue processing as compared to published methods, it was hypothesized that some easily solubilized bioactive components in the NP ECM may be preserved in our DNP. To investigate the cell-instructive potential of our material, cryomilled DNP was incorporated into *in situ* UV-crosslinking MCS hydrogels to create a tunable 3-D platform that mimics the native NP environment. The use of intact DNP does not allow for tuning of cell-cell and cell-ECM contact, which are known to play important roles in directing cell phenotype[142]. Although ~36% sGAG was preserved in the DNP in our finalized protocol, there was still a significant loss in GAG content from the native NP. Since chondroitin sulphate (CS) is the most abundant GAG in the NP ECM[133], incorporating the DNP particles into MCS hydrogels was a way to structurally reintroduce this important component into a 3-D platform. CS is negatively charged and is capable of absorbing water and nutrients, and it has been shown to have anti-inflammatory properties[135,136]. Since chronic inflammation is a hallmark of disc degeneration, this polymer is an attractive candidate for the development of biomaterials-based regenerative strategies. Physically, the mechanical properties of this polymer can be tailored by reducing or increasing the number of methacrylate groups on the polymer backbone. By adjusting the degree of methacrylation, as well as the ECM particle size and concentration, and cell density, the biomechanical properties, cell-cell and cell-ECM interactions within the 3-D hydrogel composites can be tuned, all of which influence cell phenotype. Commercially-sourced bovine tendon collagen (COL) was incorporated into the MCS hydrogels as a non-tissue specific control to better investigate the effects specific to the DNP. Previously, our group has used COL to fabricate bead foam scaffolds to compare the tissue-specific effects of decellularized adipose tissue (DAT) versus COL on human dermal fibrolasts[149]. This previous work demonstrated that the ECM source had tissue-specific effects on mediating cell survival and paracrine function, and supports the choice of the purified COL as a comparator for probing possible tissue-specific effects of the DNP.

Recognizing that cell response is mediated by the scaffold biomechanical properties in addition to the biochemical environment[162–164], physical characterization of the hydrogel was performed. First, the DNP and COL particles were characterized to confirm the particle size distributions were similar, as variations in size could influence cell-cell and cell-ECM interactions. While a range of particle sizes was observed, the majority of particles were in the expected size range of 45 μm to 125 μm. The results revealed that there were no

significant differences in the size distributions of the DNP and COL particles, suggesting that particle size was not a confounding factor in the observed response. The presence of particles <45 μm may be attributed to aggregation of smaller particles during sieving, and the presence of particles >125 μm could be due to swelling and aggregation following particle rehydration. Next, analysis of gel content revealed no significant differences between MCS+DNP, MCS+COL and single-phase MCS hydrogel constructs, indicating that integration of the DNP and COL at 5 w/v% did not compromise the hydrogel crosslinking efficacy. Finally, unrestricted bulk compression testing results suggested that single-phase MCS constructs were significantly stiffer than MCS+COL constructs, while there were no significant differences between the other groups. The COL matrix may be functioning as a spacer, resulting in fewer crosslinks between polymer chains of the MCS, introducing defects or inhomogeneities into the polymer network and resulted in a less stiff substrate. Since the DNP has a high amount of GAG content as compared to the previously characterized COL[149], it is possible that the DNP may bind to water and contribute to the compressive properties of the MCS+DNP constructs more-so than the COL. Importantly, there were no significant differences between MCS+DNP and MCS+COL bulk compressive moduli, suggesting that the bulk mechanical properties were not a major influencing factor in the cell response in the subsequent studies.

Following physical characterization of the hydrogel constructs, *in vitro* studies focused on examining the effects of DNP on human NP progenitor-like cell viability, retention and differentiation, with COL and single-phase MCS controls. Since primary notochord cells are difficult to obtain and current protocols for NP cell monolayer culture do not effectively maintain cell phenotype *in vitro*, the human chordoma-derived U-CH1 cell line was used as a model of human NP progenitors[143]. These cells demonstrate a stable notochord-like phenotype *in vitro*, marked by the expression of the embryonic notochord markers brachyury, CD24, KRT19, epithelial marker antigen, vimentin, and cytokeratin[144–146]. A cell density of 10 x 10^6 cells/mL of final gel volume was selected based on previous work with adipose-derived stem/stromal cells (ASCs) encapsulated within MCS + adipose ECM constructs[139]. This cell density was found to be favourable in promoting adipogenesis by increasing cell-cell contact[140]. In future studies further investigating the MCS ± DNP/COL constructs, the cell density could be adjusted to tune cell-cell contact. However, for the

purpose of this study, this cell density was selected as a starting point and was kept constant between constructs.

The U-CH1 cells were cultured within the MCS ± DNP/COL constructs for up to 7 days, and cell viability and retention following encapsulation within the hydrogels were qualitatively assessed by confocal imaging with LIVE/DEAD® staining. While the viability and abundance of U-CH1 cells within all of the groups were qualitatively similar at the 24 h timepoint, the MCS groups incorporating ECM particles showed qualitatively enhanced cell viability and retention over time as compared to the single-phase MCS group. At both 3 and 7 days, there was noticeable cell death and a marked decrease in the cell density of the U-CH1 cells encapsulated within the single-phase MCS hydrogels. Similarly, preliminary studies with U-CH1 cells cultured within thermally-crosslinked constructs at longer timepoints showed that there were qualitatively more viable cells present within the MCS+DNP hydrogels after 14 days of culture as compared to MCS+COL and single phase MCS constructs. These results suggest that the ECM particles provided cell-instructive cues that supported the viability and retention of the U-CH1 cells within this 3-D hydrogel platform, and preliminary work may suggest that the DNP may provide tissue-specific cues that better support these NP progenitor-like cells within the constructs at later timepoints.

Previous work has shown that the NP ECM alone is cell supportive, likely due to its native microarchitecture and biochemical signalling[118,152,165,166]. Composite DNP hydrogel scaffolds fabricated using chemical crosslinking[156], agarose[120], or pepsin digestion[121] maintained this cell-supportive microenvironment by promoting ASC[156], MSC[120] or NP cell viability[120,121] in long-term *in vitro* culture (over 14[156] or 21 days[120,121]), and promoting the production of GAG[120,121,156]. While our study is the first to culture the U-CH1 cells within MCS hydrogels, previous studies have successfully cultured other notochordal cells isolated from porcine[167], canine[168] or bovine[169] IVDs within 3-D hydrogels, such as alginate, and have been able to maintain cell viability[167–169]. The cells used in these studies were not chordoma-derived, so it is difficult to elucidate the exact reason for the marked U-CH1 cell death within our constructs. While speculative, the dramatic decrease in cell density in the single-phase MSC hydrogels may be attributed in part to the stiffness of the gels. Following 3 and 7 days of culturing, a noticeable number of cells were found in the

media during media changes. Scaffold stiffness has been shown to influence cell adhesion, cytoskeleton organization, motility and differentiation capacity[162–164]. For example, rat kidney epithelial cells and fibroblasts were found to have reduced spreading and increased rates of motility on stiff substrates as compared to softer substrates[170]. Another possible reason for the loss of U-CH1 cells within the MCS hydrogels may be due to pore size. Peyton *et al.* found that migration speed, displacement, and total path length of mesenchymal stem cells cultured within a 3-D poly(ethylene oxide) hydrogel scaffold depend strongly on pore diameter[171]. Future work could investigate the effects of modifying the degree of methacrylation to tune the scaffold stiffness and pore size with the goal of improving cell retention and promoting cell viability within the MCS constructs. Alternatively, more clinically relevant cell populations, such as mesenchymal stem/stromal cells (MSCs) sourced from adipose or bone marrow tissue, that may not exhibit the same migration profile as U-CH1 cells, could be tested within the constructs.

In the final *in vitro* studies, the effects of DNP on directing cell differentiation were examined by quantifying the expression of a panel of notochord-associated (*T* and *CD24*), NP-associated (*FOXA1* and *SOX9*), and ECM (*ACAN, COL2A1* and *COL1A1*) genes in the MCS+DNP and MCS+COL constructs at 24 h and 3-day timepoints using RT-qPCR, with cells maintained on 2-D tissue culture plastic (TCP) serving as controls. Consistent with the decrease in cell densities noted in the viability analyses, gene expression analysis could not be performed at the 7-day timepoint or for the single-phase MCS group due to low RNA yields. U-CH1 cells encapsulated within the MCS+DNP hydrogels showed a significant decrease in notochord-associated gene expression (*T* and *CD24*), a significant increase in NP-associated gene expression (*SOX9*), and a significant decrease in ECM gene expression (*ACAN* and *COL2A1*), as compared to TCP controls. Similarly, cells encapsulated within the MCS+COL hydrogels showed a significant decrease in expression of one notochord-associated marker (*CD24*), with a significant increase in expression of the NP-associated marker *FOXA1*, along with a significant decrease in ECM gene expression (*ACAN* and *COL2A1*) as compared to TCP controls. Notochord cells have been found to have a higher expression of *T* and *CD24* as compared to the NP cells[74,84]. These two markers are commonly used to identify cells with a notochord-like phenotype. *FOXA1* is a transcription factor that is involved in the formation of the notochord and maintenance of the NP[172]. *SOX9* is a transcription factor that is strongly expressed in healthy human NP

cells[173] and has been shown to promote aggrecan expression in human chondrocyte cells[174]. Loss of *SOX9* results in the complete absence of cartilage[175], and its expression in the IVD continues to be essential after skeletal maturity[176], making it an important marker when assessing an NP-like phenotype. Interestingly, although *SOX9* expression was significantly enhanced in cells within MCS+DNP, *ACAN* expression was noticeably downregulated. The expression of *ACAN* was also significantly downregulated in the cells cultured within the MCS+COL hydrogels. These findings suggest that culturing the U-CH1 cells in the GAG-rich environment of the MCS hydrogels resulted in the downregulation of *ACAN* expression. When cultured in an environment rich in a specific protein, cells have been shown to downregulate gene expression of that protein. For example, human dermal fibroblasts cultured within collagen type I gels show significantly reduced mRNA levels of the collagen type I gene after 2 days of culture[177]. The expression of *COL2A1* in our study was also downregulated over time in both groups. While collagen type II has not specifically been characterized in the DNP or COL, previous studies assessing the presence of ECM proteins in the COL have shown that it is rich in several types of collagens, including collages type IV, V and VI[149]. More than 85% of the collagen in the native NP is collagen type II[178] and it is likely abundant in our resulting DNP based on the histological, SEM and biochemical analyses. Future characterization of aggrecan and collagen type II in both ECM by immunohistochemistry could confirm the above interpretation.

Interestingly, the changes in gene expression patterns differed between the two ECM hydrogel groups, suggesting that the DNP and COL particles have cell-instructive cues unique to their biochemical/structural composition. Since the confounding effects associated with particle size, biomechanical properties and cell density were controlled for between the MCS+DNP and MCS+COL groups, the differences in gene expression seen between these groups is likely attributed to the differing effects of the specific ECM proteins. Given that both notochord-associated markers tested were downregulated in the cells within MCS+DNP and NP-associated marker *SOX9* was upregulated, it appears that the DNP may have a slightly more pronounced bioactive effect in modulating the maturation of notochord cells towards an NP-like phenotype, as compared to the COL, although further studies are warranted to assess these possible differences using cell populations that show superior long-term viability and retention as compared to the U-CH1

cell line . While the gene expression patterns we assessed suggest progression towards an NP-like phenotype, it is challenging to definitively interpret the results since there are no markers that clearly distinguish notochord cells from mature NP cells, since the temporal regulation of the gene expression from notochord to NP is not well characterized. Genes expressed in the notochord are also expressed in mature NP cells, in keeping with the finding that all cells of the NP have a shared ontogeny[83]. This highlights the need to better characterize expression profiles of notochord and NP cells to understand changes in the cell populations that may represent different stages of development. Further work in characterizing the gene and protein expression of other notochord-like and NP-like markers at longer timepoints would aid in better understanding the effects of the DNP on NP progenitor cells.

Chapter 5

5 Conclusion

5.1 Summary of findings

In the first aim, a new protocol was developed to decellularize bovine nucleus pulposus (NP), with the goal of enabling cell extraction, while retaining glycosaminoglycan (GAG) and collagen, key extracellular matrix (ECM) components predicted to be favourable for bioactivity. Parameters investigated included freeze-thaw cycles in varying hypotonic solutions, enzymatic digestion methods, and the effects of detergent washes. Applying a systematic approach, the initial 10-day cartilage decellularization protocol (Flynn Lab, unpublished) tested on the bovine NP was refined to a simple 1-day detergent-free method. Treatment with 1 freeze-thaw cycle in deionized water, followed by a 2 h enzymatic digestion with DNase and RNase in Sorensen's phosphate buffer digest solution effectively extracted ~89% double stranded DNA content. The decellularized tissues maintained collagen structure, and retained ~36% of total sulphated GAG, as compared to <14% for the initial methods tested. Standardizing the NP surface area exposed, the tissue-to-solution volume ratio, and the speed of agitation during incubation were found to be important factors in NP decellularization. Scanning electron microscope imaging suggested preservation of the mesh-like ECM ultrastructure of the native bovine NP in the decellularized NP (DNP). To create a tunable 3-D platform that mimics the native NP environment, cryomilled DNP was incorporated into *in situ* UV-crosslinking methacrylated chondroitin sulphate (MCS) hydrogels. Commercially sourced bovine tendon collagen (COL) was incorporated into the MCS hydrogels as a non-tissue specific control for experimental comparisons.

In the second aim, composite MCS ± DNP/COL hydrogels scaffolds were successfully fabricated, and the physical properties of the gels were characterized to control for confounding effects associated with particle size, biomechanical properties and cell density. The MCS ± DNP/COL constructs did not have significant differences in swelling from each other, and were stable in culture after 7 days. The particles size distributions of the cryomilled DNP were not significantly different from those of the COL, minimizing confounding factors of differing cell-cell interactions between the two groups. Gel content

analysis revealed that integration of the DNP or COL particles at 5 w/v% within the MCS did not compromise crosslinking efficacy. The bulk compressive modulus of single phase MCS was significantly higher than MCS+COL, indicating that incorporation of COL may have introduced defects or inhomogeneities into the polymer network. Importantly, there were no significant differences between MCS+DNP and MCS+COL constructs, minimizing the influence of bulk mechanical properties in the cell response between these two groups.

For the final aim, *in vitro* studies assessed the viability, retention, and differentiation of the U-CH1 human notochord-like cell line encapsulated within MCS ± DNP/COL constructs. While the viability and abundance of the cells after 24 hours of culture appeared qualitatively similar between groups, the constructs incorporating ECM particles better supported cells over time as compared to the single-phase MCS, which had overt cell death and a marked decrease in the cell density at both 3 and 7 days. This suggested that the ECM particles have some structural and/or biochemical cues that better support these NP progenitor-like cells within the constructs. The gene expression analyses revealed that notochord-related markers *T* and *CD24* were downregulated in U-CH1 cells within MCS+DNP, and the NP-associated marker *SOX9* was upregulated. In contrast, U-CH1 cells cultured in MCS+COL showed downregulation of the notochord-associated marker *CD24*, and upregulation of the NP-associated marker *FOXA1*. U-CH1 cells cultured for 7 days within MCS ± DNP/COL constructs and single phase MCS groups could not be assessed by RT-qPCR due to low RNA yields, consistent with the marked decrease in cell density seen in the viability analyses. Taken together, the results suggest that the ECM particles provided cell-instructive cues that supported the viability and retention of the U-CH1 cells within this 3-D hydrogel platform and promoted the differentiation of the notochord-like cells towards an NP-like phenotype.

5.2 Conclusion

For the first time in literature to date, a simple detergent-free method was developed to decellularize bovine NP without the need of excessive physical processing or prolonged incubation times. The protocol was successful in effectively and consistently reducing cellular and nuclear content, while retaining GAG and collagen, and qualitatively preserving the mesh-like ECM ultrastructure of the native bovine NP. In addition to

minimizing processing that may reduce the innate bioactivity of the ECM, the simple treatment steps in this protocol also allow the DNP to be easily scaled-up for possible future commercialization. The collective findings in this thesis highlight the potential of the DNP as a cell-instructive material that may promote the lineage-specific differentiation of human notochord-like cells into an NP-like phenotype. These studies established a flexible 3-D platform that mimics the native NP microenvironment and has the potential to restore mechanical function in the spine. Detailed *in vitro* studies using this system will provide valuable insight into the effects of tissue-specific ECM on NP progenitor cell fate.

5.3 Future directions

While the work in this thesis served as a basis for the rational design of a scaffold for NP regeneration or repair, future studies should focus on improving the viability and retention of encapsulated cells. Refinement of the cell density, ECM particle size and concentration, scaffold pore size and/or stiffness, complimented with *in vitro* assessment of the cells would enable detailed time course studies that further investigate the cell-instructive potential of the DNP.

Previous work suggests that cell density, ECM particle size and concentration, and scaffold pore size and stiffness are factors that affect cell viability, motility and differentiation capacity[142,170,171]. It may be of importance to modulate these factors within the MCS ± DNP/COL constructs to find a balance that enables appropriate cell-cell and cell-ECM contact, while maintaining access to nutrients. While high cell-cell contact may mimic the early stages of NP development and may promote the differentiation of notochord-like cells towards an NP-like phenotype, there is also an increase in competition for nutrients, which may result in greater cell death within the scaffolds and migration into the media. It might be of interest to test higher and lower concentrations of DNP within the scaffolds, as well to find a favourable balance of ECM that promotes retention of cells and differentiation towards an NP-like phenotype. Smaller scaffold pore sizes have been shown to increase cell motility[171], thus the effects of increasing pore size of the MCS constructs could be investigated. Finally, decreasing the scaffold stiffness to promote the retention of U-CH1 cells could also be assessed. Future work focusing on tuning these parameters individually or in combination with one another may improve the viability and retention of U-CH1 cells within the hydrogel scaffolds. Moreover, these studies should be repeated

using a stable NP cell line (i.e. primary bovine NP cells) to determine if properties of enhanced cell migration associated with the tumour-derived U-CH1 cell line affected our experimental outcome.

While confocal imaging allowed for the visualization of cells within the gels, the technique was limited to a focal depth of ~200 μm. When assessing viability and proliferation of cells within the scaffolds, future work could analyze metabolic activity by the Alamar Blue assay to compliment the confocal findings. To further support the gene expression findings in this thesis, the addition of other notochord-associated markers (e.g. *KRT8/18/19*) and NP-associated markers (e.g. *PAX1*, *FOXF1*) could be explored over a longer time course (e.g. 24 hours, 7, 14 and 21 days). The 24-hour timepoint could capture initial changes in the gene expression, while the later timepoints could highlight the progression of changes in response to the DNP over time. In addition, assessment of these markers at the protein level by western blot, ELISA and/or immunohistochemistry should be used to validate changes in cell phenotype at the protein level.

Finally, more clinically relevant cell populations, such as mesenchymal stem/stromal cells (MSCs) sourced from adipose or bone marrow tissue, that may not exhibit the same migration profile as U-CH1 cells, could be tested within the MCS ± DNP/COL constructs. Previously, MCS has been shown to be a supportive environment for adipose-derived stem/stromal cells (ASCs)[139,142,179]. Multiple studies have explored the use of ASCs for NP regeneration; however, their analysis did not differentiate NP from cartilage-associated gene expression in the differentiated cell types[154,156,180]. Markers commonly used to identify an NP-like phenotype are also expressed highly in chondrocytes, which are distinct from the NP cells in ECM composition[10] and phenotype[181]. As such, it would be of importance to assess the expression of NP positive/articular cartilage (AC) negative markers (e.g. *KRT18/19*, *PAX1*, *CA12*) and NP negative/AC positive markers (e.g. *GDF10*, *CYTL1*, *IBSP*) to assure the cells are not differentiating towards a cartilage-like phenotype instead of an NP-like phenotype.

Collectively, these studies would aid in the rational design of an engineered cellular microenvironment that promotes an NP-like phenotype, as a step towards establishing this scaffold as a potential biomaterial-based therapy for the eventual long-term goal of clinical application.

References

1. Vos, T. *et al.* Global, regional, and national incidence, prevalence, and years lived with disability for 328 diseases and injuries for 195 countries, 1990-2016: A systematic analysis for the Global Burden of Disease Study 2016. *Lancet* **390**, 1211–1259 (2017).
2. Hartvigsen, J. *et al.* What low back pain is and why we need to pay attention. *Lancet* **391**, 2356–2367 (2018).
3. Bussières, A. E. *et al.* Spinal Manipulative Therapy and Other Conservative Treatments for Low Back Pain: A Guideline From the Canadian Chiropractic Guideline Initiative. *J. Manipulative Physiol. Ther.* **41**, 265–293 (2018).
4. Hoy, D. *et al.* A systematic review of the global prevalence of low back pain. *Arthritis Rheum.* **64**, 2028–2037 (2012).
5. Deyo, R. A. & Phillips, W. R. Low Back Pain: A Primary Care Challenge. *Spine (Phila. Pa. 1976).* **21**, 2826–2832 (1996).
6. DePalma, M. J., Ketchum, J. M. & Saullo, T. What Is the Source of Chronic Low Back Pain and Does Age Play a Role? *Pain Med.* **12**, 224–233 (2011).
7. Luoma, K. *et al.* Low Back Pain in Relation to Lumbar Disc Degeneration. *Spine (Phila. Pa. 1976).* **25**, 487–492 (2000).
8. Friedman, B. W. *et al.* One-week and 3-month outcomes after an emergency department visit for undifferentiated musculoskeletal low back pain. *Ann. Emerg. Med.* **59**, 128–133 (2012).
9. McCann, M. R. & Séguin, C. A. Notochord Cells in Intervertebral Disc Development and Degeneration. *J Dev Biol.* **4**, 1–18 (2016).
10. Mwale, F. *et al.* Distinction between the extracellular matrix of the nucleus pulposus and hyaline cartilage: A requisite for tissue engineering of intervertebral disc. *Eur. Cells Mater.* **8**, 58–64 (2004).
11. Buckwalter, J. A. Aging and Degeneration of the Human Intervertebral Disc. 20:1307-1314 (1995).
12. Lundon, K. & Bolton, K. Structure and Function of the Lumbar Intervertebral Disk in Health, Aging, and Pathologic Conditions. *J. Orthop. Sport. Phys. Ther.* **31**, 291–306 (2001).
13. Setton, L. A. & Chen, J. Cell mechanics and mechanobiology in the intervertebral disc. *Spine (Phila. Pa. 1976).* **29**, 2710–2723 (2004).
14. Iu, J., Santerre, J. P. & Kandel, R. A. Inner and outer annulus fibrosus cells exhibit differentiated phenotypes and yield changes in extracellular matrix protein composition in vitro on a polycarbonate urethane scaffold. *Tissue Eng. - Part A* **20**, 3261–3269 (2014).
15. Bruehlmann, S. B., Rattner, J. B., Matyas, J. R. & Duncan, N. A. Regional variations in the cellular matrix of the annulus fibrosus of the intervertebral disc. *J. Anat.* **201**, 159–171 (2002).

16. Pattappa, G. *et al.* Diversity of intervertebral disc cells: Phenotype and function. *J. Anat.* **221**, 480–496 (2012).

17. Roberts, S., Urban, J. P. G., Evans, H. & Eisenstein, S. M. Transport properties of the human cartilage endplate in relation to its composition and calcification. *Spine* **21**, 415–420 (1996).

18. Daly, C., Ghosh, P., Jenkin, G., Oehme, D. & Goldschlager, T. A Review of Animal Models of Intervertebral Disc Degeneration: Pathophysiology, Regeneration, and Translation to the Clinic. *Biomed Res. Int.* **2016**, (2016).

19. Adams, M. A., McNally, D. S. & Dolan, P. 'Stress' distributions inside intervertebral discs. *J. Bone Jt. Surg.* **78**, 965–972 (1996).

20. Wang, C. *et al.* Advances in Magnetic Resonance Imaging for the Assessment of Degenerative Disc Disease of the Lumbar Spine. *Semin. Spine Surg.* **19**, 65–71 (2007).

21. Schizas, C., Kulik, G. & Kosmopoulos, V. Disc degeneration: Current surgical options. *Eur. Cells Mater.* **20**, 306–315 (2010).

22. Sakai, D. & Andersson, G. B. J. Stem cell therapy for intervertebral disc regeneration: obstacles and solutions. *Nat. Rev. Rheumatol.* **11**, 243–256 (2015).

23. Badylak, S. F. The extracellular matrix as a scaffold for tissue reconstruction. *Semin. Cell Dev. Biol.* **13**, 377–383 (2002).

24. Badylak, S. F. Xenogeneic extracellular matrix as a scaffold for tissue reconstruction. *Transpl. Immunol.* **12**, 367–377 (2004).

25. Bissell, M. J., Hall, H. G. & Parry, G. How does the extracellular matrix direct gene expression? *J. Theor. Biol.* **99**, 31–68 (1982).

26. Ingber, D. Extracellular matrix and cell shape: Potential control points for inhibition of angiogenesis. *J.Cell.Biochem.* **47**, 236–241 (1991).

27. Boudreau, N., Myers, C. & Bissell, M. J. From laminin to lamin: regulation of tissue-specific gene expression by the ECM. *Trends Cell Biol.* **5**, 1–4 (1995).

28. Yue, B. Biology of the Extracellular Matrix: An Overview. *J Glaucoma* **23**, 20–23 (2014).

29. Barczyk, M. & Carracedo, S. Integrins. *Cell Tissue Res.* **339**, 269–280 (2010).

30. Luo, T., Mohan, K., Iglesias, P. A. & Robinson, D. N. Molecular mechanisms of cellular mechanosensing. *Nat. Mater.* **12**, 1064–1071 (2013).

31. Frantz, C., Stewart, K. M. & Weaver, V. M. The extracellular matrix at a glance. *J. Cell Sci.* **123**, 4195–4200 (2010).

32. Aamodt, J. M. & Grainger, D. W. Extracellular Matrix-based Biomaterial Scaffolds and the Host Response. *Biomaterials* **4**, 68–82 (2016).

33. Kular, J. K., Basu, S. & Sharma, R. I. The extracellular matrix: Structure, composition, age-related differences, tools for analysis and applications for tissue engineering. *J. Tissue Eng.* **5**, (2014).

34. Ricard-Blum, S. The Collagen Family. *Cold Spring Harb. Perspect. Biol.* **3**, 1–19

(2011).

35. Gelse, K., Pöschl, E. & Aigner, T. Collagens - Structure, function, and biosynthesis. *Adv. Drug Deliv. Rev.* **55**, 1531–1546 (2003).

36. Knupp, C. & Squire, J. M. Molecular packing in network-forming collagens. *Adv. Protein Chem.* **70**, 375–403 (2005).

37. Pawelec, K. M., Best, S. M. & Cameron, R. E. Collagen: A network for regenerative medicine. *J. Mater. Chem. B* **4**, 6484–6496 (2016).

38. Shoulders, M. D. & Raines, R. T. Collagen Structure and Stability. *Annu. Rev. Biochem.* **78**, 929–958 (2009).

39. Orgel, J. P., Wess, T. J. & Miller, A. The in situ conformation and axial location of the intermolecular cross- linked non-helical telopeptides of type I collagen. *Structure* **8**, 137–142 (2000).

40. Shaw, L. M. & Olsen, B. R. FACIT collagens: diverse molecular bridges in extracellular matrices. *Trends Biochem. Sci.* **16**, 191–194 (1991).

41. Olsen, B. R. Collagen IX. *Int. J. Biochem. Cell Biol.* **29**, 555–558 (1997).

42. Cescon, M., Gattazzo, F., Chen, P. & Bonaldo, P. Collagen VI at a glance. *J. Cell Sci.* **128**, 3525–3531 (2015).

43. Debelle, L. & Tamburro, A. M. Elastin: Molecular description and function. *Int. J. Biochem. Cell Biol.* **31**, 261–272 (1999).

44. Patel, A., Fine, B., Sandig, M. & Mequanint, K. Elastin biosynthesis: The missing link in tissue-engineered blood vessels. *Cardiovasc. Res.* **71**, 40–49 (2006).

45. Halper, J. & Kjaer, M. Basic Components of Connective Tissues and Extracellular Matrix: Elastin, Fibrillin, Fibulins, Fibrinogen, Fibronectin, Laminin, Tenascins and Thrombospondins. in *Progress in Heritable Soft Connective Tissue Diseases* **802**, 31–47 (2014).

46. Gandhi, N. S. & Mancera, R. L. The structure of glycosaminoglycans and their interactions with proteins. *Chem. Biol. Drug Des.* **72**, 455–482 (2008).

47. Jackson, R. L., Busch, S. J. & Cardin, A. D. Glycosaminoglycans: Molecular properties, protein interactions, and role in physiological processes. *Physiol. Rev.* **71**, 481–539 (1991).

48. Hynes, R. O. Extracellular matrix: not just pretty fibrils. *Science (80-.).* **326**, 1216–1219 (2009).

49. Varki, A., Cummings, R., Esko, J. & Al, E. Proteoglycans and Glycosaminoglycans. in *Essentials of Glycobiology* (1999).

50. Stanley, P. What Have We Learned from Glycosyltransferase Knockouts in Mice? *J. Mol. Biol.* **428**, 3166–3182 (2016).

51. Mizumoto, S., Yamada, S. & Sugahara, K. Human genetic disorders and knockout mice deficient in glycosaminoglycan. *Biomed Res. Int.* **2014**, (2014).

52. Iozzo, R. V & Schaefer, L. Proteoglycan form and function: A comprehensive nomenclature of proteoglycans. *Matrix Biol.* **42**, 11–55 (2015).

53. Couchman, J. R. & Pataki, C. A. An Introduction to Proteoglycans and Their Localization. *J. Histochem. Cytochem.* **60**, 885–897 (2012).

54. Heinegård, D. Proteoglycans and more - From molecules to biology. *Int. J. Exp. Pathol.* **90**, 575–586 (2009).

55. Shylaja, M. & Seshadri, H. S. GLYCOPROTEINS: AN OVERVIEW. *Biochem. Educ.* **17**, 170–178 (1989).

56. Miyamoto, S., Katz, B.-Z., Lafrenie, R. & Yamada, K. M. Fibronectin and Integrins in Cell Adhesion, Signaling, and Morphogenesis. *Ann. New York Acad. Sci.* **23**, 119–129 (1998).

57. Zhu, J., Beamish, J. A., Tang, C., Kottke-Marchant, K. & Marchant, R. E. Extracellular matrix-like cell-adhesive hydrogels from RGD-containing poly(ethylene glycol) diacrylate. *Macromolecules* **39**, 1305–1307 (2006).

58. Francisco, A. T. *et al.* Injectable laminin-functionalized hydrogel for nucleus pulposus regeneration. *Biomaterials* **34**, 7381–7388 (2013).

59. Singh, P., Carraher, C. & Schwarzbauer, J. E. Assembly of Fibronectin Extracellular Matrix. *Annu. Rev. Cell Dev. Biol.* **26**, 397–419 (2010).

60. Ruoslahti, E. Rgd and Other Recognition Sequences for Integrins. *Annu. Rev. Cell Dev. Biol.* **12**, 697–715 (1996).

61. Akhmanova, M., Osidak, E., Domogatsky, S., Rodin, S. & Domogatskaya, A. Physical, Spatial, and Molecular Aspects of Extracellular Matrix of in Vivo Niches and Artificial Scaffolds Relevant to Stem Cells Research. *Stem Cells Int.* **2015**, (2015).

62. Tzu, J. & Marinkovich, M. P. Bridging structure with function: Structural, regulatory, and developmental role of laminins. *Int. J. Biochem. Cell Biol.* **40**, 199–214 (2008).

63. Chandran, P. L. & Horkay, F. Aggrecan, an Unusual Polyelectrolyte: Review of Solution Behavior and Physiological Implications. *Acta Biomater.* **8**, 3–12 (2013).

64. Whatley, B. R. & Wen, X. Intervertebral disc (IVD): Structure, degeneration, repair and regeneration. *Mater. Sci. Eng. C* **32**, 61–77 (2012).

65. Comper, W. D. & Laurent, T. C. Physiological functions of connective tissue polysaccharides. *Physiol. Rev.* **58**, 255–315 (1978).

66. Masuda, K., Oegema, T. R. & An, H. S. Growth factors and treatment of intervertebral disc degeneration. *Spine (Phila. Pa. 1976).* **29**, 2757–2769 (2004).

67. Hwang, P. Y., Chen, J., Jing, L., Hoffman, B. D. & Setton, L. A. The Role Of Extracellular Matrix Elasticity and Composition In Regulating the Nucleus Pulposus Cell Phenotype in the Intervertebral Disc: A Narrative Review. *J. Biomech. Eng.* **136**, 021010 (2014).

68. van Uden, S., Silva-Correia, J., Oliveira, J. M. & Reis, R. L. Current strategies for treatment of intervertebral disc degeneration: Substitution and regeneration possibilities. *Biomater. Res.* **21**, 1–19 (2017).

69. Frapin, L. *et al.* Lessons learned from intervertebral disc pathophysiology to guide

rational design of sequential delivery systems for therapeutic biological factors. *Adv. Drug Deliv. Rev.* (2019). doi:10.1016/j.addr.2019.08.007

70. Hardingham, T. E. Cartilage; Aggrecan-Link Protein-Hyaluronan Aggregates. (1998).

71. Ricardo, R.-P., Richardson, S. M. & Hoyland, J. A. An understanding of intervertebral disc development, maturation and cell phenotype provides clues to direct cell-based tissue regeneration therapies for disc degeneration. *Eur. spine J.* **23**, 1803–1814 (2014).

72. Hunter, C. J., Matyas, J. R. & Duncan, N. A. The notochordal cell in the nucleus pulposus: A review in the context of tissue engineering. *Tissue Eng.* **9**, 667–677 (2003).

73. Trout, J. J., Buckwalter, J. A. & Moore, K. C. Ultrastructure of the human intervertebral disc: II. Cells of the nucleus pulposus. *Anat. Rec.* **204**, 307–314 (1982).

74. McCann, M. R., Tamplin, O. J., Rossant, J. & Seguin, C. A. Tracing notochord-derived cells using a Noto-cre mouse: implications for intervertebral disc development. *Dis. Model. Mech.* **5**, 73–82 (2012).

75. Choi, K. S., Cohn, M. J. & Harfe, B. D. Identification of nucleus pulposus precursor cells and notochordal remnants in the mouse: Implications for disk degeneration and chordoma formation. *Dev. Dyn.* **237**, 3953–3958 (2008).

76. Erwin, W. M., Islam, D., Inman, R. D., Fehlings, M. G. & Tsui, F. W. L. Notochordal cells protect nucleus pulposus cells from degradation and apoptosis: implications for the mechanisms of intervertebral disc degeneration. *Arthritis Res. Ther.* **13**, R215 (2011).

77. Aguiar, D. J., Johnson, S. L. & Oegema, T. R. Notochordal cells interact with nucleus pulposus cells. *Exper Cell Res* **246**, 129–137 (1999).

78. Colombier, P., Clouet, J., Hamel, O., Lescaudron, L. & Guicheux, J. The lumbar intervertebral disc: From embryonic development to degeneration. *Jt. Bone Spine* **81**, 125–129 (2014).

79. Mwale, F. *et al.* Effect of a Type II Collagen Fragment on the Expression of Genes of the Extracellular Matrix in Cells of the Intervertebral Disc. *Open Orthop. J.* **2**, 1–9 (2008).

80. Erwin, W. M. The Notochord, Notochordal cell and CTGF/CCN-2: Ongoing activity from development through maturation. *J. Cell Commun. Signal.* **2**, 59–65 (2008).

81. Abreu, J. G., Ketpura, N. I., Reversade, B. & De Robertis, E. M. Connective-tissue growth factor (ctgf) modulates cell signalling by bmp and TGF-β. *Nat. Cell Biol.* **4**, 599–604 (2002).

82. Richardson, S. M. *et al.* Notochordal and nucleus pulposus marker expression is maintained by sub-populations of adult human nucleus pulposus cells through aging and degeneration. *Sci. Rep.* **7**, 1–11 (2017).

83. Risbud, M. V *et al.* Defining the Phenotype of Young Healthy Nucleus Pulposus

Cells: Recommendations of the Spine Research Interest Group at the 2014 Annual {ORS} Meeting. *J. Orthop. Res.* **33**, 283–293 (2014).

84. Liu, Z. *et al.* CD24 identifies nucleus pulposus progenitors/notochordal cells for disc regeneration. *J. Biol. Eng.* **12**, 1–15 (2018).

85. Kerr, G. J., Veras, M. A., Kim, M. K. M. & Séguin, C. A. Decoding the intervertebral disc: Unravelling the complexities of cell phenotypes and pathways associated with degeneration and mechanotransduction. *Semin. Cell Dev. Biol.* **62**, 94–103 (2017).

86. Vergroesen, P. P. A. *et al.* Mechanics and biology in intervertebral disc degeneration: A vicious circle. *Osteoarthr. Cartil.* **23**, 1057–1070 (2015).

87. Roughley, P. J. Biology of intervertebral disc aging and degeneration: Involvement of the extracellular matrix. *Spine (Phila. Pa. 1976).* **29**, 2691–2699 (2004).

88. Boxberger, J. I., Sounok, S., Yerramalli, C. S. & Elliott, D. M. Nucleus Pulposus Glycosaminoglycan Content Is Correlated with Axial Mechanics in Rat Lumbar Motion Segments. *J. Orthop. Res.* **24**, 1906–1915 (2006).

89. Le Maitre, C. L., Freemont, A. J. & Hoyland, J. A. Accelerated cellular senescence in degenerate intervertebral discs: A possible role in the pathogenesis of intervertebral disc degeneration. *Arthritis Res. Ther.* **9**, 1–12 (2007).

90. Inoue, N. & Espinoza Orías, A. Biomechanic of disc degeneraion. *Orthop. Clin. North Am.* **42**, 487–499 (2011).

91. Barbir, A. *et al.* Effects of Torsion on Intervertebral Disc Gene Expression and Biomechanics, Using a Rat Tail Model. *Spine (Phila. Pa. 1976).* **36**, 607–614 (2011).

92. Latridis, J. C., Godburn, K., Wuertz, K., Alini, M. & Roughley, P. J. Region-dependent aggrecan degradation patterns in the rat intervertebral disc are affected by mechanical loading in vivo. *Spine (Phila. Pa. 1976).* **36**, 203–209 (2011).

93. Jim, B., Steffen, T., Moir, J., Roughley, P. & Haglund, L. Development of an intact intervertebral disc organ culture system in which degeneration can be induced as a prelude to studying repair potential. *Eur. Spine J.* **20**, 1244–1254 (2011).

94. Roughley, P. J., Melching, L. I., Heathfield, T. F., Pearce, R. H. & Mort, J. S. The structure and degradation of aggrecan in human intervertebral disc. *Eur. Spine J.* **15**, 326–332 (2006).

95. Risbud, M. V. & Shapiro, I. M. Role of cytokines in intervertebral disc degeneration: Pain and disc content. *Nat. Rev. Rheumatol.* **10**, 44–56 (2014).

96. Handa, T. *et al.* Effects of hydrostatic pressure on matrix synthesis and matrix metalloproteinase production in the human lumbar intervertebral disc. *Spine* **22**, 1085–1091 (1997).

97. Mcnally, S. *et al.* Effects of hydrostatic pressure on matrix in different regions of the intervertebral synthesis disk. *J. Appl. Physiol.* **80**, 839–846 (1996).

98. Priyadarshani, P., Li, Y. & Yao, L. Advances in biological therapy for nucleus

pulposus regeneration. *Osteoarthr. Cartil.* **24**, 206–212 (2016).

99. Calderon, L. *et al.* Type II Collagen-Hyaluronan Hydrogel - A Step Towards A Scaffold For Intervertebral Disc Tissue Engineering. *Eur. Cells Mater.* **20**, 134–148 (2010).

100. Collin, E. C. *et al.* An injectable vehicle for nucleus pulposus cell-based therapy. *Biomaterials* **32**, 2862–2870 (2011).

101. Renani, H. B. *et al.* Determination and comparison of specifics of nucleus pulposus cells of human intervertebral disc in alginate and chitosan-gelatin scaffolds. *Adv. Biomed. Res.* **1**, 81 (2012).

102. Huang, Y. C., Hu, Y., Li, Z. & Luk, K. D. K. Biomaterials for intervertebral disc regeneration: Current status and looming challenges. *J. Tissue Eng. Regen. Med.* **12**, 2188–2202 (2018).

103. Allen, A. B., Priddy, L. B., Li, M. T. A. & Guldberg, R. E. Functional Augmentation of Naturally-Derived Materials for Tissue Regeneration. *Ann. Biomed. Eng.* **43**, 555–567 (2015).

104. Bowles, R. D. & Setton, L. A. Biomaterials for intervertebral disc regeneration and repair. *Biomaterials* **129**, 54–67 (2017).

105. Lutolf, M. P. & Hubbell, J. A. Synthetic biomaterials as instructive extracellular microenvironments for morphogenesis in tissue engineering. *Nat. Biotechnol.* **23**, 47–55 (2005).

106. Bhatia, S. K. *Biomaterials for Clinical Applications*. (Springer, New York, Dordrecht Heidelberg London, 2010). doi:10.1017/CBO9781107415324.004

107. Anderson, J. M., Rodriguez, A. & Chang, D. T. Foreign body reaction to biomaterials. *Semin. Immunol.* **20**, 86–100 (2008).

108. Bornstein, P. & Sage, E. H. Matricellular proteins : extracellular modulators of cell function. *Curr. Opin. Cell Biol.* **14**, 608–616 (2002).

109. Badylak, S. F., Freytes, D. O. & Gilbert, T. W. Extracellular matrix as a biological scaffold material: Structure and function. *Acta Biomater.* **5**, 1–13 (2009).

110. Gilbert, T. W., Freund, J. & Badylak, S. F. Quantification of DNA in biological scaffolds. *J Surg Res* **152**, 135–139 (2010).

111. Crapo, P. M., Gilbert, T. W. & Badylak, D. V. M. An Overview of tissue and whole organ decellularisation. *Biomaterials* **32**, 3233–3243 (2011).

112. Keane, T. J., Londono, R., Turner, N. J. & Badylak, S. F. Consequences of ineffective decellularization of biologic scaffolds on the host response. *Biomaterials* **33**, 1771–1781 (2012).

113. Keane, T. J., Saldin, L. T. & Badylak, S. F. Decellularization of mammalian tissues: preparing extracellular matrix bioscaffolds. in *Characterisation and Design of Tissue Scaffolds* (Elsevier Ltd, 2015). doi:10.1016/b978-1-78242-087-3.00004-3

114. Robb, K. P., Shridhar, A. & Flynn, L. E. Decellularized Matrices As Cell-Instructive Scaffolds to Guide Tissue-Specific Regeneration. *ACS Biomater. Sci.*

Eng. **4**, 3627–3643 (2018).

115. Chan, B. P. & Leong, K. W. Scaffolding in tissue engineering: General approaches and tissue-specific considerations. *Eur. Spine J.* **17**, (2008).

116. Mercuri, J. J., Gill, S. S. & Simionescu, D. T. Novel tissue-derived biomimetic scaffold for regenerating the human nucleus pulposus. *J. Biomed. Mater. Res. - Part A* **96 A**, 422–435 (2011).

117. Chan, L. K. Y. *et al.* Decellularized bovine intervertebral disc as a natural scaffold for xenogenic cell studies. *Acta Biomater.* **9**, 5262–5272 (2013).

118. Lin, X. *et al.* Decellularized allogeneic intervertebral disc: natural biomaterials for regenerating disc degeneration. *Oncotarget* **7**, 12121–12136 (2016).

119. Fernandez, C., Marionneaux, A., Gill, S. & Mercuri, J. Biomimetic nucleus pulposus scaffold created from bovine caudal intervertebral disc tissue utilizing an optimal decellularization procedure. *J. Biomed. Mater. Res. - Part A* **104**, 3093–3106 (2016).

120. Illien-Jünger, S. *et al.* Development of a bovine decellularized extracellular matrix-biomaterial for nucleus pulposus regeneration. *J. Orthop. Res.* **34**, 876–888 (2016).

121. Wachs, R. A. *et al.* Creation of an injectable in situ gelling native extracellular matrix for nucleus pulposus tissue engineering. *Spine J.* **17**, 435–444 (2017).

122. Chan, L. K. Y. *et al.* Decellularized bovine intervertebral disc as a natural scaffold for xenogenic cell studies. *Acta Biomater.* **9**, 5262–5272 (2013).

123. Buwalda, S. J. *et al.* Hydrogels in a historical perspective: From simple networks to smart materials. *J. Control. Release* **190**, 254–273 (2014).

124. Jabbari, E., Leijten, J., Xu, Q. & Khademhosseini, A. The matrix reloaded: The evolution of regenerative hydrogels. *Mater. Today* **19**, 190–196 (2016).

125. Geckil, H., Zhang, X., Moon, S. & Demirci, U. Engineering hydrogels as extracellular matrix mimics R eview. *Lab Chip* **11**, 469–484 (2013).

126. Zhu, J. Design properties of hydrogel tissue-engineering scaffolds. *Expert Rev. Med. Devices* **8**, 607–626 (2012).

127. Hou, Q., De Bank, P. A. & Shakesheff, K. M. Injectable scaffolds for tissue regeneration. *J. Mater. Chem.* **14**, 1915–1923 (2004).

128. Oryan, A., Kamali, A., Moshiri, A., Baharvand, H. & Daemi, H. Chemical crosslinking of biopolymeric scaffolds: Current knowledge and future directions of crosslinked engineered bone scaffolds. *Int. J. Biol. Macromol.* **107**, 678–688 (2018).

129. Thorpe, A. A., Boyes, V. L., Sammon, C. & Le Maitre, C. L. Thermally triggered injectable hydrogel, which induces mesenchymal stem cell differentiation to nucleus pulposus cells: Potential for regeneration of the intervertebral disc. *Acta Biomater.* **36**, 99–111 (2016).

130. Thorpe, A. A. *et al.* Thermally triggered hydrogel injection into bovine intervertebral disc tissue explants induces differentiation of mesenchymal stem

cells and restores mechanical function. *Acta Biomater.* **54**, 212–226 (2017).

131. Tsaryk, R. *et al.* Biological performance of cell-encapsulated methacrylated gellan gum-based hydrogels for nucleus pulposus regeneration. *J. Tissue Eng. Regen. Med.* **11**, 637–648 (2017).

132. Silva-Correia, J. *et al.* Biocompatibility evaluation of ionic- and photo-crosslinked methacrylated gellan gum hydrogels: In vitro and in vivo study. *Adv. Healthc. Mater.* **2**, 568–575 (2013).

133. Liu, X. *et al.* A Method for Characterising Human Intervertebral Disc Glycosaminoglycan Disaccharides using Liquid Chromatography-Mass Spectrometry with Multiple Reaction Monitoring. *Eur. Cells Mater.* **35**, 117–131 (2018).

134. Uebelhart, D. Clinical review of chondroitin sulfate in osteoarthritis. *Osteoarthr. Cartil.* **16**, 19–21 (2008).

135. Ronca, F., Palmieri, L., Panicucci, P. & Ronca, G. Anti-inflammatory activity of chondroitin sulfate. *Osteoarthr. Cartil.* **6**, 14–21 (1998).

136. Du Souich, P., García, A. G., Vergés, J. & Montell, E. Immunomodulatory and anti-inflammatory effects of chondroitin sulphate. *J. Cell. Mol. Med.* **13**, 1451–1463 (2009).

137. Wang, D. A. *et al.* Multifunctional chondroitin sulphate for cartilage tissue-biomaterial integration. *Nat. Mater.* **6**, 385–392 (2007).

138. Li, Q. *et al.* Photocrosslinkable polysaccharides based on chondroitin sulfate. *J. Biomed. Mater. Res. - Part A* **68**, 28–33 (2004).

139. Arthi, S., Gillies, E., Amsden, B. G. & Flynn, L. E. Composite Bioscaffolds Incorporating Decellularized ECM as a Cell-Instructive Component Within Hydrogels as In Vitro Models and Cell Delivery Systems. in *Methods in Molecular Biology* 257–284 (2017). doi:10.1007/7651

140. Brown, C. F. C. *et al.* Effect of decellularized adipose tissue particle size and cell density on adipose-derived stem cell proliferation and adipogenic differentiation in composite methacrylated chondroitin sulphate hydrogels. *Biomed. Mater.* **10**, (2015).

141. Cheung, H. K. *et al.* Composite hydrogel scaffolds incorporating decellularized adipose tissue for soft tissue engineering with adipose-derived stem cells. *Biomaterials* **35**, 1914–1923 (2014).

142. Brown, C. F. C. *et al.* Effect of decellularized adipose tissue particle size and cell density on adipose-derived stem cell proliferation and adipogenic differentiation in composite methacrylated chondroitin sulphate hydrogels. *Biomed. Mater.* **10**, 45010 (2015).

143. Scheil, S. *et al.* Genome-wide analysis of sixteen chordomas by comparative genomic hybridization and cytogenetics of the first human chordoma cell line, U-CHI. *Genes Chromosom. Cancer* **32**, 203–211 (2001).

144. Fujita, N. *et al.* Chordoma-derived cell line U-CH1-N recapitulates the biological properties of notochordal nucleus pulposus cells. *J. Orthop. Res.* **34**, 1341–1350

(2016).

145. Lehtonen, E., Stefanovic, V. & Saraga-Babic, M. Changes in the expression of intermediate filaments and desmoplakins during development of human notochord. *Differentiation* **59**, 43–49 (1995).

146. Salisbury, J. Demonstration of cytokeratins and an epithelial membrane antigen in chordomas and human fetal notochord. *Am. J. Surg. Pathol.* **9**, 791–797 (1985).

147. Graham, M. E., Gratzer, P. F., Bezuhly, M. & Hong, P. Development and characterization of decellularized human nasoseptal cartilage matrix for use in tissue engineering. *Laryngoscope* **126**, 2226–2231 (2016).

148. Yu, C., Kornmuller, A., Brown, C., Hoare, T. & Flynn, L. E. Decellularized adipose tissue microcarriers as a dynamic culture platform for human adipose-derived stem/stromal cell expansion. *Biomaterials* **120**, 66–80 (2017).

149. Morissette Martin, P., Grant, A., Hamilton, D. W. & Flynn, L. E. Matrix composition in 3-D collagenous bioscaffolds modulates the survival and angiogenic phenotype of human chronic wound dermal fibroblasts. *Acta Biomater.* **83**, 199–210 (2019).

150. Antoine, E. E., Vlachos, P. P. & Rylander, M. N. Review of Collagen I Hydrogels for Bioengineered Tissue Microenvironments: Characterization of Mechanics, Structure, and Transport. *Tissue Eng. Part B Rev.* **20**, 683–696 (2014).

151. Sukarto, A., Yu, C., Flynn, L. E. & Amsden, B. G. Co-delivery of adipose-derived stem cells and growth factor-loaded microspheres in RGD-grafted N-methacrylate glycol chitosan gels for focal chondral repair. *Biomacromolecules* **13**, 2490–2502 (2012).

152. Yuan, M., Pai, P.-J., Liu, X., Lam, H. & Chan, B. P. Proteomic Analysis of Nucleus Pulposus Cell-derived Extracellular Matrix Niche and Its Effect on Phenotypic Alteration of Dermal Fibroblasts. *Sci. Rep.* **8**, 1512 (2018).

153. Xu, H. *et al.* Comparison of decellularization protocols for preparing a decellularized porcine annulus fibrosus scaffold. *PLoS One* **9**, 1–14 (2014).

154. Zhou, X. *et al.* Injectable decellularized nucleus pulposus-based cell delivery system for differentiation of adipose-derived stem cells and nucleus pulposus regeneration. *Acta Biomater.* **81**, 115–128 (2018).

155. Akbari Zahmati, A. H., Alipoor, R., Rezaei Shahmirzadi, A., Khori, V. & Abolhasani, M. M. Chemical Decellularization Methods and Its Effects on Extracellular Matrix. *Intern. Med. Med. Investig. J.* **2**, 76 (2017).

156. Mercuri, J. J. *et al.* Regenerative Potential of Decellularized Porcine *Nucleus Pulposus* Hydrogel Scaffolds: Stem Cell Differentiation, Matrix Remodeling, and Biocompatibility Studies. *Tissue Eng. Part A* **19**, 952–966 (2013).

157. Vincent, K. *et al.* Aging of mouse intervertebral disc and association with back pain. *Bone* **123**, 246–259 (2019).

158. Mohanty, S., Pinelli, R., Pricop, P., Albert, T. J. & Dahia, C. L. Chondrocyte-like nested cells in the aged intervertebral disc are late-stage nucleus pulposus cells. *Aging Cell* e13006 (2019). doi:10.1111/acel.13006

159. Novais, E. J., Diekman, B. O., Shapiro, I. M. & Risbud, M. V. p16 Ink4a deletion in cells of the intervertebral disc affects their matrix homeostasis and senescence associated secretory phenotype without altering onset of senescence. *Matrix Biol.* **82**, 1–17 (2019).

160. Zhang, Y. *et al.* Early onset of disc degeneration in SM/J mice is associated with changes in ion transport systems and fibrotic events. *Matrix Biol.* **70**, 123–139 (2018).

161. Burk, J. *et al.* Freeze-Thaw Cycles Enhance Decellularization of Large Tendons. *Tissue Eng. Part C Methods* **20**, 276–284 (2014).

162. Kim, I. L., Khetan, S., Baker, B. M., Chen, C. S. & Burdick, J. A. Fibrous hyaluronic acid hydrogels that direct MSC chondrogenesis through mechanical and adhesive cues. *Biomaterials* **34**, 5571–5580 (2014).

163. Dado, D. & Levenberg, S. Cell-scaffold mechanical interplay within engineered tissue. *Semin. Cell Dev. Biol.* **20**, 656–664 (2009).

164. Breuls, R. G. M., Jiya, T. U. & Smit, T. H. Scaffold Stiffness Influences Cell Behavior: Opportunities for Skeletal Tissue Engineering. *Open Orthop. J.* **2**, 103–109 (2008).

165. Liu, Y., Rahaman, M. N. & Bal, B. S. Modulating notochordal differentiation of human induced pluripotent stem cells using natural nucleus pulposus tissue matrix. *PLoS One* **9**, e100885 (2014).

166. Liu, Y., Fu, S., Rahaman, M. N., Mao, J. J. & Bal, B. S. Native nucleus pulposus tissue matrix promotes notochordal differentiation of human induced pluripotent stem cells with potential for treating intervertebral disc degeneration. *J. Biomed. Mater. Res. - Part A* **103**, 1053–1059 (2015).

167. Potier, E., de Vries, S., van Doeselaar, M. & Ito, K. Potential application of notochordal cells for intervertebral disc regeneration: An in vitro assessment. *Eur. Cells Mater.* **28**, 68–81 (2014).

168. Arkesteijn, I. I. T. *et al.* Effect of coculturing canine notochordal, nucleus pulposus and mesenchymal stromal cells for intervertebral disc regeneration. *Arthritis Res. Ther.* **17**, 1–12 (2015).

169. Saggese, T., Redey, P. & McGlashan, S. R. Same-species phenotypic comparison of notochordal and mature nucleus pulposus cells. *Eur. Spine J.* **24**, 1976–1985 (2015).

170. Pelham, R. J. & Wang, Y.-L. Cell locomotion and focal adhesions are regulated by substrate flexibility. *Proc. Natl. Acad. Sci.* **94**, 13661–13665 (1997).

171. Peyton, S. R. *et al.* Marrow-Derived Stem Cell Motility in 3D Synthetic Scaffold Is Governed by Geometry Along With Adhesivity and Stiffness. *Biotechnol. Bioeng.* **108**, 1181–1193 (2011).

172. Lawson, L. Y. & Harfe, B. D. Developmental mechanisms of intervertebral disc and vertebral column formation. *WIREs Dev. Biol.* **6**, e283 (2017).

173. Sive, J. I. *et al.* Expression of chondrocyte markers by cells of normal and degenerate intervertebral discs. *J. Clin. Pathol. - Mol. Pathol.* **55**, 91–97 (2002).

174. Sekiya, I. *et al.* SOX9 enhances aggrecan gene promoter/enhancer activity and is up- regulated by retinoic acid in a cartilage-derived cell line, TC6. *J. Biol. Chem.* **275**, 10738–10744 (2000).

175. Bi, W., Deng, J. M., Zhang, Z., Behringer, R. R. & Crombrugghe, B. De. Sox9 is required for cartilage formation. *Nat. Genet.* **22**, 85–89 (1999).

176. Séguin, C. A., Chan, D., Dahia, C. L. & Gazit, Z. Latest advances in intervertebral disc development and progenitor cells. *JOR Spine* **1**, e1030 (2018).

177. Hata, R. I., Akai, J. & Kimura, A. Cell position-dependent reciprocal feedback regulation of type I collagen gene expression in cultured human skin fibroblasts. *Cell Biol. Int.* **22**, 185–191 (1998).

178. Eyre, D. R. & Muir, H. Quantitative analysis of types I and II collagens in human intervertebral discs at various ages. *Biochim. Biophys. Acta* **492**, 29–42 (1977).

179. Cheung, H. K. *et al.* Composite hydrogel scaffolds incorporating decellularized adipose tissue for soft tissue engineering with adipose-derived stem cells. *Biomaterials* **35**, 1914–1923 (2014).

180. Zhang, Z. C. *et al.* Differentiation of adipose-derived stem cells toward nucleus pulposuslike cells induced by hypoxia and a three-dimensional chitosanalginate gel scaffold in vitro. *Chin. Med. J. (Engl).* **127**, 314–321 (2014).

181. Lee, C. R. *et al.* A phenotypic comparison of intervertebral disc and articular cartilage cells in the rat. *Eur. Spine J.* **16**, 2174–2185 (2007).

Appendix: Supplemental Figures

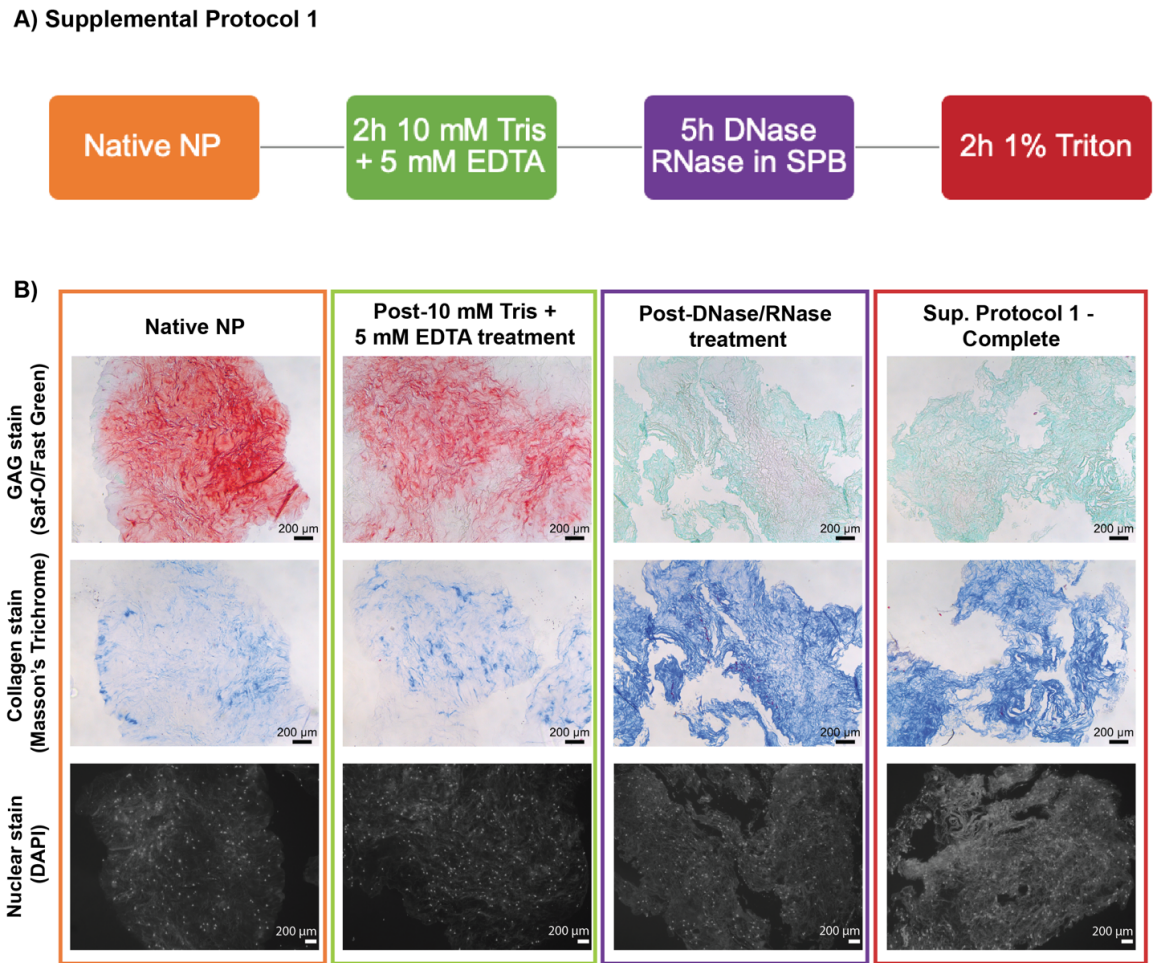

Supplemental Figure 1: Histological analysis of tissue processed with decellularization Supplemental Protocol 1. A) Protocol overview, with sampling points shown in colour. Acronyms: Tris = tris (hydroxymethyl)aminomethane, EDTA = ethylenediaminetetraacetic acid, SPB = Sorensen's phosphate buffer. **B)** Representative safranin-O/fast green staining of GAG (pink) and collagen (blue-green), Masson's trichrome staining of collagen (blue), and DAPI nuclear staining (white), (n=3, serial sections throughout the whole tissue sample). Scale bars = 200 µm. This study demonstrated that the freeze-thaw cycles were important for the effective removal of nuclei from the tissues at the end of processing.

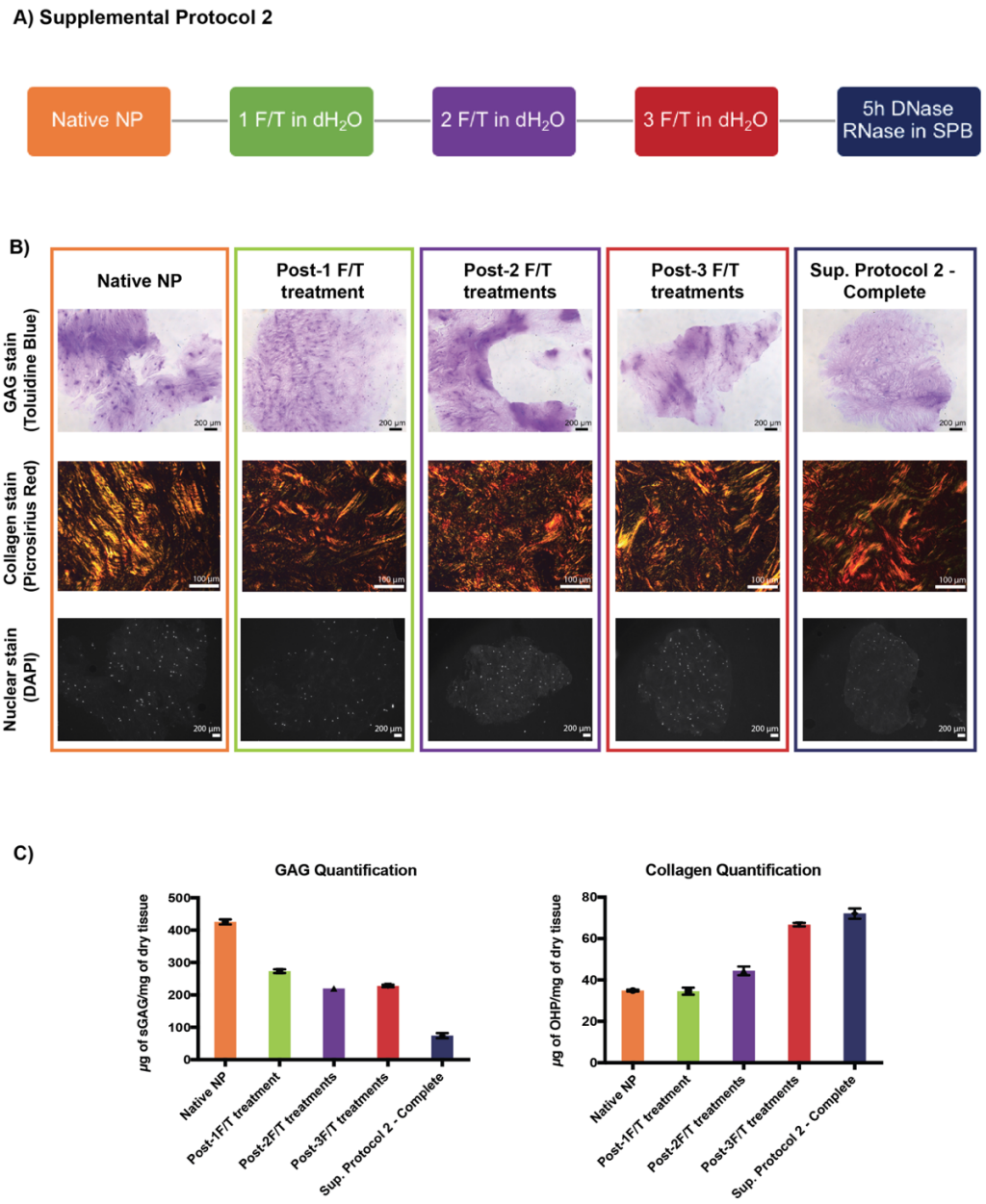

Supplemental Figure 2: Histological and quantitative analyses of tissue processed with decellularization Supplemental Protocol 2. A) Protocol overview, with sampling points shown in colour. Acronyms: F/T = freeze-thaw cycle, SPB = Sorensen's phosphate buffer. **B)** Representative Toluidine blue staining of GAG (purple), Picrosirius red staining of collagen (orange), and DAPI nuclear staining (white), (n=3, serial sections throughout the whole tissue sample). Scale bars for Toluidine blue and DAPI staining = 200 µm. Scale bars for Picrosirius red staining = 100 µm. **C)** Quantitative biochemical analysis of the processed DNP and native tissues including sGAG content as determined by the DMMB assay, hydroxyproline content as a measure of total collagen content by the hydroxyproline assay, and dsDNA content as determined by the PicoGreen assay (n=3, N=1 for all assays). Data are presented as mean ± SD. This study demonstrated that GAG was lost with each freeze-thaw cycle.

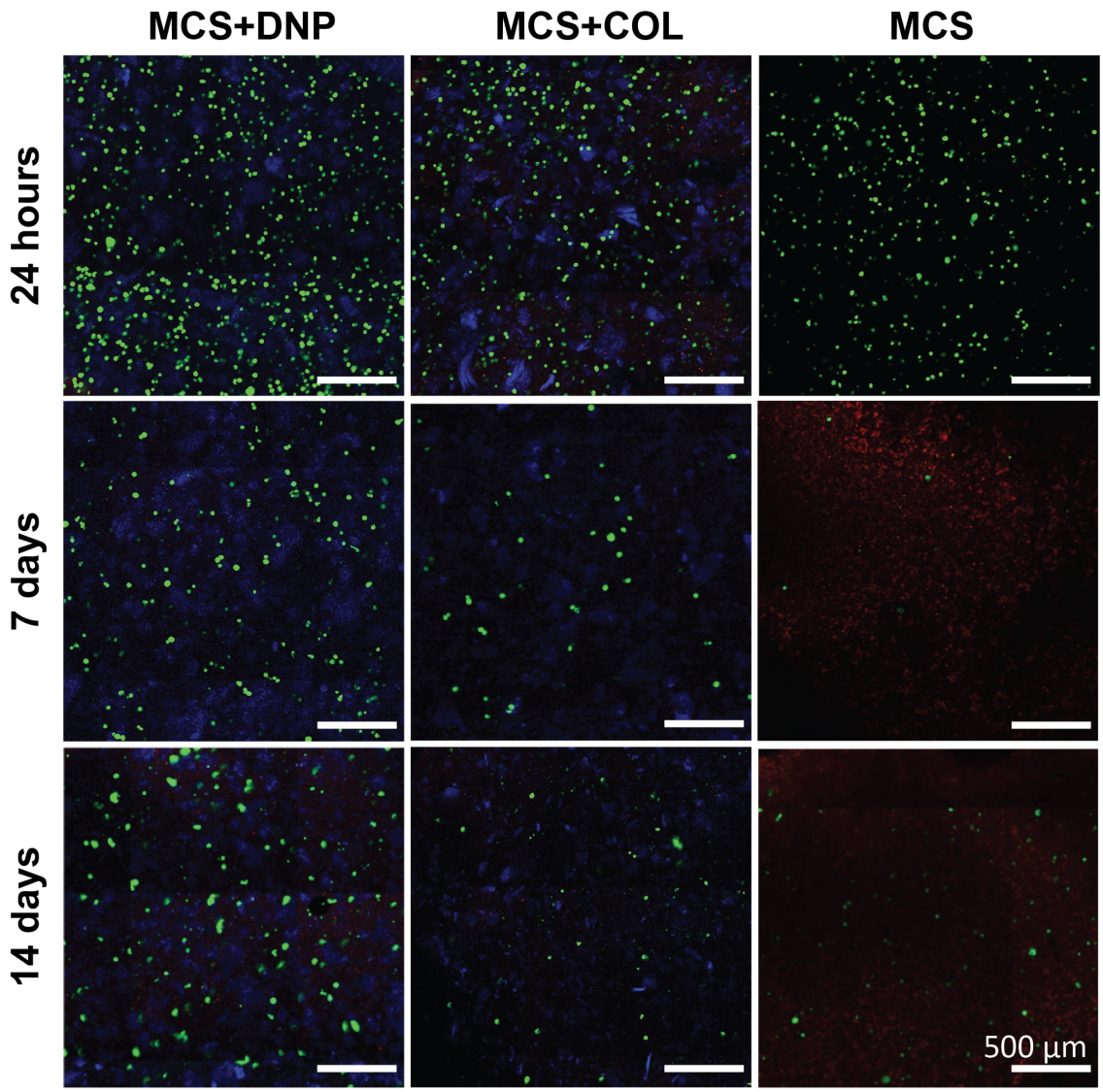

Supplemental Figure 3: Representative confocal microscopy images showing LIVE/DEAD® staining of U-CH1 cells encapsulated within the MCS ± DNP/COL hydrogel constructs through thermal crosslinking and cultured *in vitro* over 14 days. Live cells were stained with calcein-AM (green) and dead cells were stained with ethidium homodimer-1 (red). The DNP and COL particles appear blue due to ECM autofluorescence. Images were captured at a depth of ~100 µm. Scale bars = 500 µm.

Supplemental Table 1: All iterations of treatment steps tested to decellularize bovine nucleus pulposus and their results and conclusions. * = sampling points. Acronyms: ABAM = antibiotic-antimycotic, PMSF = phenylmethylsulfonyl fluoride, NP = nucleus pulposus, ECM = extracellular matrix, GAGs = glycosaminoglycans, F/T = freeze-thaw cycles, Tris = tris(hydroxymethyl)aminomethane, EDTA = ethylenediamine-tetraacetic acid, SPB = Sorensen's phosphate buffer, TBP = tributyl phosphate, PBS = phosphate buffered saline, dH_2O = deionized water, DMMB = dimethylmethylene blue, dsDNA = double stranded DNA. All solutions, with the exception of the enzymatic digestion steps, were supplemented with 1 v/v% ABAM and 0.27 mM PMSF; the enzymatic digestions (15,000 U DNase Type II and 12.5 mg RNase Type III) were supplemented with only 1 v/v% ABAM. Solution volumes were kept constant at 100 mL of solution in a 500 mL tissue tub for all treatment steps, with ~15 g of NP per 100 mL. Freezing was performed at -80°C overnight and thaw at 37°C with 125 rpm for all freeze-thaw cycles. All incubations were performed at 37°C with 125 rpm unless noted otherwise. Tissues were rinsed in dH_2O for 3 x 30 min and PBS for 3 x 30 min (iterations 1-8), or only PBS for 3 x 30 min (iterations 9-11) at room temperature under 125 rpm agitation prior to collection.

Iteration	Treatment Steps	Summary of Results & Conclusions
1 Presented as "Protocol 1" in Thesis (e.g. Fig. 3.1)	NP sectioned into quarters following dissection*. 1. **3 F/T** in 10 mM Tris + 5 mM EDTA. 2. 10 mM Tris + 5 mM EDTA for 24 h (37°C; 125 rpm). 3. **2% Triton X-100** in 1.5M KCl + 50 mM Tris for 48 h (37°C; 125 rpm for the first 24 h, 200 rpm for the next 24 h). 4. PBS rinse for 3 x 30 min (37°C; 200 rpm). 5. **DNase RNase** in SPB for 5 h (37°C; 200 rpm). 6. **1% TBP** in 50 mM Tris for 72 h (37°C; 200 rpm). 7. dH_2O rinse for 3 x 30 min (37°C; 200 rpm). 8. PBS rinse for 3 x 30 min (37°C; 200 rpm). 9. 50 mM Tris for 48 h (37°C; 200 rpm)*. Replacing with fresh solution following each thaw and every ~12 h.	Effects on NP ECM: • **GAGs:** no detectable GAGs in processed NP visualized by safranin-O/fast green staining. • **Collagen:** darker staining for collagen in processed NP visualized by Masson's trichrome stain. • **Nuclei:** no detectable nuclei in processed NP visualized by DAPI fluorescent stain. **Conclusions:** Treatments in iteration 1 reduced nuclei, but resulted in a substantial qualitative loss in GAG in the processed NP. **Plan:** In an attempt to preserve more GAG, explore effects of reduced treatment time by eliminating the 24 h incubation in 10 mM Tris + 5 mM EDTA and reducing the 1% TBP incubation from 72 h to 18 h. Explore effects of 1% Triton X-100 detergent incubation, since Triton may better preserve more soluble ECM components as compared to TBP. Perform incubations in future iterations at 125 rpm as tissues had greater aggregation at 200 rpm. *Note:* stains used to visualize GAG, collagen and nuclei remain consistent in following iterations unless specified.

2	NP sectioned into eighths to increase surface area treated and reduce variability*. 1. **3 F/T** in 10 mM Tris + 5 mM EDTA. 2. 10 mM Tris + 5 mM EDTA for 24 h. 3. **2% Triton X-100** in 1.5M KCl + 50 mM Tris for 48 h. 4. PBS rinse for 3 x 30 min. 5. **DNase RNase** in SPB for 5 h*, then samples split equally into: ⇒ *Iteration 2A:* 6. **1% TBP** in 50 mM Tris for 18 h*. ⇒ *Iteration 2B:* 6. **1% Triton X-100** for 18 h*. Replacing with fresh solution following each thaw, and every ~12 h.	Effects on NP ECM: • **GAGs:** qualitative loss in processed NP post-DNase/RNase treatment. No detectable staining in NP processed through both iteration 2A and 2B. • **Collagen:** similar qualitative structure between native NP and post-DNase/RNase treatment processed NP. Collagen distribution appeared disrupted (looser-looking structure) in NP processed through 2A and 2B. • **Nuclei:** Qualitative reduction in nuclei in NP throughout processing. **Conclusions:** treatment with TBP and Triton had similar qualitative effects on NP ECM. Triton X-100 detergent was selected for subsequent testing since it has previously been reported to better preserve protein–protein interactions that may be disrupted with the use of TBP in other tissues[1]. **Plan:** Eliminate the 2% Triton wash before DNase/RNase treatment and explore effects of reduced 1% Triton incubation time from 18 h to 2 h in an effort to preserve more GAGs.
3	NP sectioned into eighths*. 1. **3 F/T** in 10 mM Tris + 5 mM EDTA.* 2. PBS rinse for 3 x 30 min. 3. **DNase RNase** in SPB for 5 h*, 4. **1% Triton X-100** for 2 h*. Replacing with fresh solution following each thaw.	Effects on NP ECM: • **GAGs:** qualitatively increased loss of GAGs with each added treatment step. No detectable GAGs in processed NP following detergent treatment. • **Collagen:** similar qualitative structure and staining in processed NP before the DNase/RNase treatment step. The intensity of staining qualitatively increased in the processed NP following treatment with 1% Triton. • **Nuclei:** no noticeable loss of nuclei following F/T. Marked decrease in visible nuclei post-DNase/RNase treatment.

[1] Keane, T. J., Saldin, L. T. & Badylak, S. F. Decellularization of mammalian tissues: preparing extracellular matrix bioscaffolds. in *Characterisation and Design of Tissue Scaffolds* (Elsevier Ltd, 2015). doi:10.1016/b978-1-78242-087-3.00004-3

		Conclusions: GAG is lost with each added treatment, and the F/T did not reduce visible nuclei. **Plan:** Explore effects of incubation in 10 mM Tris + 5 mM EDTA to determine the importance of F/T.
4 Presented in the thesis as "Supplemental Protocol 1" in Supplemental Fig. 1	NP sectioned into eighths*. 1. 10 mM Tris + 5 mM EDTA for 2 h* 2. PBS rinse for 3 x 30 min. 3. **DNase RNase** in SPB for 5 h* 4. **1% Triton X-100** for 2 h*.	Effects on NP ECM: • **GAGs:** increased qualitative loss with each added treatment. No detectable positive staining in processed NP treated with 1% Triton. • **Collagen:** similar structure and staining intensity post-incubation in 10 mM Tris + 5 mM EDTA. Qualitatively increased staining intensity post-DNase/RNase and 1% Triton detergent treatments. • **Nuclei:** no qualitative reduction of nuclei in NP processed through all treatments. **Conclusions:** F/T are important in cell lysis and removal of nuclei. **Plan:** Explore effects of reducing 3 F/T to 2 F/T in an effort to preserve more GAGs.
5	NP sectioned into eighths*. 1. **2 F/T** in 10 mM Tris + 5 mM EDTA* 2. PBS rinse for 3 x 30 min. 3. **DNase RNase** in SPB for 5 h*, 4. **1% Triton X-100** for 2 h*. Replacing with fresh solution following each thaw.	Effects on NP ECM: • **GAGs:** increased qualitative and quantitative loss with each added treatment. • **Collagen:** quantitative increasing trend of relative collagen content in keeping with the quantitative loss of GAGs. • **Nuclei:** detectable nuclei in processed NP post-detergent treatment. **Conclusions:** 2 F/T in 10 mM Tris + 5 mM EDTA was found to be insufficient in reducing nuclei in NP segments at this size range. **Plan:** reduce size of NP sections in an effort to enhance cell extraction. *Notes:* The safranin-o/fast green stained samples in iteration 5 appeared to lose almost all GAGs post-F/T, whereas the quantitative results by DMMB assay showed ~72% retention of sulphated GAGs post-F/T. The staining intensity visualized by toluidine blue

		was in keeping with the quantitative trends in GAGs within processed NP. Thus, toluidine blue staining was selected to visualize GAGs in subsequent treatments. Total collagen content was quantified by hydroxyproline assay.
6	NP biopsy punched into 5 mm sections to increase surface area treated and reduce variability in processed NP*. 1. **3 F/T** in 10 mM Tris + 5 mM EDTA, then samples split equally into: ⇒ *Iteration 6A:* 2. 10 mM Tris + 5 mM EDTA for 18 h*. ⇒ *Iteration 6B:* 2. **DNase RNase** in SPB for 5 h*. ⇒ *Iteration 6C:* 2. **DNase RNase** in SPB for 5 h. 3. **1% Triton X-100** for 2 h*. Replacing with fresh solution following each thaw.	Effects on NP ECM: • **GAGs:** Processed NP showed a marked qualitative decrease in staining intensity, with Iteration 6B having better qualitative preservation of GAGs. Quantitative results revealed ~10% greater loss of sulphated GAGs in NP processed through 6A. • **Collagen:** similar qualitative structure in NP processed though 6A-C, with an increasing quantitative trend of relative collagen content. • **Nuclei:** qualitative reduction in NP processed through 6A-C. **Conclusions:** the greater quantitative loss of GAGs in 6A may indicate that the EDTA in the solution may destabilize matrix. **Plan:** Investigate the effects of performing F/T in dH_2O versus 10 mM Tris + 5 mM EDTA.
7 Presented in the thesis as "Protocol 2" in Fig. 3.2	NP biopsy punched and sectioned into 2 mm x 2 mm to further increase the surface area and reduce variability*. Native NP samples split equally into: ⇒ *Iteration 7A:* 1. **3 F/T** in **dH_2O**. 2. **DNase RNase** in SPB for 5 h*. 3. **1% Triton X-100** for 2 h*. ⇒ *Iteration 7B:* 1. **3 F/T** in **10 mM Tris + 5 mM EDTA**. 2. **DNase RNase** in SPB for 5 h. 3. **1% Triton X-100** for 2 h*.	Effects on NP ECM: • **GAGs:** increased qualitative and quantitative loss with each added treatment as seen previously, with higher qualitative GAG retention in NP processed through iteration 7A as compared to 7B (~17% versus ~14% retention, respectively). • **Collagen:** similar distribution between NP processed through 7A and 7B, with an increasing quantitative trend of relative collagen content within processed tissues. • **Nuclei:** marked qualitative and quantitative decrease in nuclear content in NP processed through both 7A and 7B, with greater reduction of dsDNA in 7A as compared to 7B (~77% versus ~61% reduction, respectively). Interestingly, the post-DNase/RNase

	Replacing with fresh solution following each thaw.	processed NP in 7A had similar levels of qualitative and quantitative nuclei as compared to the processed NP post-detergent treatment. **Conclusions:** F/T in dH_2O had a better qualitative preservation of GAG and more effectively reduced dsDNA content as compared to F/T in 10 mM Tris + 5 mM EDTA. Treatment with DNase/RNase following 3 F/T in dH_2O effectively reduces nuclear content while better preserving GAG as compared to the added Triton detergent treatment. **Plan:** Omit the detergent treatment and explore effects of each F/T in dH_2O. *Note:* dsDNA content was determined by PicoGreen assay. Since staining for collagen by Masson's trichrome was very faint and collagen distribution was difficult to visualize, subsequent testing employed the use of picrosirius red staining to better visualized collagen.
8 Presented in the thesis as "Supplemental Protocol 2" in Supplemental Fig. 2	NP biopsy punched and sectioned into 2 mm x 2 mm*. 1. **3 F/T** in dH_2O***. 2. **DNase RNase** in SPB for 5 h*. ***sampling following each thaw. Replacing with fresh solution following each thaw.	Effects on NP ECM: • **GAGs:** qualitative and quantitative decrease with each F/T, and following treatment with DNase/RNase. • **Collagen:** similar distribution and increasing quantitative trend with each added treatment. • **Nuclei:** noticeable reduction in nuclei following treatment with DNase/RNase. No noticeable reduction in nuclei following each F/T. **Conclusions:** GAG lost with each F/T. **Plan:** Explore effects of reducing F/T from 3 to 1, and explore the effects of enzymatic digestion in dH_2O versus SPB in an effort to preserve more GAGs.
9	NP biopsy punched and sectioned into 2 mm x 2 mm*.	Effects on NP ECM: • **GAGs:** greater qualitative and quantitative loss in NP processed through 9A as compared to 9B (~22%

	1. **1 F/T** in dH_2O*, then samples split equally into: ⇒ *Iteration 9A:* 2. **DNase RNase** in **dH_2O** for 5 h*. ⇒ *Iteration 9B:* 2. **DNase RNase** in **SPB** for 5 h*.	versus ~27% preservation, respectively). • **Collagen:** similar qualitative distribution and an increasing quantitative trend of collagen content consistent with the loss of GAGs. • **Nuclei:** marked reduction of dsDNA content in NP processed through 9A and 9B (~85% versus ~90% reduction, respectively),with some visible nuclei present. Treatment with 1 F/T alone resulted in an ~44% reduction in dsDNA content. **Conclusions:** enzymatic digestion in SPB better preserves GAGs and reduces nuclear content as compared to digestion performed in dH_2O. The 1 F/T alone is insufficient in reducing nuclear content. **Plan:** Investigate the effects of reducing digestion incubation time from 5 h to 2 h, and explore the effects of PBS as the digestion solution.
10 Presented in the thesis as "Protocol 3" in Fig. 3.3	NP biopsy punched and sectioned into 2 mm x 2 mm*. 1. **1 F/T** in dH_2O*, then samples split equally into: ⇒ *Iteration 10A:* 2. **DNase RNase** in **SPB** for **5 h***. ⇒ *Iteration 10B:* 2. **DNase RNase** in **SPB** for **2 h***. ⇒ *Iteration 10C:* 2. **DNase RNase** in **PBS** for **2 h***.	Effects on NP ECM: • **GAGs:** increased quantitative and qualitative preservation in NP processed with 10B and 10C as compared to 10A, with similar levels of GAG in 10B and 10C. • **Collagen:** similar qualitative distribution and an increasing quantitative trend of collagen content consistent with the loss of GAGs • **Nuclei:** some visible nuclei present in NP, with 10A containing qualitatively fainter staining for nuclei. Quantitative results showed that NP processed through 10A and 10B has a greater reduction of dsDNA content than 10C, with similar levels between 10A and 10B (~88% and ~89% reduction, respectively). **Conclusions:** enzymatic digestion in SPB for 2 h better preserved GAG while effectively reducing nuclear content as compared to incubation for 5 h in SPB, as well as for 2 h in PBS.

		Plan: In a final attempt to further preserve GAG, the effects of shortening the enzymatic digestion step to 1 h was explored.
11	NP biopsy punched and sectioned into 2 mm x 2 mm*. 1. **1 F/T** in dH_2O, then samples split equally into: ⇒ *Iteration 11A:* 2. **DNase RNase** in SPB for **2 h***. ⇒ *Iteration 11B:* 2. **DNase RNase** in SPB for **1 h***.	Effects on NP ECM: • **GAGs:** increased quantitative and qualitative preservation in NP processed with 11B as compared to 11A (~64% versus ~35% retained, respectively). • **Collagen:** similar qualitative distribution and an increasing quantitative trend of collagen content consistent with the loss of GAGs • **Nuclei:** some visible nuclei present in NP processed through 11A and 11B, with 11A having a greater reduction of dsDNA content than 10C, (~48% versus ~83% reduction, respectively). **Conclusions:** while enzymatic digestion in SPB for 1 h better preserved GAG, it insufficiently reduced nuclear content. Iteration 11A was selected as the final NP decellularization protocol for subsequent studies.

Curriculum Vitae

Name:	Nadia Sharma
Post-secondary Education and Degrees:	The University of Western Ontario London, Ontario, Canada 2013-2017 B.Sc. (Honors Specialization in Chemistry) The University of Western Ontario London, Ontario, Canada 2017-2019 M.E.Sc. Candidate
Honours and Awards:	CMHR Transdisciplinary Bone and Joint Training Award 2017-2019 CONNECT! NSERC CREATE Program in Soft Connective Tissue Regeneration/Therapy Training Award 2017-2019 Western Graduate Research Scholarship 2017-2019 Canadian Biomaterials Society 1st Distinguished Oral Presentation Award 2019
Related Work Experience	Teaching Assistant The University of Western Ontario 2017-2018 Internship CellScale Biomaterials Testing Waterloo, Ontario 2018-2019